Università degli Studi di Palermo

AREA QUALITÀ, PROGRAMMAZIONE E SUPPORTO STRATEGICO
SETTORE STRATEGIA PER LA RICERCA
U. O. DOTTORATI

Dottorato in Ingegneria dell'Innovazione Tecnologica
Scuola Politecnica
Settore Scientifico Disciplinare (ING-IND/14)

The role of patient specific morphology and contractility of the left atrial appendage on the thromboembolic risk in atrial fibrillation

IL DOTTORE
GIULIO MUSOTTO

IL COORDINATORE
SALVATORE GAGLIO

I TUTOR
BERNARDO ZUCCARELLO
GAETANO BURRIESCI

I CO-TUTOR
ANTONIO PANTANO
GIUSEPPE PITARRESI

XXXIV Ciclo
2020/2021

“Σπεῦδε βραδέως”

“Festina lente”

Index

Index of figures

Index of tables

Abstract

The vast majority of thrombi that cause ischemic complications in atrial fibrillation originate in the left atrial appendage. The left atrial appendage is an anatomical structure that starts from the left atrium, characterized by a wide morphological variability between individuals. This work analyses simulated hemodynamic for different patient-specific models of the left atrial appendage, using computational fluid-structure interaction studies, modelling the effect of changes in contractility and shape resulting from atrial fibrillation.

Three operating conditions were analysed: sinus rhythm, acute atrial fibrillation, and chronic atrial fibrillation. These were simulated on four patient-specific left atrial appendage morphologies, each associated with one of the major morphological variants identified by the common classification: chicken wing, cactus, windsock, and cauliflower.

The active contractility of the wall muscle was calibrated on the basis of clinical assessments of the filling and emptying volumes and boundary conditions were imposed on the fluid to replicate physiological and pathological atrial pressures, typical of the different operating conditions.

The volume of the left atrial appendage and the shear strain rates were analysed over time and space for the different models.

Globally, under conditions of atrial fibrillation, all models were found to be well aligned in terms of shear rate values and expected risk level.

Regions of low shear velocity, typically associated with an increased risk of clot, appeared to be promoted by sudden turns and focused on the trabeculae and lobes. These become substantially more pronounced and extensive with atrial fibrillation, especially in acute conditions.

This work clarifies the role of active and passive contraction on healthy hemodynamic in the left atrial appendage, analysing the changes produced by atrial fibrillation that produce hemodynamic conditions that promote clot formation.

The study indicates that the local topological features of the left atrial appendage are more directly associated with the onset of risk than the global form of the appendage, suggesting that more effective classification criteria should be identified.

Preamble

This PhD project is the result of the collaboration between the Ri.MED Foundation and the University of Palermo, as part of the XXXIV PhD cycle in Engineering of Technological Innovation, active at the Engineering Department of the University of Palermo.

It is a scholarship financed, with DDG of the MIUR n. 2983 of 05.11.2018 and admitted for funding by the University of Palermo, among the additional grants for innovative research doctorates with industrial characterization, as part of the PON Research and Innovation program 2014-2020.

The research activities were carried out under the joint supervision of Prof. Bernardo Zuccarello (UniPA), Prof. Gaetano Burriesci (University College London, GB and Ri.MED Foundation) and co-tutors Prof. Antonio Pantano (UniPA) and Prof. Giuseppe Pitarresi (UniPA).

The research project was funded with the aim of carrying out a study on the contractility of the heart chambers and highlighting the values of the physical parameters capable of providing an indication of any thromboembolic risk that arises in conditions of atrial fibrillation.

The research activities were largely carried out at the Bioengineering unit of the Ri.MED Foundation, in the Bioengineering Group coordinated by Prof. Gaetano Burriesci, currently housed in the premises of Building 18 of the University of Palermo.

Much of the research work was mainly aimed at the implementation of a numerical model based on computational simulations of fluid-structure interaction, capable of carrying out a study on the hemodynamic of the left atrial appendage and of better investigating the responsible mechanisms that trigger the formation of a clot within the atrial appendage itself.

The clinical focus of the research activities is therefore entirely based on the pathological condition of atrial fibrillation and on the mechanisms responsible for thromboembolic risk within the left atrial appendage.

A bibliographic study was made of the pathological condition, the anatomical structures involved, the pharmacological treatments, the thromboembolic risk and the numerical methods used to treat the problem from a computational point of view. Various tests were carried out which led to the election of an adequate numerical method to model the problem from a pathophysiological point of view.

The goal of introducing patient-specific geometries into the numerical model was achieved and a code was developed that made it possible to obtain an evaluation of the anatomical areas of the left atrial appendage most exposed to thrombus formation.

The research activity resulted in some new elements that can be recognized and summarized below in three main aspects:

- the development of numerical models based on patient-specific geometries, made from radiological images produced with computerized axial tomography;
- the use of a working computational model, based on numerical methods of bidirectional fluid-structure interaction that allow to model the effect of active and passive contraction of the walls of the left atrial appendage in conditions of sinus rhythm and atrial fibrillation (before and after remodelling);
- the indication of a possible criterion that exceeds the current morphological classification and that provides information directly related to the factors that promote the risk of coagulation, more related to local topological characteristics such as folds, trabeculations and lobes.

This suggests that more effective classification criteria should be identified to implement reliable thromboembolic risk stratification approaches.

The issues dealt with were analysed with methodological rigor, supporting the numerical approach, initially based on hemodynamic evaluations performed with purely fluid dynamics computational methods, through numerical simulations that proved how this study improves the current understanding of the mechanisms related to atrial fibrillation responsible for clot formation in the left atrial appendage by fluid structure interaction analysis.

The research activities led to the publication of a scientific article in an international journal of the first quartile and high impact factor (> 5), and to the submission of another work, currently being evaluated by one of the international peers reviewed scientific journals of sector.

Part of the research activities were of interest from a stay abroad, where it was possible to receive training at UCL Mechanical Engineering, University College London, GB. Here, adequate high-profile training was provided by international experts. This activity was characterized by learning the techniques used in the section of biological tissues and in performing both biaxial and mono-axial mechanical tests on various components of cardiovascular tissue, with particular attention to the left atrial appendage.

The activity abroad was abruptly interrupted by the pandemic caused by COVID-19 and continued in smart-working mode from Italy according to the indications provided by the Ministry and in compliance with the law. The remote support provided by UCL was fundamental for the morphological classification and for the creation of the geometric models necessary to develop patient-specific computational analyses.

Work Outline

The work outline of this PhD programme includes the following work packages:

- Pathophysiological analysis of the condition of atrial fibrillation;

- Anatomical analysis of the left atrial appendage as the anatomical part involved in the numerical study;

- Analysis of the various numerical methods used in the field of computational simulations related to clinical and bioengineering problems;

- Evaluation of the most suitable numerical tools for studying the problem that is the subject of the PhD research;

- Development of patient-specific models to perform numerical simulations representative of the four morphological families;

- Identification of adequate surrounding conditions capable of reproducing both physiological and pathological cardiac activity;

- Identification of the adequate mechanical characteristics to be attributed to the cardiac tissue and of those relating to the characterization of the fluid;

- Analysis and development of three different analysis conditions: sinus rhythm, acute atrial fibrillation and chronic atrial fibrillation;

- Identification and analysis of the correct physical parameters related to thromboembolic risk such as the Shear Strain Rate (SSR);

- Development of colour maps related to the various levels of SSR within the cardiac cycle, for each morphology and for each condition of analysis;

- Development of the SSR curves diagrams related to the various operating conditions;

- Development of a code for reading the results capable of offering a graphic evaluation of the risk percentages and of the relative anatomical portions exposed overall to low values of SSR for the entire cardiac cycle;

- Open questions

1. Introduction

Atrial fibrillation is a heart rate disorder (see Figure 1) and is characterised by a rapid and asynchronous heartbeat. The incidence of this pathology affects between 1% -2% of the population, with about 9%, and increases considerably with advancing age, reaching a prevalence of almost 10% in the over 80s (Colilla et al., 2013; Krahn et al., 1995). In Italy this aspect has even more relevant characteristics, as there are over 150 elderly people for every 100 young people, compared to a European average of 116.5; and it is expected that by 2050 more than a third of the population will be over 65 years of age.

Atrial fibrillation is the leading cause of thromboembolic events, causing pathological phenomena such as stroke and vascular dementia or TIA (transient ischemic attack) (Gorelick, 2004). In particular, stroke is the second leading global cause of mortality, whilst vascular dementia affects 6% of people over 60 and currently has no cure (Kalaria et al., 2008). These percentages give us an idea of the extent of the phenomenon and its consequences.

It has been shown that 90% of the thrombi responsible for thromboembolic events in the condition of atrial fibrillation originate in the left atrial appendage (Yaghi et al., 2015). This is a protrusion between 2 and 4 cm in size that departs from the main body of the left atrium (Al-Saady et al., 1999a). In atrial fibrillation condition, the normal function of the left atrial appendage is altered, with reduction in the normal contractility and function of the appendage.

This phenomenon favours the establishment of haemostatic areas which are more likely to promote the formation of any clots with a consequent increase in thromboembolic risk (Al-Saady et al., 1999a). Although these phenomena are of considerable importance, the hemodynamic processes induced by atrial fibrillation in the left atrial appendage are still poorly understood. This research work has investigated the phenomenon of atrial fibrillation, trying to obtain a more complete view of the hemodynamic processes present in the different morphologies of the left atrial appendage and their contribution to thromboembolic events, through the use of experimental and computational biomechanical models.

This work aims to lay the foundations for the stratification of patients at higher risk of thrombus formation, on the basis of patient-specific anatomical morphologies. Although the computational models can be improved and extended to a larger sample of morphologies, the information obtained can offer valid support for the development of new tools that allow a more effective and sustainable therapeutic planning, based on specific patient and population approaches.

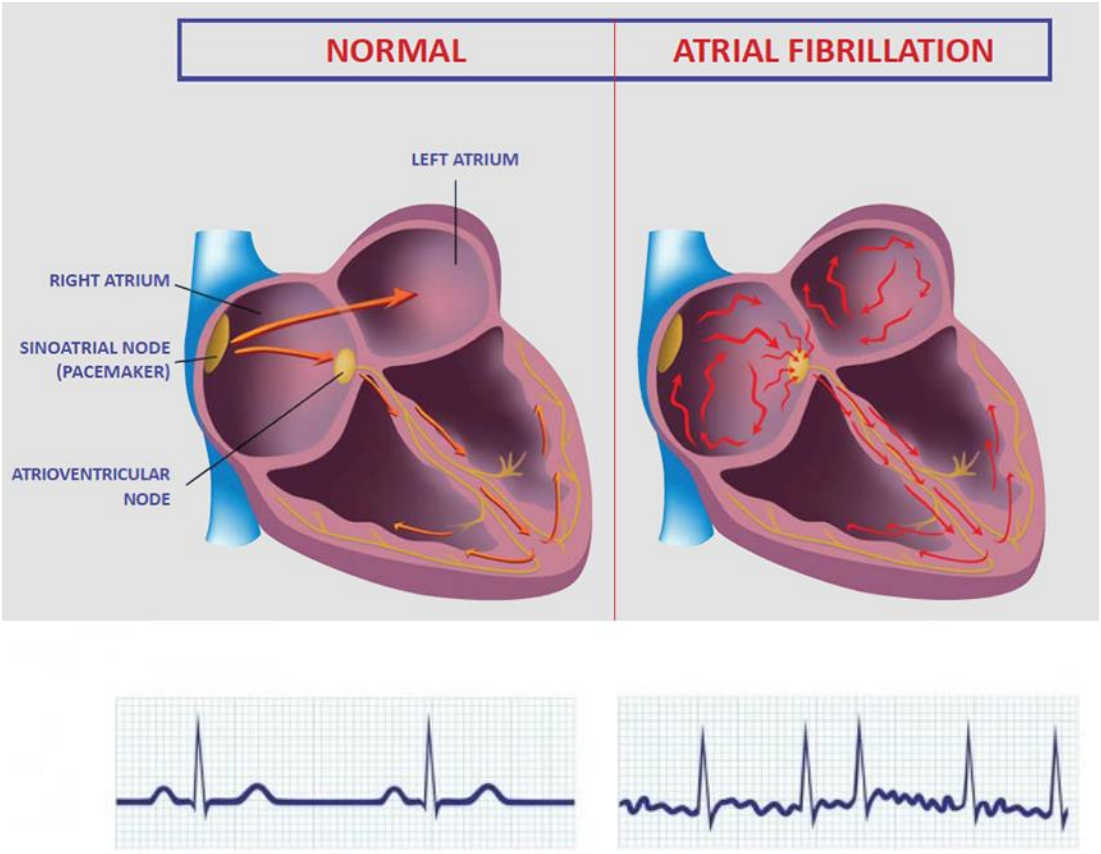

Figure 1 The left part of the figure describes the trigger points and the conduction pathways and the related tracing identifiable in the sinus rhythm condition. The right part of the figure describes the condition of atrial fibrillation through the schematization of different trigger points in the atrial surface and the relative anomaly in the electrocardiographic trace where the absence of the P wave and the periodicity of the R-R segment emerge (imagine from: https://www.feinberg.northwestern.edu/giving/stories/_stories/arrhythmia-research-center-2019.html)

2. Background

2.1 Left Atrial Appendage (LAA)

The left atrial appendage is an anatomical structure adjacent to the left atrium (see Figure 2). It has a structural continuity with the left atrium and is partly placed on the outer wall of the left ventricle and plays the role of a decompression chamber in the phases in which the atrial pressure is high as in ventricular systole (Al-Saady et al., 1999b).

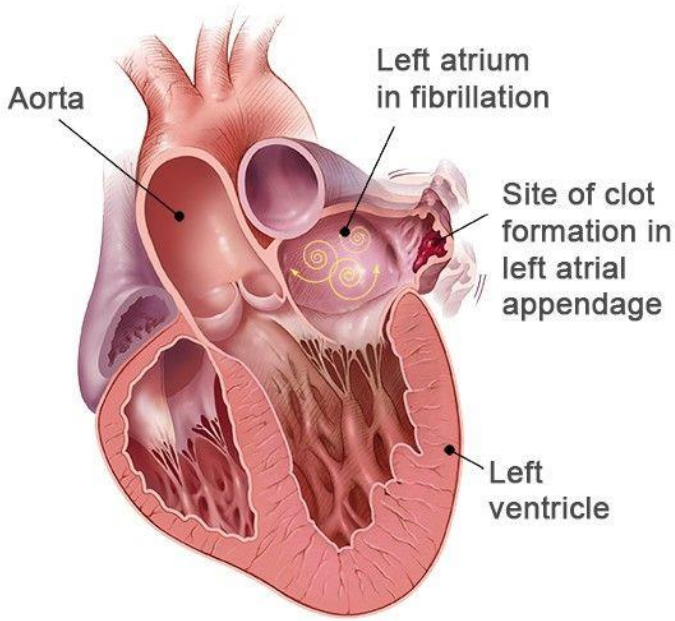

Figure 2 Anatomical view of the left atrium in atrial fibrillation condition. In this figure it is possible to see in section: the aorta, the left atrium, the left ventricle and the left atrial appendage which appears to be the site of formation of the clot (from https://www.pinterest.it/pin/379639443571345737/).

From a hormonal point of view, the left atrial appendage is an anatomical structure characterised by a high presence of atrial natriuretic peptide (ANP).

The presence of ANP within the left atrial appendage gives it a role in regulating atrial pressure through the activation of specific receptors. Although the left atrial appendage is considered non-functional, some doppler-echocardiographic studies reveal an active contraction (Petty et al., 1999).

One of the aspects to underline about the left atrial appendage is the morphological classification. There is a high variability among the classifiable shape of this anatomical portion which changes from patient to patient. However, a common classification includes four large families, defined on the basis of the shape that the appendage recalls: the "chicken wing" morphology is the most common (48%), followed by the "cactus" (30%), "Windsock" ("windsock") (19%) and "cauliflower" ("cauliflower") (3%) morphologies (see Figure 3). Although these anatomical features are still the subject of debate, recent studies have suggested an association of the morphology with the risk of thrombus formation.

Still, the association between the anatomical characteristics and the risk of thrombosis remain an open question. This research project aims to elucidate the role of the left atrial appendage in healthy and pathological conditions by studying the relationship between the left atrial appendage morphology and dynamics and the risk of thrombus formation, by applying modern computational and experimental approaches available in engineering.

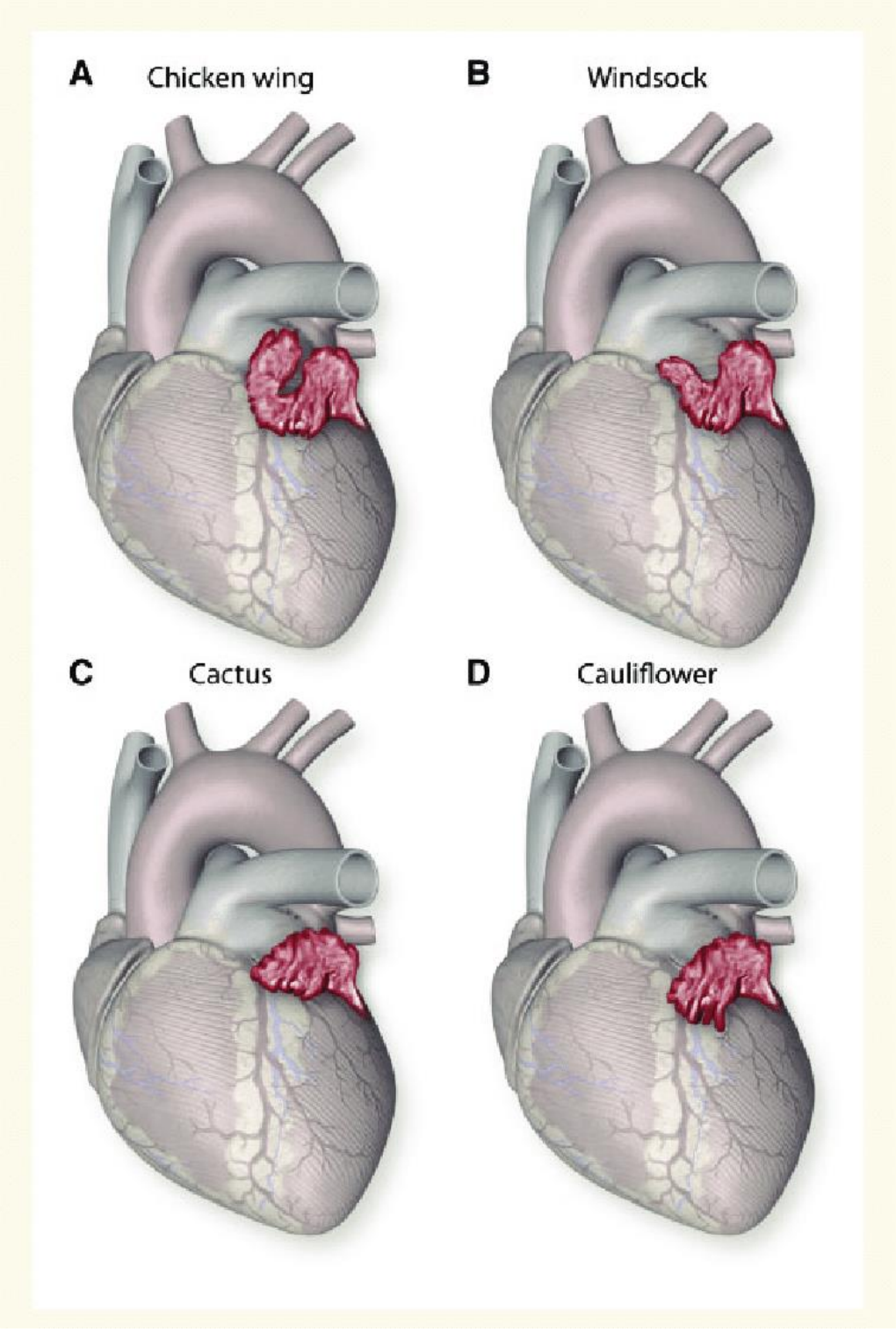

Figure 3 This figure shows the various types of morphology of the left atrial appendage, integrated with the rest of the cardiac anatomic structure. They are present in sequence: Chicken Wing (A), Windsock (B), Cactus (C) and Cauliflower (D) (from Khan & Lip, 2019).

2.2 Clinical need (Atrial Fibrillation)

Atrial fibrillation is defined as a heart rhythm disorder, characterised by the presence of multiple trigger points on the atrial surface and identifiable in the electrocardiographic trace by the absence of the P wave (wave relative to the atrial contraction) and by the aperiodicity of the R-R segment (see Figure 1).

The presence of atrial fibrillation increases the probability of onset of ischemic events and the related neurological consequences (Hagiwara et al., 2018; Nattel, 2002; Stoddard et al., 1995).

The treatment of atrial fibrillation requires a multidisciplinary approach, and can be done pharmacologically through the administration of anticoagulants or by a surgical approach (Hindricks et al., 2021).

Although the pathogenesis has not yet been fully clarified and about 30-40% of ischemic strokes is of unknown cause, the left atrial appendage is undoubtedly related to the thrombo-embolic risk, as it is reported that 90% of clots responsible for these events originates inside this chamber (Yaghi et al., 2015).

Currently, the most effective and most widespread drug therapy for the prevention of thrombus formation in patients with atrial fibrillation consists in the use of oral anticoagulants. The best known and most used oral anticoagulant for this pathology is Warfarin (Björck et al., 2013). However, this treatment has some contraindications in 44% of patients with atrial fibrillation (Björck et al., 2013), including considerable increase in the bleeding risk associated with it, the cost, and the need for frequent

laboratory checks for the evaluation of the prothrombin time (PT = Prothrombin time), which quantifies the time required for the formation of a clot.

In addition to drug therapy, there are also surgical treatments that alter the left atrial appendage in the attempt to reduce the likelihood of a clot forming in the site of atrial fibrillation.

One of these options consists in the surgical exclusion of the left atrial appendage through external ligation, which avoids the need of drug therapy. However, this is an invasive open-chest operation, that involves high risks, especially in elderly. This procedure is in fact practiced in a secondary surgical regime, wherever the patient is undergoing a primary surgery that already involves invasiveness (Dawson et al., 2010; Whitlock et al., 2021).

Trans-catheter ablation is another procedure developed for the non-pharmacological treatment of atrial fibrillation. This is a minimally invasive procedure performed through the introduction of a catheter into the blood vessels and led to the heart, with the aim of identifying and interrupting the abnormal electrical pathways present in the heart tissues.

Finally, the most recent development is represented by percutaneous occluding devices, which isolate the left atrial appendage chamber by plugging its access orifice from the atrial chamber (OSTERMAYER et al., 2003). These devices are typically designed with self-expanding nitinol structures that are implantable via access from peripheral vessels.

The most relevant complications of these solutions include lateral leakages, that require long-term anticoagulant therapy, effectively compromising the main interned purposes of the procedure (Holmes et al., 2009)

This doctoral work aims to help clarifying role and biomechanics of the left atrial appendage in sinus rhythm and pathological conditions, distinguishing the chronic condition from the acute one.

2.3 Clinical Issue

The clinical problem presented has a growing incidence, and as previously pointed out, has a strong correlation with advancing age. Considering that in today's society the average age is continuously increasing, the impact of this pathological condition is expected to become major in terms of both numbers and social costs. Therefore, this PhD project addresses a problem that falls within the national and regional thematic area of 'health', defined in the National Strategy of Intelligent Specialization (SNSI) and approved by the European Commission. In fact, this is an issue related to the aging of the population and the consequent incidence of chronic degenerative diseases. These aspects must be identified as relevant factors for the development and management perspective of a given area. The clinical problem can be summarised as follows:

- ✓ High pathological incidence;
- ✓ Affected population group of high average age;
- ✓ High clinical and social management costs;
- ✓ The left atrial appendage is the site of clot formation in atrial fibrillation regime;
- ✓ The left atrial appendage exhibits great morphological variability, which may play a role in promoting thrombosis;

- ✓ Neurological consequences related to thromboembolic risk such as: stroke, TIA and vascular dementia;
- ✓ Pharmacological treatment with continuous monitoring of certain blood chemistry parameters;
- ✓ Invasive surgical treatment that is not always justified or practicable;
- ✓ Endovascular treatment that does not exceed any pharmacological treatment;

3. Literature Review

3.1 Thrombogenicity

Platelets activation and thrombosis are the blood mechanisms that cause blood coagulation to stop its leakage following an injury to a blood vessel. This is also called haemostasis. Following trauma, in addition to the intervention of platelets aggregation (primary haemostasis), coagulation factors, defined in the coagulation cascade, vascular factors are triggered to form more stable fibrin/red cells clots, in the attempt to further control blood loss (secundary haemostasis). A mechanism of local vasoconstriction and compression of the vessels is also triggered due to the pressure exerted by the blood which is extravasated into the surrounding tissues.

The coagulation process, in conditions that alter the biochemical balance of blood, can lead to two extreme conditions that trigger a clinical condition:

• **Thrombosis**: process that leads to the formation of a clot capable of obstructing a blood vessel;

• **Haemorrhage:** blood leaking from a blood vessel, both venous and arterial.

The triggering of a coagulation process can occur, as a result of endothelial damage, such as a lesion following, for example, an inflammatory process. Following an endothelial damage or a vascular trauma, circulating platelets are recruited to the injury site, where they are activated and aggregate, change their shape, and through the production of mediators such as ADP they favour the aggregation and activation of other platelets at the level of the lesion.

This results in the formation of a platelet plug primary haemostasis which, however, may not sufficient, alone, to generate haemostasis. Hence, the coagulation cascade may be triggered.

The term coagulation cascade takes on this name as the activation of the processes occurs sequentially. The process involves the activation of a number of proteins, called 'factors', identified by a Roman numeral in the sequence they were chronologically discovered. The factors (see Table 1) are activated sequentially, with each element involved responsible for the activation of the following factor (Furie & Furie, 2008). The process culminated with the formation of fibrin.

Table 1 Coagulation cascade factor

Factor	***Name***	***Form activated***	***Type***	***Way***
I	Fibrinogen	Fibrin	Protein	Common
II	Prothrombin	Thrombin	Serine protease	Common
III	Tissue factor		Cofactor	Extrinsic
IV	Calcium ion		Chemical element	Common
V	Proaccelerin		Cofactor	Common
VI	-	-	-	-
VII	Proconvertine		Serine protease	Extrinsic
VIII	Antihemophilic factor A.		Cofactor	Intrinsic
IX	Christmas factor		Serine protease	Intrinsic

X	Stuart factor		Serine protease	Common
XI	Plasma antecedent of thromboplastin		Serine protease	Intrinsic
XII	Hageman factor		Serine protease	Intrinsic
XIII	Fibrin stabilizing factor		Enzyme	Common

In relation to the cause that triggers the coagulation process and in relation to the number of activated factors, we can distinguish two pathways that lead to the formation of fibrin:

Extrinsic way:

- It is activated in the presence of tissue damage or trauma;
- Fibrin formation occurs more quickly;
- The number of activated factors is reduced with respect to the intrinsic pathway.

Intrinsic way:

- It is activated when the blood comes into contact with a surface other than the vascular one;
- Fibrin formation occurs more slowly;
- The number of activated factors is greater than in the extrinsic way.

From the activation of factor X into factor Xa they are common to both the extrinsic and intrinsic pathways.

Vitamin K acts as a co-enzyme in the carboxylation process of glutamic acid, allowing the activation of some coagulation proteins (prothrombin, factors VII, IX, X and proteins C and S).

This process presents significant variability in terms of comparative physiology, between different species and between members of the same species. The study of this phenomenon mainly requires a multidisciplinary approach, as it involves different branches of knowledge from basic medicine to mathematical modelling.

However, developing a mathematical model capable of describing the mechanism in its entirety, including the multitude of variables involved, is still an open question (Anand et al., 2005; Leiderman & Fogelson, 2011) .

3.2 The risk of thrombosis with atrial fibrillation

Due to the complexity of blood and the biochemical aspects that regulates the described phenomenon (Furie & Furie, 2008), the coagulation process can also be triggered and influenced by external stimuli or unphysiological conditions. For example, excessive amounts of thrombin promote thrombosis, which is a critical event leading to conditions such as stroke and myocardial infarction, and venous thrombosis is the second leading cause of death in cancer patients. In general, any flow conditions that cause stagnation, high residence time, or excessive levels of shear rate can promote the phenomenon, and atrial fibrillation is one of the main causes of pathological thrombosis.

The stratification of thromboembolic risk is particularly important to identify if a therapy is needed, and in the selection of the treatment. Clinicians currently rely on score criteria relative to the patient's clinical condition and related appropriate drug therapy. These are used to determine which patients have a risk of stroke which justifies the bleeding risk associated with these oral anticoagulants (Mason et al., 2012).The most common scoring systems in use are $CHADS_2$ and especially CHA_2DS_2-Vasc (Olesen et al., 2012). The second scoring method has gradually replaced the first one (see Figure 4).

The main differences of the two scoring methods are listed below:

• *The $CHADS_2$ score is commonly used for stroke risk stratification for atrial fibrillation, but is not of great predictive value.*

• *The CHA_2DS_2-VASc scheme has been validated and appears to have improved value, doubling the number of patients' candidates for oral anticoagulation*.

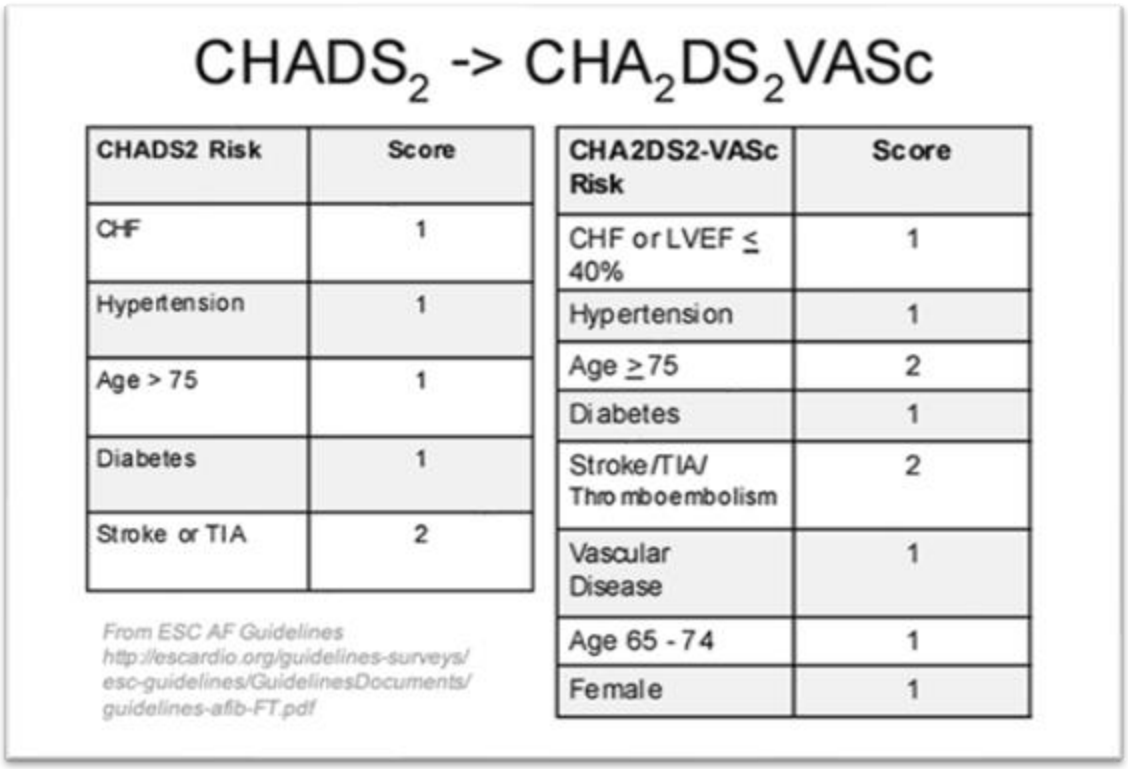

Figure 4 This figure illustrates the score sheets relating to the $CHADS_2$ and CHA_2DS_2-VASc risk score. These scores, relating to the condition of atrial fibrillation, were created with the aim of assessing the risk of stroke in patients with atrial fibrillation in the absence of heart valve disease. The $CHADS_2$ score is no longer in use in recent years and has been replaced by CHA_2DS_2-VASc, as it has been shown that patients who score low on the CHADS2 may still have a significant risk of stroke (from European Heart Association).

3.3 Pharmacological treatment

As mentioned above, atrial fibrillation is a heart rhythm disorder which, in non-pathological conditions, is defined as sinus rhythm.

Being a rapidly increasing pathology, with an epidemiological increase in old age, it has a strong social impact, especially in conjunction with other chronic pathologies which, in the presence of atrial fibrillation, strongly increase the thromboembolic risk (Abrignani & Colivicchi, 2015).

Therefore, since it is a pathology related to thromboembolic risk, drug treatments aimed at linting formation of clot and the resulting clinical consequences are commonly adopted (di Fusco et al., 2017).

3.3.1 Anticoagulants

Anticoagulant drug treatments have shown evidence of therapeutic efficacy, especially in the prevention phase of the thromboembolic risk (Cabral, 2013).

Anticoagulants are classified according to the mechanism of action and the type of administration:

• **Coumarins:** they are administered orally and are coumarin derivatives. They are classified as antagonists of vitamin K, already involved in the mechanism that triggers the coagulation cascade.

• **Heparinises:** they are administered parenterally; they include heparin and its derivatives. They work by activating antithrombin III, a plasma glycoprotein synthesized by the liver that is classified as a physiological inhibitor of coagulation.

• **Factor Xa inhibitors:** the action of this category of drugs is directed on the coagulation factor Xa. They have the ability to hinder the transformation of prothrombin I into thrombin (factor IIa).

• **Factor IIa inhibitors:** the action of this category of drugs is directed on factor IIa, that is, on thrombin. They have the ability to prevent the formation of the fibrin network that traps erythrocytes and gives rise to the blood clot.

Treatment with anticoagulant is characterised by some complication linked to potential haemorrhagic events that may arise due to an inadequate calibration of the treatment. A well-known problem, linked for example to the use of oral anticoagulants, is the evaluation of the INR (International Normalized Ratio), which is a parameter used to more accurately estimate the prothrombin time (PT).

It is therefore a necessary parameter to periodically monitor patients and consequently manage the pharmacological dosage. An oral anticoagulant belonging to the coumarins and well known for some time is **Warfarin**. The family of drugs to which warfarin belongs is grouped among vitamin K antagonists and, as such, is capable of inhibiting the activation of factors of the coagulation cascade that depend on vitamin K (factors II, VII, IX and X). Determination of INR is therefore useful to ensure that the drug is effective and the prothrombin time is appropriate.

The heparin anticoagulants currently used are basically of two types:

Standard or non-fractionated heparin (high molecular weight): this is a molecule that has a short duration of action, but is characterised by a very rapid anticoagulant effect. This feature configures the use of standard heparin ideal for emergency cases.

Low molecular weight heparins (or **LMWH**): compared to unfractionated heparin, these types of heparins have a prolonged action over time. They are therefore ideal to be administered when an emergency condition is not present.

Heparin therefore has the characteristic of enhancing the process linked to the inhibition of coagulation factors Xa and IIa.

Heparin binds to antithrombin III and acts as a physiological inhibitor of the coagulation process. The binding affinity between antithrombin III and coagulation factors Xa and IIa is increased by the heparin action. This mechanism significantly increases the physiological action of antithrombin III.

The action of low molecular weight heparins compared to high molecular weight ones are distinguished from each other in relation to the coagulation factor that is inhibited. Those with low molecular weight, for example, increase the action of antithrombin III against coagulation factor Xa. In the same way, they exert a reduced action against factor IIa, negligible from a clinical point of view. The result is a greater selectivity towards the coagulation factor Xa compared to the family of so-called standard or high molecular weight heparins.

In oral pharmacological therapy, a distinction can be made between direct inhibitors of factor Xa and factor IIa:

Direct factor Xa inhibitors prevent thrombus formation by acting selectively on the active site. They have the ability to interrupt the action of the coagulation mechanism and therefore prevent the clot from forming.

The related active ingredients on the market are listed below:

- Rivaroxaban
- Edoxaban
- Apixaban

Direct factor IIa inhibitors act in the clotting process directly on factor IIa. They are antagonists of factor IIa (thrombin) which breaks down fibrinogen into fibrin monomers. They prevent the formation of the fibrin network that traps erythrocytes and gives rise to the blood clot. Their mechanism of action is therefore able to block the last stages of the coagulation process, preventing the formation of the thrombus.

The related active ingredients on the market are listed below:

- Bivalirudin (parenteral route);
- Argatroban (injection);
- Dabigatran (oral);

The last two families of anticoagulants described above, capable of acting on factor Xa and factor IIa, which are administered orally are also identified as NAO. The new oral anticoagulants (NAO) are a class of drugs indicated for the prevention of stroke, embolism and atrial fibrillation.

NAO have advantages over the classic oral anticoagulant therapy (TAO) identified in the use of warfarin. The advantages are linked to the following features:

- No blood chemistry assessment of INR
- Fixed dosage
- Less interaction with other drug therapies
- Fewer side effects
- Fewer interactions with the diet

It should be emphasised that NAO are not indicated in the anticoagulant treatment in patients undergoing surgery for valve diseases and related prosthetic implant.

3.3.2 Anti-platelet drugs

Another category of drugs used to reduce the thromboembolic risk associated with the formation of blood clots are the so-called antiplatelet drugs. They act through different mechanisms of action with the aim of inhibiting platelet activation. They are used in therapies associated with cardiovascular diseases. They can also be used in atrial fibrillation conditions, in association with anticoagulant therapy.

There is a broad classification of antiplatelet drugs. Their identity is related to the relative mechanism of action.

Below is a bulleted list of the pharmacological families of antiplatelet agents:

- COX-1 inhibitors
- PDE-3 inhibitors
- P2Y receptor antagonists
- GP IIb / IIIa receptor antagonists
- Other antiplatelet agents

Therapeutic indications are substantially linked to the prevention of cardiovascular events.

Among the best-known antiplatelet agents, there is acetylsalicylic acid (aspirin), identified among NSAIDs (non-steroidal anti-inflammatory drugs), which is one of the irreversible inhibitors of the COX-1 enzyme responsible for the synthesis of PGH2 from which thromboxane A2 (TXA2) derives. Blocking thromboxane prevents clot formation (Mega & Simon, 2015).

Dipyridamole, on the other hand, is one of the inhibitors of type 3 phosphodiesterase (PDE-3), an enzyme responsible for the degradation of cAMP (cyclic adenosine monophosphate, or cyclic AMP if you prefer) into AMP (adenosine monophosphate). AMP promotes platelet degranulation and therefore dipyridamole exerts an antiplatelet action.

The use of this drug has decreased over time. Another type of antiplatelet drugs is represented by the P2Y receptor antagonists present in platelets. They are sometimes associated with acetylsalicylic acid and are known as Clopidogrel and Ticlopidine, they act by preventing the bond with ADP, reducing the thromboembolic risk.

Another family of antiplatelet agents is identified among the antagonists of the GP IIb/IIIa receptor used in the hospital and administered intravenously. They have the function of inhibiting the bond with fibrinogen, consequently hindering platelet aggregation. Also, in this case the, aforesaid mechanism favours a lowering of the thromboembolic risk. Finally, other antiplatelet agents include the drugs inhibitors of the receptors and of the synthesis of TXA2 and those inhibitors of the PAR-1 receptor of thrombin. The former inhibits thromboxane synthetase while the latter hinder the induced activation of thrombin. Both reduce processes involved in clot formation.

3.4 Numerical methods

The phenomena occurring in the cardiovascular system involve the coupling of highly deformable tissues with pulsatile blood flows. The structural and fluid problems cannot be described and solved independently, as the coexistence of their different physical nature operates synergically in a single environment, defined as multi-physical. Within the multi-physical problems, the fluid-structural interactions (FSI) can be described as a problem where the action of the fluid has an impact on the structural component which, conversely, acts on the fluid part in response to the primary action.

Through continuum mechanics, it is possible to describe problems of a structural nature as well as of a fluid nature. There are several numerical solution methodologies for FSI problems best described in the literature as monolithic or partitioned methods. A further difference to underline within the partitioned methods is that between unidirectional methods and bidirectional methods.

In turn, there is a coupling classification within bidirectional methods, understood as strongly coupled and weakly coupled.

There is a wide range of documents in the literature that illustrate the differences in terms of partitioned monolithic methods; mixed; loosely coupled and strongly coupled (Benra et al., 2011).

3.4.1 Numerical Approach

The architecture of the numerical model involved the **ANSYS TRANSIENT STRUCTURAL** software for the structural part. The fluid side part was covered by the **ANSYS CFX** fluid dynamics software, while the **ANSYS SYSTEM COUPLING** algorithm was used for two-way coupled simulations. System Coupling is a component of ANSYS Workbench. It is an infrastructure suitable for simulations in the multidisciplinary field. The data involved in the numerical modelling of both one-way and two-way solid fluid interaction analysis involve transfers of:

- **force**
- **displacement**
- **temperature**
- **heat**

3.4.2 FSI in the cardiovascular field

Finite element analysis (FEA) and computational fluid dynamics (CFD) are among the numerical methods used to carry out computational analyses of an engineering problem or, more generally, of a specific physical system, whether of a structural or fluid dynamic nature. However, these methods are not sufficient to model cardiovascular systems satisfactorily, individually.

A numerical tool suitable for analysing these issues are fluid-structure interaction simulations (FSI). In this way it is possible to describe a system where the flow of a fluid causes the deformation of a solid structure or vice versa.

Thanks to this aptitude, numerical simulations of the FSI type lend themselves well to describing problems typical of bioengineering. For this reason, the use of FSI simulations in the field has expanded over time, with various methods being used to model biomechanics of problem such as aneurysms, heart valve dynamics, atherosclerosis, etc (Hirschhorn et al., 2020a).

A typical issue of cardiovascular simulations is the complexity of the geometries involved in the analyses, with patient-specific models playing a fundamental role in the modelled phenomena. Patient-specific models are commonly created through data retrieved through two main diagnostic imaging approaches:

• MRI Imaging: These are nuclear magnetic resonance scans. The data is acquired during the scan and processed through specific anatomical segmentation software; The operating principle of this investigation method relating to the field of diagnostic imaging exploits the magnetic fields produced by a large magnet. The output is to obtain three-dimensional images of the internal anatomy. MRI not involve the use of ionizing radiation.

• CT scan imaging: these are radiological scans based on high resolution X-ray technology. The aim is always to obtain three-dimensional images of a specific anatomical portion. As well as MRI, a contrast agent could be used under certain conditions related to clinical reasons. Also, in this case it is necessary to implement

the images on software suitable for segmenting the images (Fedorov et al., 2012; Lansberg et al., 2000).

The choice of one method of investigation over other falls on clinical reasons that involve investigating a specific type of tissue.

In both cases, these images must be carefully and manually processed by an operator, in order to obtain 3D models that can be edited in a numerical environment.

Although in recent times artificial intelligence has also been making progress in the field of patient-specific modelling, traditional tools, such as MIMICS or 3DSclicer software remain the main tools for creating these geometries.

Despite the complexity of the model preparation, the level of accuracy of FSI methods with patient-specific geometries is opening up new important scenarios in terms of both numerical and clinical impact of the results and their evaluations.

In these terms, FSI model coupled to a patient-specific geometry offers a more accurate and precise description of the pathophysiological process. A reading of any physical parameters that determine a condition more or less exposed to a clinical problem is the result of a dedicated and specific analysis process for a single patient. This approach brings us closer to precision medicine and opens the way to scenarios with a strong therapeutic and social impact.

We can give some examples of the quantities used to make a precise assessment of a pathophysiological process:

• Shear Strain Rate (SSR): is a measure of the flow velocity correlated to the dimensions of the space crossed, and is linked to the rheological response as well as to the thrombogenicity of the blood;

• Wall Shear Stress (WSS): Direct measurement of the wall shear stress (WSS) in a blood vessel within the body is currently impossible. It should be noted that pathologically low WSS is an important risk factor for the onset and progression of atherosclerosis (Badimon et al., 1986).

4. Materials and Methods

The research project developed in the following work packages:

1. **Acquisition** of the theoretical and practical skills necessary for the development of the project, including: study of the literature relating to atrial fibrillation, soft biological materials, the principles of finite element modelling and computational fluid dynamics.

2. **Morphological analysis** of the left atrial appendage. This activity was carried out at UCL, UK, in collaboration with the UCL Institute of Cardiovascular Science & Great Ormond Street Hospital for Children, London, United Kingdom. Different wild pig hearts were analysed, the tissues of the various anatomical parts considered of interest were dissected and mechanical tests performed as per protocol. 3D morphology analysis of the left atrial appendage and parameterization based on geometric measurements, such as the number and size of lobes and trabeculae, and the size of the access orifice of the left atrial appendage.

3. **Preliminary study**, based on fluid dynamics simulations and implemented on population specific geometries. The geometries developed consider the presence of the both the left atrium and appendage, and are designed to represent conditions of functioning of sinus rhythm and atrial fibrillation.

The results of the preliminary study confirm the importance of atrial contraction in the evaluation of the parameters used in the evaluation of thromboembolic risk.

4. **The images** produced by computed tomography scans were recovered from patients who did not have pathological conditions of atrial fibrillation. These scans, after appropriate morphological classification, were used to create the three-dimensional models used for numerical simulations. This activity was carried out in part physically and in part in flexible working mode at the foreign academic partner, who offered tutoring and access to the archive of the UCL Institute of Cardiovascular Science, UK. The already segmented anatomical acquisitions available were processed with the free Meshmixer software to obtain geometric models in STL format to be implemented on CAD software such as Rhinoceros. The final aim was to obtain detailed 3D morphologies of the left atrial appendage and adjacent structures for both the structural part and the fluid part.

5. **Computational modelling** of hemodynamic in the left atrial appendage. This phase of the project was carried out entirely at the company partner UPMC-Italy, within the Bioengineering laboratory of the Ri.MED foundation. The purpose of this activity is related to the morphological-functional correlation of the left atrial appendage with the thrombogenic risk.

The models developed in the previous phase have now been used to perform numerical simulations with fluid-structure interaction (FSI), using software present in the ANSYS Workbench suite.

In particular, the structure of the numerical model is formed by the Transient software for the structural part, the **ANSYS CFX** software for the fluid dynamics part, and the System Coupling software for the coupling of the two domains, so as to obtain a two-way numerical simulation of fluid interaction. The properties of the materials of the left atrium and left atrial appendage to be used in the computational models were obtained from the data available in the literature and on swine heart samples. Scientific works related to uniaxial and biaxial characterisation tests on sheep hearts were also analysed.

4.1 Anatomical Analyses

4.1.1 Morphological analysis of anatomical tissues

This part of the work concerns the study of the various morphologies characterising the left atrial appendage on wild pig hearts. These tissues were stored at the UCL Division of Cardiac Surgery, suitably frozen and catalogued. A working protocol was developed to examine, and subsequently dissect, anatomical tissues for mechanical testing.

The first phase involved training related to the management and dissection of anatomical tissues.

The didactic and training support related to the anatomical aspects was provided by Prof Andrew Cook, Professor of Research and Education in Fetal Cardiac Development, Surgical and Interventional Cardiac Anatomy, Institute of Cardiovascular Science, UCL.

In addition to developing an analysis of the morphologies of the left atrial appendage, a cutting protocol was implemented.

The portions of tissue examined go beyond the only appendage, and also involved other areas of neighbouring tissue which were considered equally interesting to evaluate such as:

- Right Atrial Appendage
- Right and Left Atrium
- Aorta
- Pulmonary Artery
- Mitral valve, leaflets and chordae tendineae
- Tricuspid valve, leaflets and chordae tendineae
- Aortic valve leaflets
- Pulmonary valve leaflets
- Coronaries

Below are some identification images of some phases of the anatomical section process (see Figure 5-Figure 8).

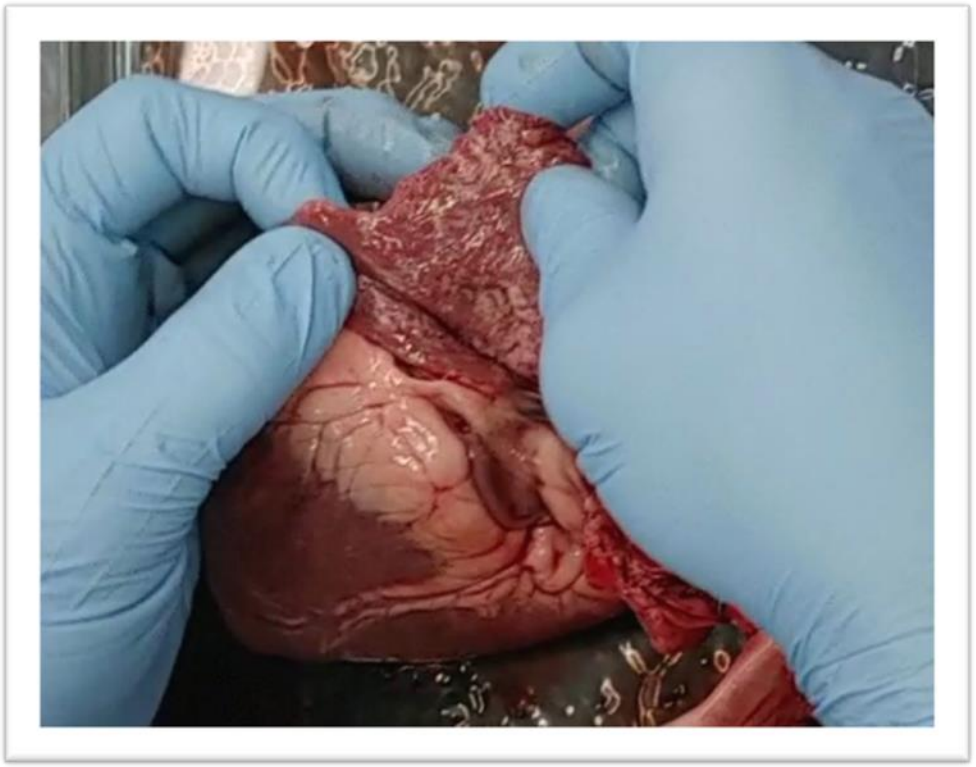

Figure 5 This figure shows the identification of the left atrial appendage and its anatomical cut.

Figure 6 In this figure it is possible to identify the outline that defines the orifice of the left atrial appendage and the trabecular structure that characterizes it.

Figure 7 This figure shows the mitral valve in a top view where it is possible to appreciate the anatomical location of the left ventricle and part of the adjacent structure relating to the aortic valve.

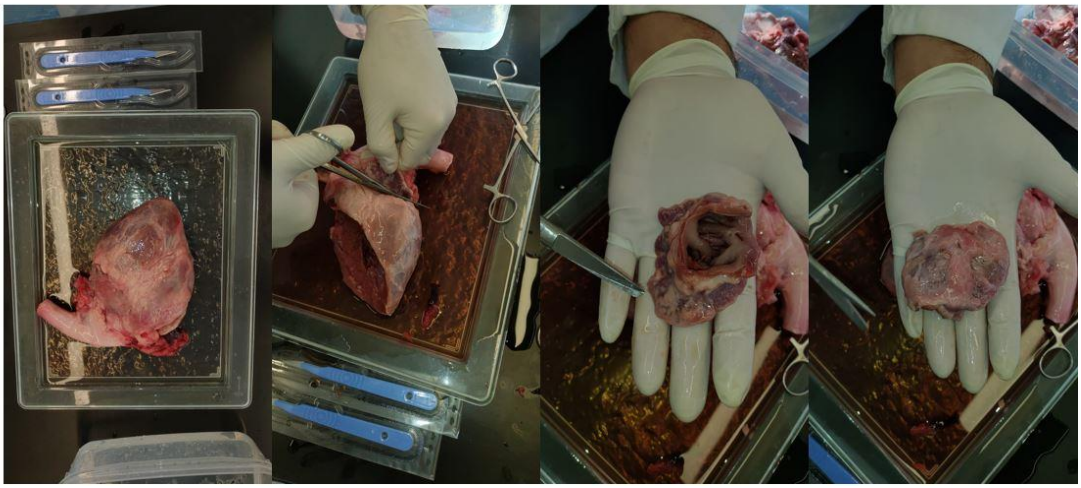

Figure 8 In this figure it is possible the relative sequence to the identification of the left atrial appendix and to its complete extraction.

4.1.2 Monoaxial and Biaxial Mechanical Tests

Mechanical tests were performed on the mentioned anatomical parts of eight different swine hearts. A total of over three hundred tests were carried out on different specimens. Tests were performed on uniaxial and biaxial tensile machines. The entire process for each heart was completed on fresh tissue, over two to three days.

Uniaxial mechanical testing was carried out in a heated bath at a temperature of 37 °C. Each specimen was placed on a plastic support, as shown in Figure 9, to facilitate the positioning of the specimen, the setting of the strain configuration and the execution of the test. Where possible, tests were performed in compliance with the ISO37 standard, with specimen dimensions of gauge length equal to 12 mm and width equal to 2 mm.

Where these dimensions were likely to alter the execution of the test due to the presence of trabeculae within the atrial appendage (these often exceeded 3 mm in width), rectangular specimens of suitable size were manually cut and used for the tests. The average thickness of each specimen was measured with a micrometre, in at least three different regions equally spaced within the sample. Tests were performed to failure, identifying the first hint of fraying as the strength of the material.

Biaxial mechanical tests were performed on a Biotester machine, Cellscale, Canada, using Digital Image correlation (DIC) for the strain measurement. Tests were carried out in a heated bath, at a temperature of 37 °C (see Figure 10). DIC required creating a speckle pattern on the specimen, that was obtained using graphite powder.

For each specimen, with dimensions of approximately 8 mm^2, the grips were arranged at a distance of 4.7 mm. A maximum strain of 60% was applied in three cyclic loading and unloading ramps, at a velocity of 0.135 mm/s

Figure 9 This figure shows how to make a specimen for a uniaxial aorta test. The implementation of the test is supported by the use of a support system for a better arrangement of the fabric in the appropriate grips.

Figure 10 In this figure it is possible to identify the preparation of the specimens of the various monoaxial and biaxial tests and in particular an extraction of a valve with the relative tendon cords is shown. Finally, the arrangement of the specimen inside the biaxial test machine.

4.1.3 Processing of the results

The initial plan was to carry out an anatomy-morphological analysis of the cardiovascular tissue. Through the anatomical sections and the mechanical tests, it would have been possible to obtain a mechanical characterisation of the tissue, providing data to be fed in the constitutive laws used in the numerical models.

Due to the global health emergency, caused by the spreading of SARS-COVID 19, access to the laboratories at UCL was suddenly suspended, and this work package interrupted. Still, the direct anatomical analysis carried out on the left atrial appendage, allowed to obtain a more in-depth knowledge and understanding of the object of the study. By way of example, typical uniaxial results on five aorta specimens are represented in Figure 12.

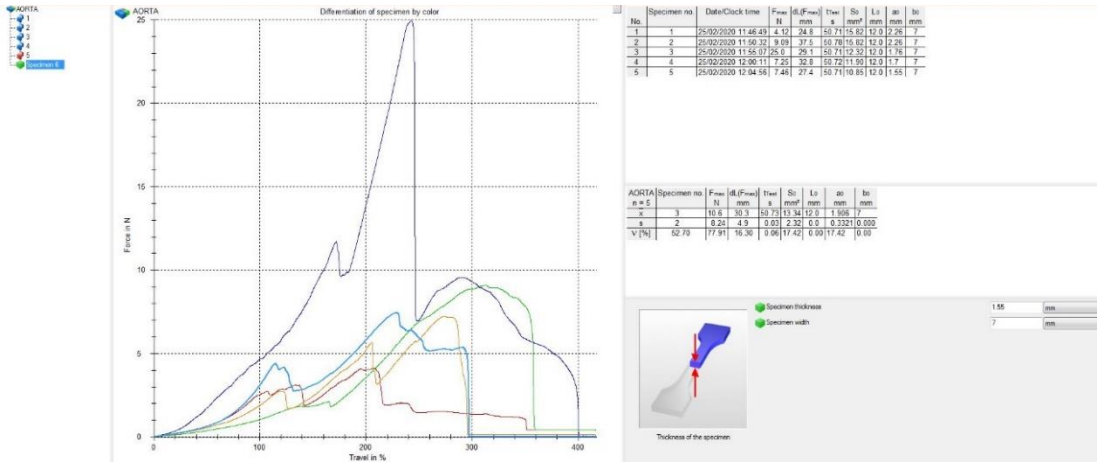

Figure 11 This figure shows the uniaxial test output. In particular, here it is possible to carry out an evaluation of the results relating to specimens taken from aortic tissue.

The same anatomical components were used to obtain the specimens used in the biaxial mechanical tests (see Figure 12, Figure 13, Figure 14).

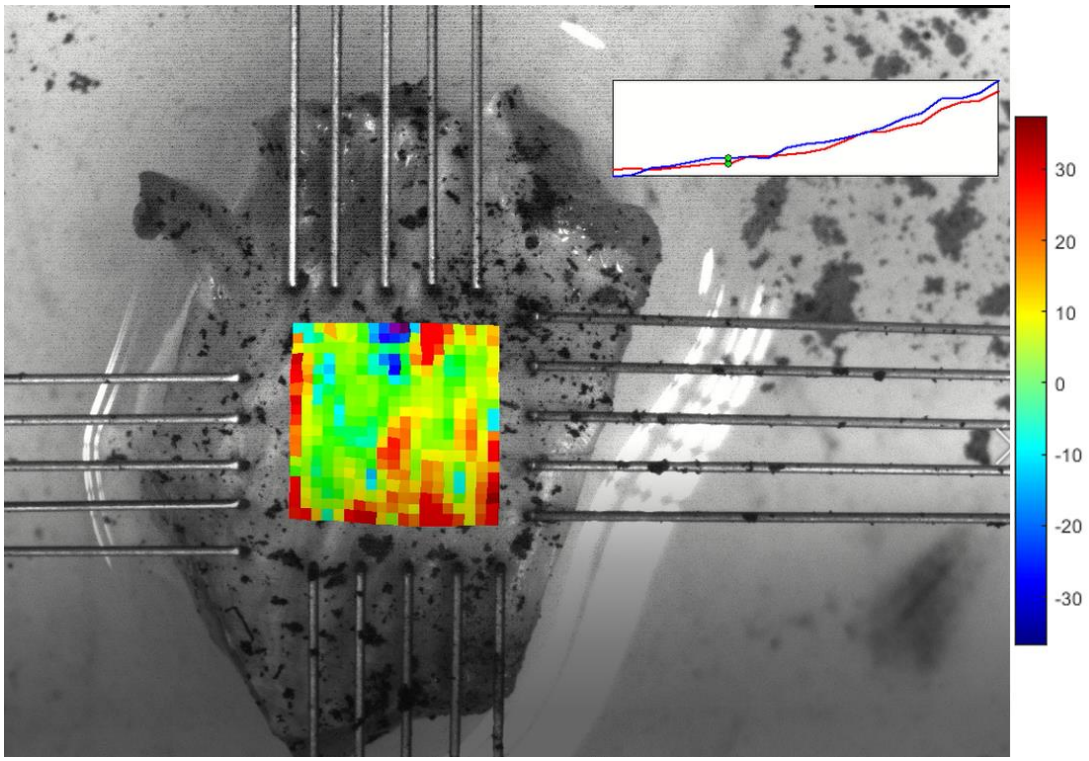

Figure 12 This figure shows one of the initial moments recorded during the biaxial test (DIC).

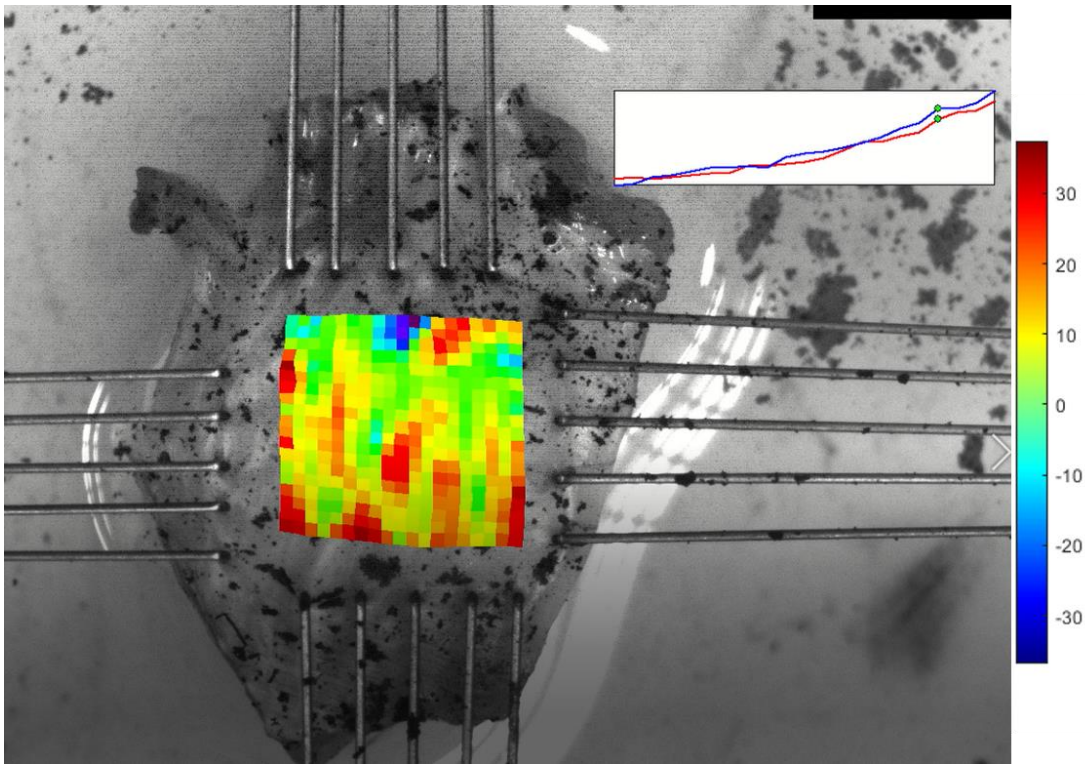

Figure 13 In this figure, one of the instants following the one shown in the previous figure can be appreciated. This is a tissue specimen taken from an atrial appendage.

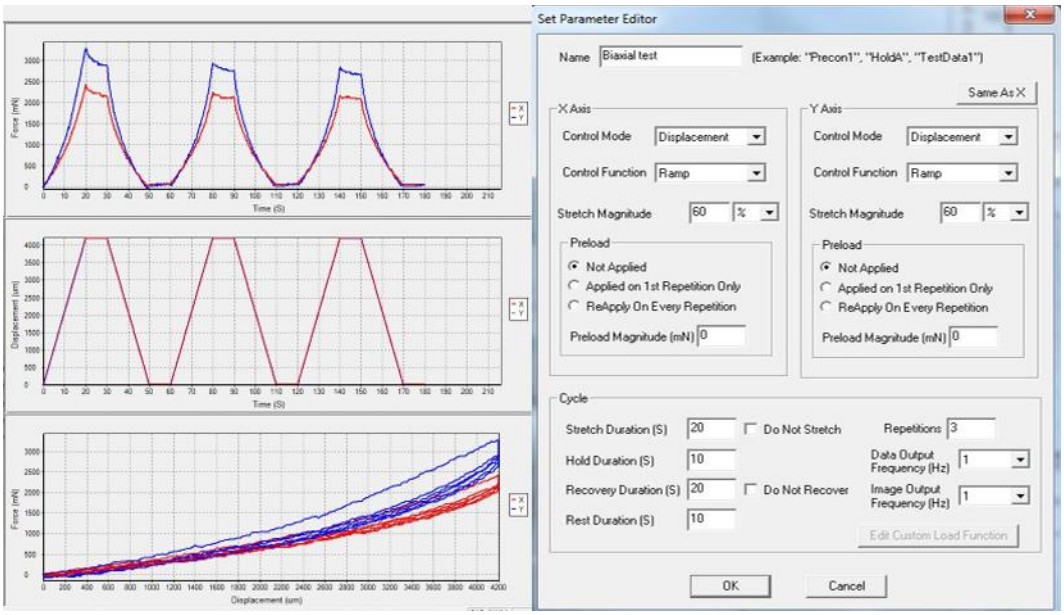

Figure 14 This figure shows the setup developed for performing the biaxial test with the DIC technique (Digital imagine correlation).

In addition, a protocol for processing and evaluating the results was drafted with the aid of the MATLAB calculation code. The map distributions of the computed strains at the maximum deformation, in the *x* and *y* directions, are displayed in Figure 15 and in Figure 16, respectively.

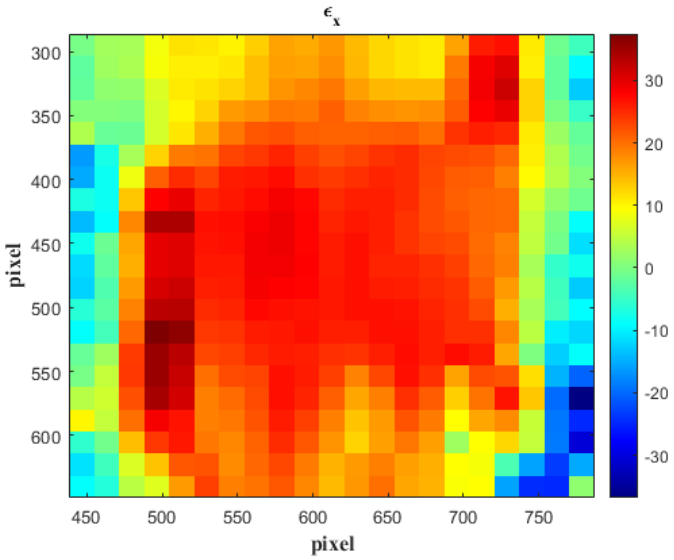

Figure 15 Digital imagine correlation (DIC) result x strain by a colour map.

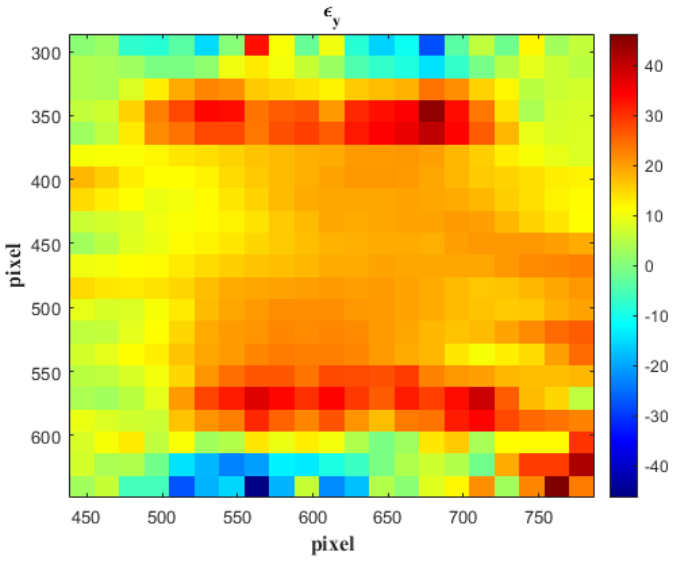

Figure 16 Digital imagine correlation (DIC) result y strain by a colour map.

4.2 Preliminary study

The first studies carried out in this research project were based on fluid dynamics simulations. Geometric models representative of a large sample of patients were generated, here identified as idealised models (see Figure 17). The geometries were elaborated to represent both a physiological condition and a pathological condition related to atrial fibrillation. In this version, the chronic effect of the pathological condition in volumetric terms was also considered, therefore modelling remodelling.

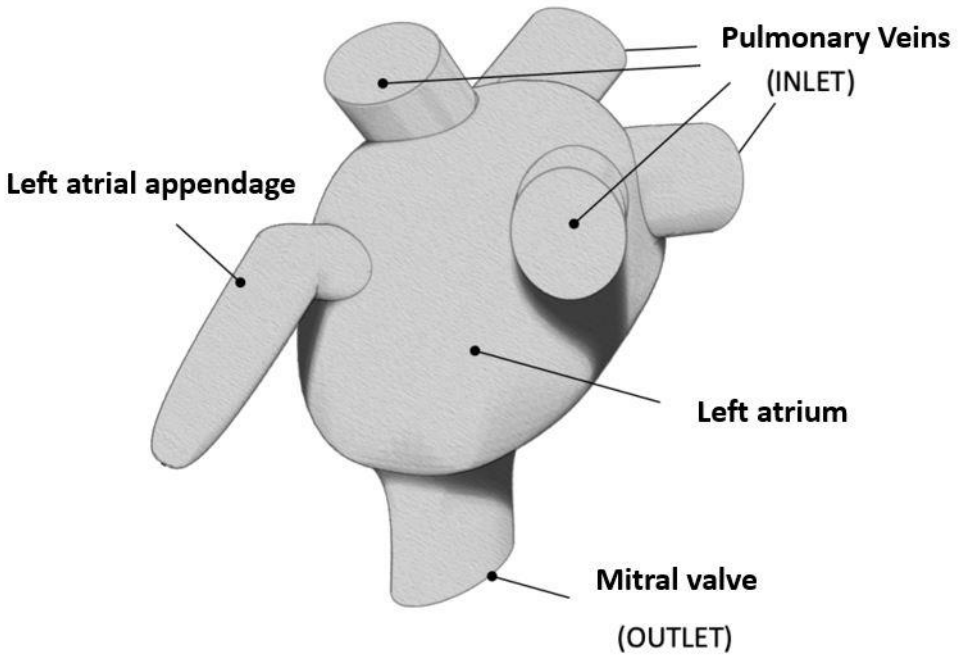

Figure 17 Geometric model of the analysed fluid domain. Geometry includes left atrium, left atrial appendage, pulmonary veins, and mitral valve schematic.

4.2.1 Idealised Model

Although numerous studies have been conducted on the subject, the hemodynamic processes that regulate the phenomenon of atrial fibrillation are still poorly understood. A main limitation is due to the fact that computational models developed to date do not include the movement and volume variation of the left atrium associated with the cardiac cycle. Consequently, fluid dynamics studies do not consider the contribution of heart muscle functioning, both in physiological and pathological conditions.

The integration of atrial contraction in existing models could lead to a better understanding of the biological phenomenon that leads to thrombus formation.

This initial numerical study, therefore, developed a computational model that includes the movement of the walls and the change in volume of the left atrial appendage, as a consequence of the atrial contraction during the cardiac cycle.

The movement was produced by imposing displacement functions on the nodes of the discretisation in the region of the left atrial appendage in a model that was defined as a deformable model. This computational model was compared with another model, based on the same geometry, which modelled the left atrial chamber and appendage as rigid wall regions, focusing the study on the estimation of some physical parameters inherent in cardio-circulatory fluid dynamics, such as shear strain rates (SSR) on selected sections of the left atrial appendage and at particular instants of the cardiac cycle.

The first comparison between the two models passes through the construction of the geometry used in the healthy and pathological conditions, identified in the numerical model as deformable and rigid. The difference between the two models is the movement of the left atrial appendage. In both cases, the same ideal geometric model was used and, in correspondence of the pulmonary veins and the mitral valve, pressure curves characteristic of the cardiac cycle were imposed (Bosi et al. 2018).

For the deformable model, displacement functions were defined for the nodes in the mesh of the left atrial appendage, obtained by integrating velocity curves of the walls of the same left appendage, measured with ultrasound, Doppler tissue imaging DTI (Farese et al. 2019).

For the mesh of the geometric model, tetrahedral elements were used for the internal volume and 5 layers of prisms for the walls, for a total of 2888185 elements, according to the method proposed by (Bosi et al. 2018).

The software used in the preliminary studies were:

- ✓ Rhinoceros for the realization of the CAD model;
- ✓ R-Studio for the calculation of pressure and displacement curves;
- ✓ ANSYS ICEM for the mesh;
- ✓ ANSYS CFX (Ansys, Inc.) for fluid dynamics analysis;

The first step was to build an ideal geometric model, which does not represent a specific case, but which includes the main features of the left atrium and the left atrial appendage. In order to obtain results that are as generalisable as possible, the geometric model of the left atrium was based on a parameterised map of the atrium, averaged over 150 subjects (Varela et al. 2017). The geometry and position of the other anatomical components, such as the pulmonary vein accesses and the mitral valve, were derived from the study by Schwartzman et al. (2003) and appropriately normalised. Finally, the ultrasound measurements obtained by Lacomis et al. (2007a) were used as a reference to generate the curves for the construction of the geometric model of the left atrial appendage (see Figure 18). The ultrasound measurements for the proximal part of the left atrial appendage, i.e., the one adjacent to the atrial wall, and for the distal part measurements, reported in Bosi et al. (2018) were used to generate the construction curves of the two parts of left atrial appendage and the angle that joins them.

4.2.2 Numerical simulations CFD Population Specific

First of all, it was necessary to verify the contribution of the alterations produced by atrial fibrillation. The design of the analysed conditions was developed on the basis of the effects due to contractility and morphology.

Ultimately, four scenarios were simulated; three of these are based on a morphology representative of health conditions, in which the wall (i) is stiff, (ii) replicates the typical contractions of SR, and (iii) replicates the contractions typical of atrial fibrillation; and one based on a pathologically enlarged morphology, subject to parietal contractions typical of atrial fibrillation.

The four scenarios were designed with the aim of analysing the effect on hemodynamic of two main factors associated with atrial fibrillation, the first concerns the impairment of contraction while the second concerns the progressive enlargement of the left atrium and left atrial appendage.

A method used to calibrate the contraction of the models was developed using instant flow control across the mitral valve (by adjusting the pressure difference between the inlet of the pulmonary veins and the mitral outlet), the atrium wall velocity and wall movement of the appendage.

The enlargement of the chambers was considered by analysing two idealised morphologies of both the atrium and the appendage, whose volumes were set to reproduce the average dimensions of the left atrium and left atrial appendage reported for healthy cases, therefore with sinus rhythm and for pathological cases therefore in atrial fibrillation (see Figure 18).

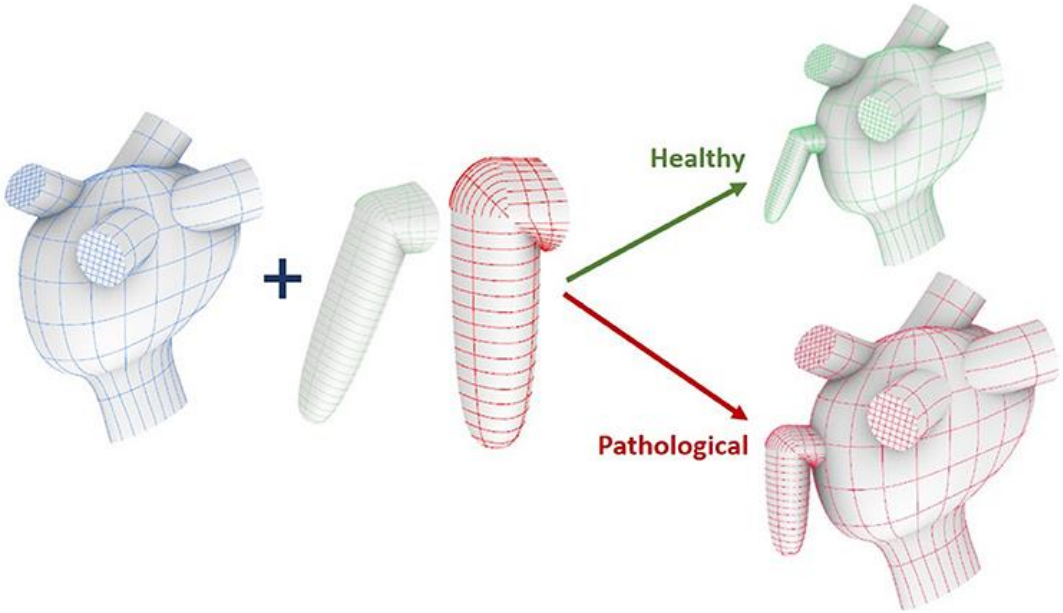

Figure 18 Construction workflow of the atrium model. From top to bottom: main ideal shape, pulmonary veins and mitral valve.

The results obtained continue to be compared in terms of Shear Strain Rate (SSR) but also with vortex structures, parameters related to thrombogenic potential (Kim et al., 2012; Otani et al., 2016). In this work, four cardiac cycles were simulated in four different scenarios.

A heart rate of 70 beats/min was assumed, and commercial software **ANSYS CFX** 19.2 was used. This work was conducted within the bioengineering laboratory of the Ri.MED foundation whose synthesis was collected in the scientific work of Vella et al., 2021b) and was divided into various phases which can be summarized below:

a) Design of two idealized models: left atrium and left atrial appendage. The models describe the mean healthy and pathological morphologies respectively;

b) Definition of boundary conditions: inlet (to the pulmonary veins) and outlet (at the orifice of the mitral valve) pressures in healthy and pathological conditions;

c) Definition of the contraction functions for the left atrial and left atrial appendage walls, in healthy and pathological conditions (in particular, the Wall Velocity conditions were applied to the left atrial, while for the and left atrial appendage portion a higher degree of accuracy was preferred, imposing Wall Motion);

d) Setting of four scenarios (see Table 2)

- **Rigid**: represents the healthy morphology in the absence of contraction;
- **Healthy**: represents healthy morphology with sinus rhythm contraction pattern;
- **Hybrid:** represents healthy morphology with atrial fibrillation contraction pattern;
- **Pathological:** represents the pathological morphology with AF contraction pattern;

Table 2 Scenarios. H, healthy; P, pathological, AWM, Appendage Wall Motion; AWV, Atrium Wall Velocity.

	Geometry	**Pressure**	**AWM**	**AWV**
Rigid	H	H	-	-
Healthy	H	H	H	H
Hybrid	H	P	P	P
Pathological	P	P	P	P

4.2.3 Model features:

The rigid model:

This model is based on the similarities modeled already in other numerical studies such as that of bosi et al Vella et al., 2021b) where the flow is structured through the application of a physiological pressure difference between the inlet pulmonary veins and the outgoing mitral valve.

The healthy model:

In this model, the concept of physiological contraction is introduced both in the atrium and in the appendage. The aim was to introduce an operating condition that more correctly describes the operating conditions of the atrium and appendage.

The hybrid model:

Also, in this case, the pressure differences are applied, which however describe the condition of atrial fibrillation, also introducing the absence of contractility.

The pathological model:

This model introduces the morphological alterations that are typical of chronic atrial fibrillation such as volumetric remodeling

The idealized geometries

In this study, idealized geometries were developed, based on representative measures of healthy adult population under sinus rhythm conditions. The geometries obtained are two and are related to the measurements carried out in the study by (Lacomis et al., 2007a) and based on clinical measurements both in conditions of sinus rhythm and in atrial fibrillation. Each of the two chambers is built separately and subsequently assembled in a single structure using the Rhinoceros CAD software.

Another aspect is related to the structure of the mesh used where in this work it was constructed in such a way as to maintain the same density of elements in the various geometric models, being computational domains with different volumes.

Icem CFD was used for the mesh of the two parts. The network was composed of tetrahedral and prismatic elements with 5 layers of prismatic elements along the wall.

To maintain the same element density in the Pathological and Healthy models, whose computational domains have different volumes (see Figure 18), the final meshes contain a total of 4548050 and 2888185 elements respectively (Bosi et al., 2018).

4.2.4 Model of the atrium

The construction of the geometry used in the numerical simulations is composed of two main parts: atrium and left atrial appendage.

The atrium model includes three main sections: main chamber, pulmonary veins and mitral valve. To design the main chamber, an average volume was assumed obtained on the basis of the study of the population analyzed in the work of (Varela et al., 2017b). The standard form of the atrium was obtained through left atrium

geometry maps obtained from magnetic resonance images 144 patients with atrial fibrillation. The left atrium was defined from the mean of all measured atrium surfaces.

Clinical measurements of orifice diameters and relative distances by (Schwartzman et al., 2003) were to define the portions of access to the pulmonary veins.

To build the pulmonary veins, the ideal main atrial chamber was first sized based on the atrium mean size (x, y, z), derived from a population study of patients with atrial fibrillation (Schwartzman et al., 2003)

Veins were created and inserted into the atrium, according to clinical measurements of the same population (Schwartzman et al., 2003).

The mitral valve was designed as a tubular shape attached to the base of the atrium, extending perpendicular to the surface and reducing the diameter with a funnel shape (Bloodworth et al., 2017; Lim et al., 2005).

The atrial geometry obtained as described above, based on the data of patients with atrial fibrillation, was resized in terms of volume in order to obtain the different health conditions.

However, it should be noted that although it is clear from the literature that atrial fibrillation causes volumetric remodeling, there is no evidence that significant shape changes occur (Mori et al., 2011; Nattel & Harada, 2014; Sanfilippo et al., 1990).

The aim was to obtain a generalized shape of the left atrium, which was able to represent a standard and ideal measure.

The references used are obtained from the clinical measurements of the groups of healthy and pathological subjects (Lacomis et al., 2007a). These two volume values (85.5 and 117.5 mL, respectively) were calculated as the average between the maximum and minimum atrial volumes measured during the cardiac cycle.

The geometric model includes three portions: left atrium; pulmonary veins and mitral valve (see Figure 19).

The model is intended to represent the shape of a standard atrium. The volume of the model can be modified based on clinical measures to represent a specific case or a specific population.

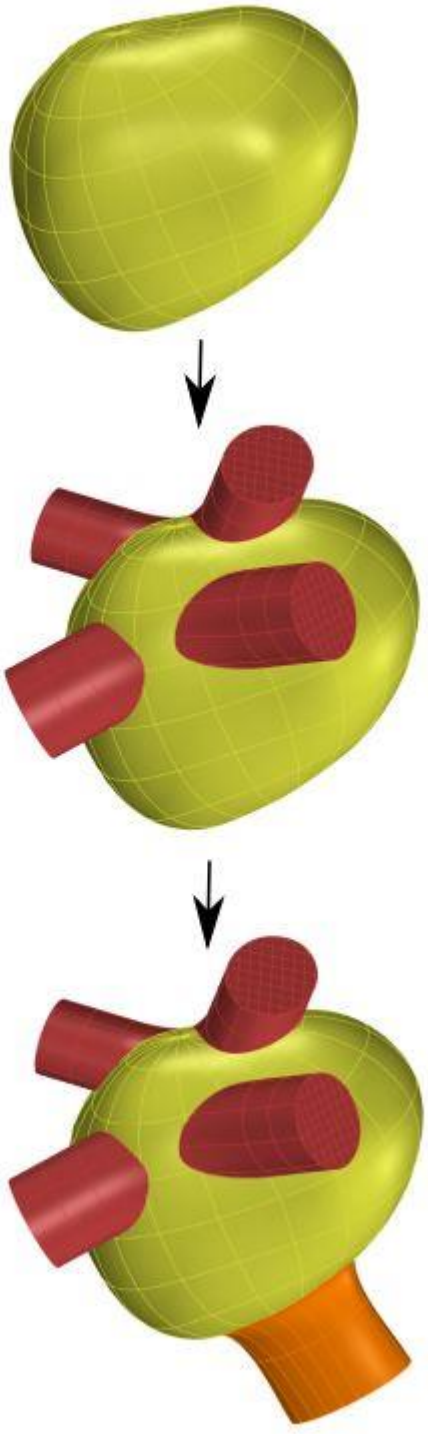

Figure 19 Construction workflow of the atrium model. From top to bottom: main ideal shape, pulmonary

The construction of the appendage

Being characterized by a morphological variability from patient to patient, obtaining a classification based on objective criteria of the left atrial appendage is very difficult. Therefore, it was appropriate to rely on the classical morphological classification: chicken wing, cactus, windsock and cauliflower (Korhonen et al., 2015; Nedios et al., 2014). The most common morphology is the chicken wing and for this reason it was also the easiest to recreate due to the clinical measurements available.

The geometry of the appendage includes two portions: the proximal region and the distal region. The first is adjacent to the atrium and consists of a tubular shape, which starts from the atrial orifice and extends to the distal part at a specific angle.

The distal region consists of a tubular ellipsoidal shape, which starts from the proximal part and ends with a tip (Budge et al., 2008).

The model is based on seven parameters:

- maximum orifice diameter (Dp; max),
- minimum orifice diameter (Dp; min)
- length of the proximal part (Lp);
- maximum orifice diameter (Dd; max),
- minimum orifice diameter (Dd; min)
- the length of the distal part (Ld)
- the connection angle (α).

From a geometric point of view, the appendage was constructed from two portions, a proximal and a distal region.

The steps followed for the construction of the appendages are described in Figure 20 and in Table 3. The appendages are connected to the left atrium and at a distance from the mitral valve twice the distance from the upper left pulmonary vein and orienting the tip towards the base, as described in (Li et al., 2015)

Table 3 Parameters defining the appendage idealized models. LAAd, appendage distal part; LAAp appendage proximal part; MV, mitral valve;

	Healthy		**Pathological**	
	LAAp	***LAAd***	***LAAp***	***LAAd***
Diameter max [mm]	19	13	22	18
Diameter min [mm]	10	10	13	14
Length [mm]	5	31	6	34
Angle α	144°		92°	

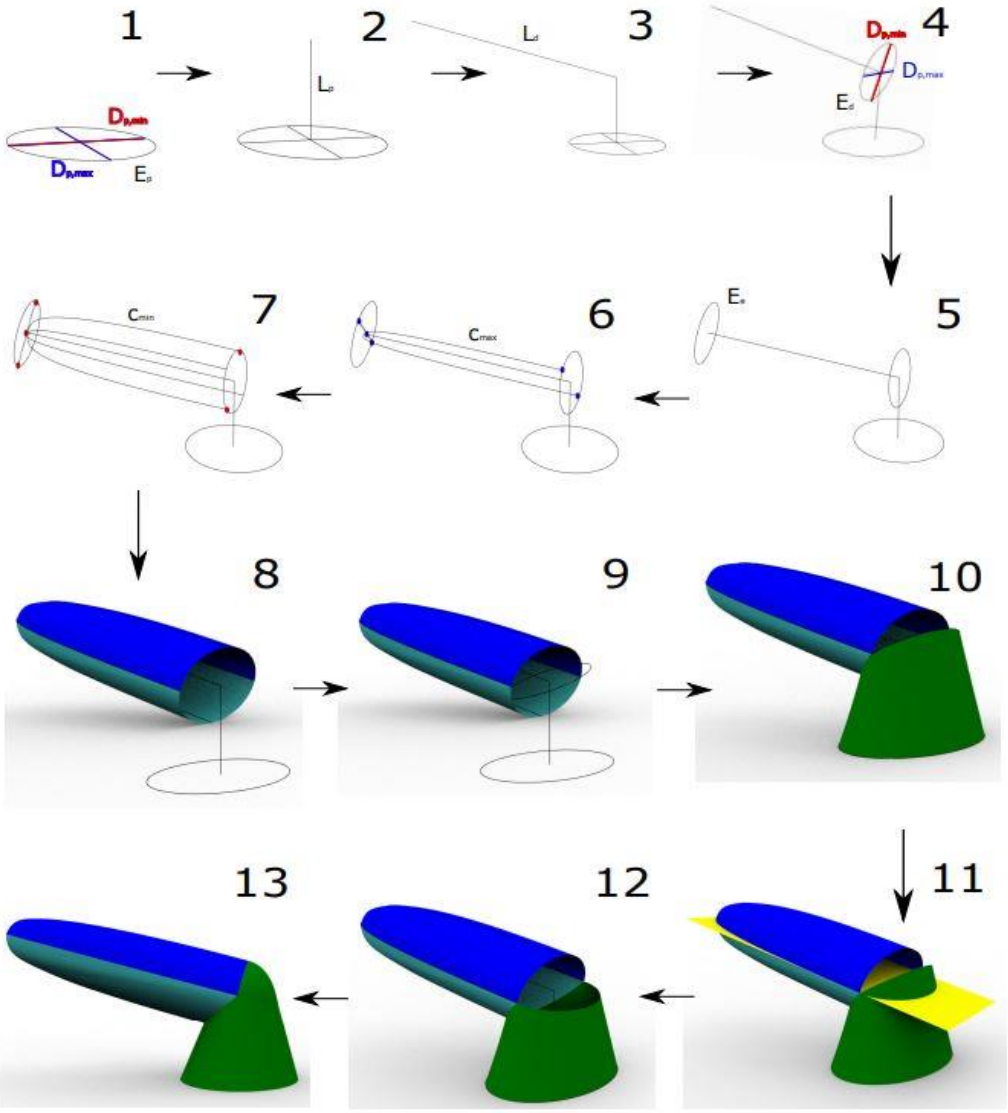

Figure 20 Construction workflow of the appendage model.

4.2.5 *Movement of the appendage wall*

The description of the left atrial appendage made previously confirms the idealized nature of the geometry and the division into two main regions: one proximal and one distal. The distal part is in turn divided into two components: the medial wall and the lateral wall. The medial wall is located just in front of the atrial chamber while the lateral wall is further away from the left atrium Figure 21.

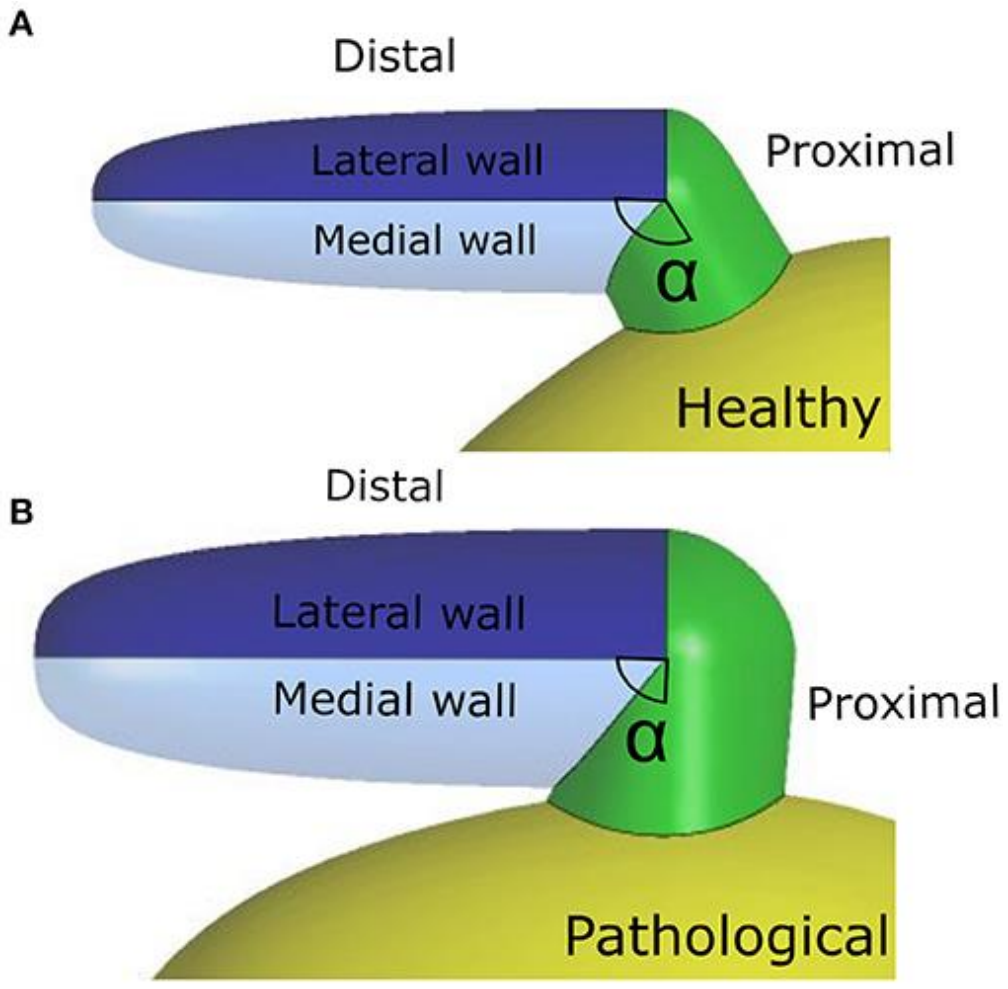

Figure 21 (A) Healthy geometry; (B) Pathological geometry.

In the designed numerical model, the contraction of the appendage was applied only to the distal part. The data used are the result of experimental measurements found in the literature (Farese et al., 2019). Contraction was defined by imposing two different displacement functions for the lateral and medial wall, FL (t) and FM (t), respectively.

These functions are the result of mathematical transformations based on two main displacement curves, sL (t) and sM (t), obtained by integrating the velocities of the two appendage walls over time. The magnitudes of the function have been varied linearly from the canter line of each wall section to the line where they join, in order to have a smooth transition in the motion imposed in the two sections.

Going into detail, regarding the wall velocities of a patient representative of a sinus rhythm condition, the relative values were extracted from the Tissue Doppler echocardiographic data reported in the literature(Farese et al., 2019).

The amplitudes of the curve and the inflection points were then adjusted to fit the mean values of the healthy and pathological populations (Figure 22, left panel). Interestingly, the direction of lateral and medial wall movement during the cardiac cycle is reset in the Pathological model, compared to Healthy Conditions (Figure 22, right panel) (Farese et al., 2019). This is due to the fact that in healthy conditions the left atrial appendage undergoes an active contraction, while during atrial fibrillation it expands more passively, under the effect of atrial pressure.

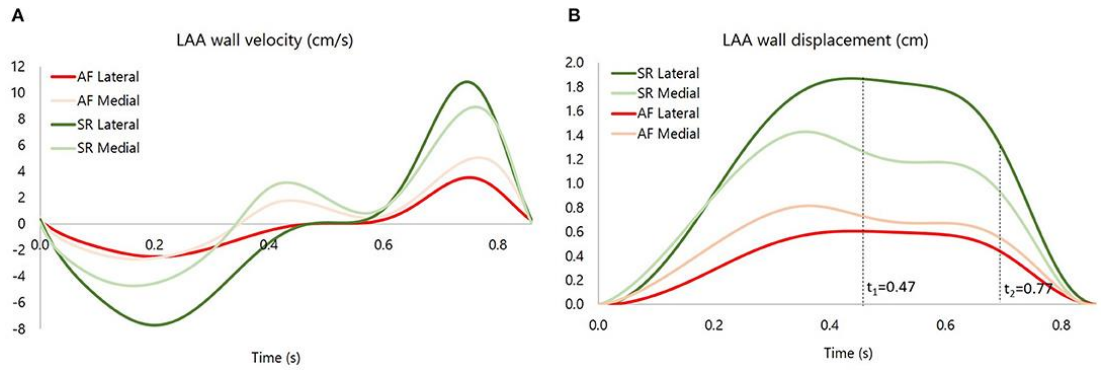

Figure 22 (A) medial and lateral wall velocity of the appendage for the Pathological (P) case and the Healthy (H) case. (B) medial and lateral wall displacement, respectively, sM and sL, for the Pathological (P) case and the Healthy (H) case.

4.2.6 Atrium wall velocity

The atrial contraction had to be considered without substantially increasing the complexity of the model. The velocity amplitude was set to reproduce the reported volume changes for patients with sinus rhythm and atrial fibrillation (Lacomis et al., 2007b), normalizing with respect to the wall area and differentiating with respect to time.

Movement was modelled by applying normal fluid velocity to the atrial wall.

Three volume values were used to define the left atrium volume change curve, corresponding to three phases of the cardiac cycle:

- Maximum volume (V_{max}), before the opening of the mitral valve;
- Precontraction volume (V_{preA}), before the A wave, corresponding to the atrial contraction;
- Minimum volume (V_{min}), at the end of the atrial contraction.

Using these values, a volume-time function was calculated as the sum of the sine curves for each case (see Figure 23 in the top panel).

The velocity of the atrium wall was first derived from the volume-time function normalizing with respect to the atrium surface, then derived with respect to time (see Figure 23 in the lower panel).

Note that in the Pathological and Hybrid models the amplitude of the curve is reduced during mitral valve closure and atrial contraction.

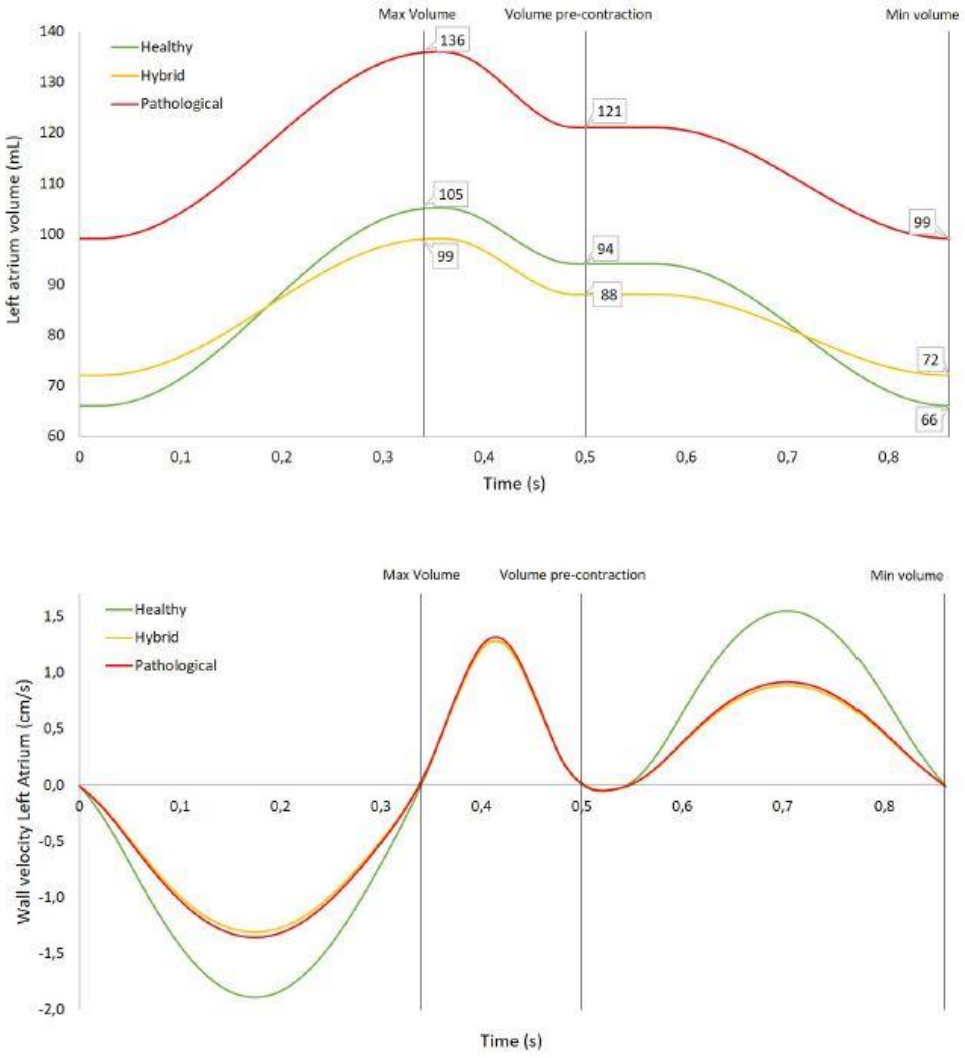

Figure 23 Top panel: volume variation of the left atrium during a cardiac cycle; k Top panel: volume variation of the left atrium during a cardiac cycle; each curve is based on three main values: Maximum Volume, Pre-contraction Volume and Minimum Volume. Bottom panel: velocity of atrium wall during a cardiac cycle, corresponding to the derivative of the volume curve in the top panel.

4.2.7 Pressure

The pressure curves were obtained as result of four CFD simulations (one for each studied case), with different flowrates applied to the mitral valve outlet.

To simulate blood flow in the atrium, pressure was imposed on both, the inlet of the pulmonary veins and the outlet of the mitral valve. For all cases, the pressure in the pulmonary veins was set to a constant zero value. An evenly distributed pressure was imposed at the outlet of the mitral valve, to produce a flow rate representative of the sinus and atrial fibrillation cases, as shown in Figure 24.

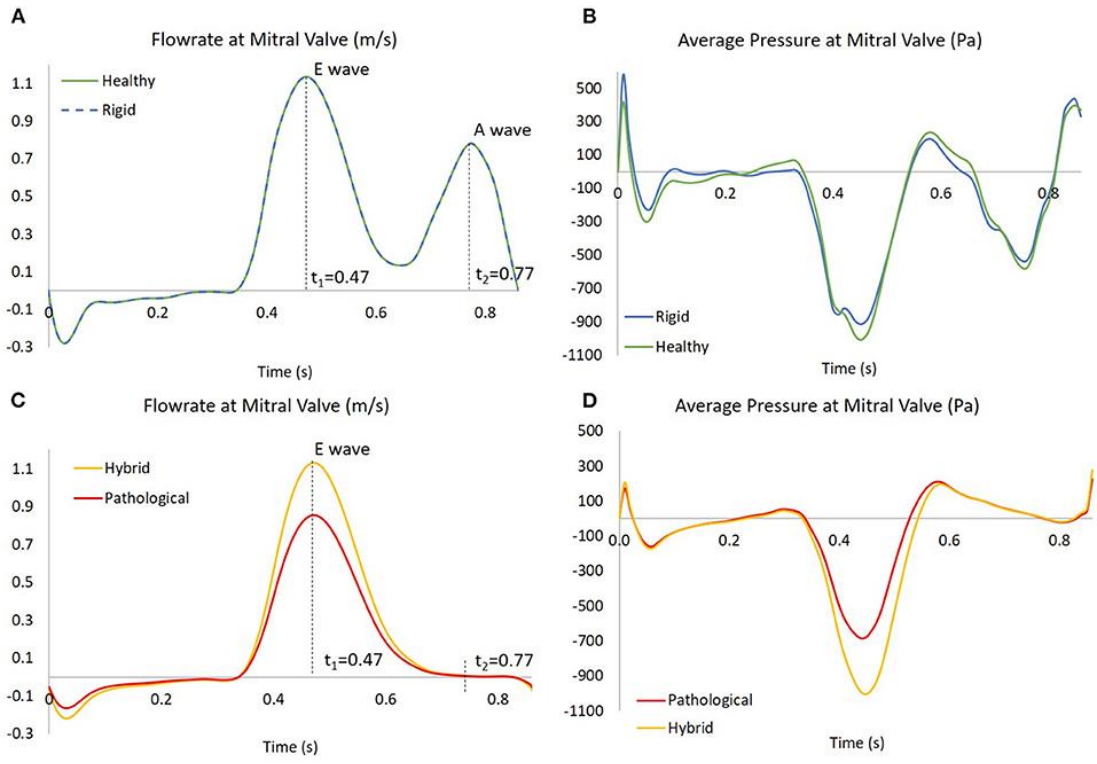

Figure 24 In (A, C), the flowrates at mitral valve for the four scenarios; the instants t_1 = 0.47 s and t_2 = 0.77 s are showed, corresponding to E wave and A wave, respectively. In (B, D), the pressures at mitral valve for the four scenarios, obtained as results of four simulations based on the flowrate in the left panel.

4.2.8 Analysis of the results on preliminary study

The parameters analysed in the four models that helped to understand hemodynamic phenomena also involve vorticity as well as SSR.

SSR is a measure of flow velocity related to the size of the space traversed, and is related to the rheological response as well as to the thrombogenicity of the blood(Cadroy et al., 1989; Casa & Ku, 2017; Ducci et al., 2016a; Vella et al., 2021a).

Speed deserves a separate observation. It must be considered that, although velocity is the most used parameter to evaluate hemodynamic (Dedè et al., 2021; Jia et al., 2019; Masci et al., 2019), the SSR better describes the flow characteristics in a context in which global velocities are different applied to the study chamber, due to the alternative left atrial appendage motion modes analysed in this study.

The Q criterion was used to calculate the vortex structures. The Q criterion is a measure based on the second invariant of the velocity gradient tensor, widely used to evaluate stagnation regions and blood wash, which are directly related to the clot formation (Chnafa et al., 2014; Ducci et al., 2016a; Masci et al., 2019; Otani et al., 2016; Seo et al., 2014; Vedula et al., 2015).

Specifically, a Q function is calculated as:

$$Q=12(\Omega 2-S2)$$

Ω and S are the antisymmetric and symmetric components of the velocity gradient tensor, respectively.

In the following description a local Cartesian system will be used as reference, with the origin positioned at the intersection between the axis of the distal and proximal portion of the left atrial appendage; the x axis in the plane separating the lateral and medial walls; the y axis directed along the normal to this plane, directed towards the side walls; and the z-axis aligned with the axis of the distal portion and directed towards the tip of the left atrial appendage (see Figure 25, bottom panel).

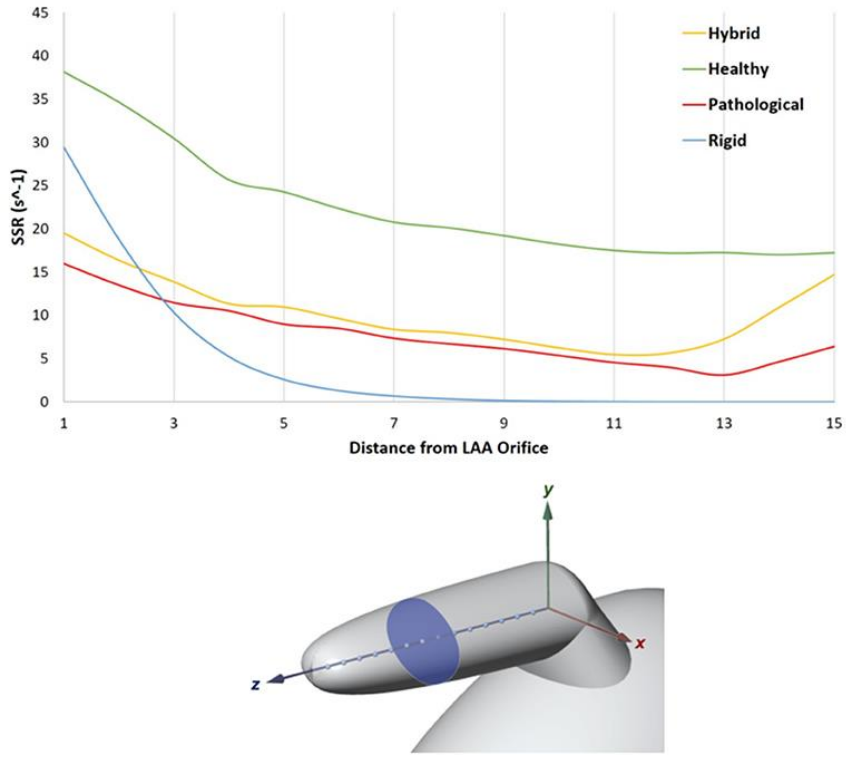

Figure 25 In the top panel SSR along the left atrial appendage axis, from the orifice to the tip. LAA axis at the fourth SSR peak of the cardiac cycle (t = 3.36 s, Rigid case).

An analysis of the SSR along the appendage axis was performed at the peak flow of the fourth cardiac cycle, (t = 3.36 s in the analysis). The z-axis of the appendage of the four models was divided into N = 15 equidistant points (Figure 25, lower panel) and the average value SSR was calculated on the cross sections passing through each of these points (one of the cross sections is highlighted in Figure 25, bottom panel). The diagram in Figure 25 (top panel) represents the SSR values obtained for all cases (the maximum and the average values for the 15 sections are reported in Table 4 last column).

Table 4 SSR maximum values (average values into brackets) for the four scenarios evaluated in sagittal (S) section planes (Superior, Central, and Inferior) and Transversal planes.

	Superior S [s^{-1}]	**Central S [s^{-1}]**	**Inferior S [s^{-1}]**	**Transversal [s^{-1}]**
Rigid	5.09 (1.32)	0.23 (0.07)	0.02 (0.005)	29.38 (4.59)
Healthy	35.49 (18.11)	22.53 (11.87)	17.84 (18.56)	38.14 (22.64)
Hybrid	16.34 (8.24)	9.58 (5.29)	6.49 (4.41)	19.49 (10.35)
Pathological	11.23 (5.85)	6.79 (3.61)	4.40 (2.74)	15.98 (7.81)

In the simulation with healthy geometry and without appendage contraction (blue line in figure), the mean cross-sectional SSR rapidly decreases to zero from the orifice to the tip of the left atrial appendage, reducing by more than one order of magnitude in the proximal first third of the 'axis. It should be noted that, under real conditions, sustained SSR values below 10 s^{-1} would lead to a substantial increase in blood viscosity (Chien, 1970; Ducci et al., 2016b). This non-Newtonian behaviour, neglected in this study, would further contribute to generating stagnation of blood in the appendage. This condition, which typically promotes clot formation, is prevented in the Healthy model, where left atrial appendage (green line) motion is applied. In this case, the results indicate a much more favourable scenario, with mean cross-sectional SSR values maintained well above 10 s^{-1} to the distal tip of the appendage. This highlights the crucial importance of including wall movement in the simulation of the phenomenon. In the pathological case (red line in the figure), due to the irregular and reduced volume contraction, the SSR values in most of the distal region are less than 10 s^{-1}. In the Hybrid case (yellow line), characterized by healthy geometry and AF contraction, a trend very similar to that of the Pathological model is observed, except for the tip region, where the SSR values increase. This effect may be due to the different chamber sizes.The SSR was also evaluated on three sagittal sections (S) (see Figure 26, lower panel) of the distal part of the appendage, named Inferior, Central and Superior. These S-sections were selected near the tip, because this is the region where thrombus development is most likely to occur. Each section has the same length along z and normal aligned with the x direction.

The mean SSR calculated for all S sections during the fourth cardiac cycle is represented in Figure 26 top panel. For the Rigid model, the average SSR varies in the range $0 \div 5\ s^{-1}$ and always remains well below $10\ s^{-1}$.

In the healthy case, the SSR is between $0 \div 35\ s^{-1}$ and decreases below $10\ s^{-1}$ only for a short period of about 0.3 s, during ventricular diastole. In the hybrid model, it varies in the range $0 \div 16\ s^{-1}$ and is less than $10\ s^{-1}$ during most of the cardiac cycle. In the pathological case it varies in the interval $0 \div 11\ s^{-1}$ and remains below $10\ s^{-1}$ for almost the entire cycle. In all cases, the SSR values gradually decrease along the z-axis, moving towards the tip, from the upper section to the lower (see Figure 26 upper panel).

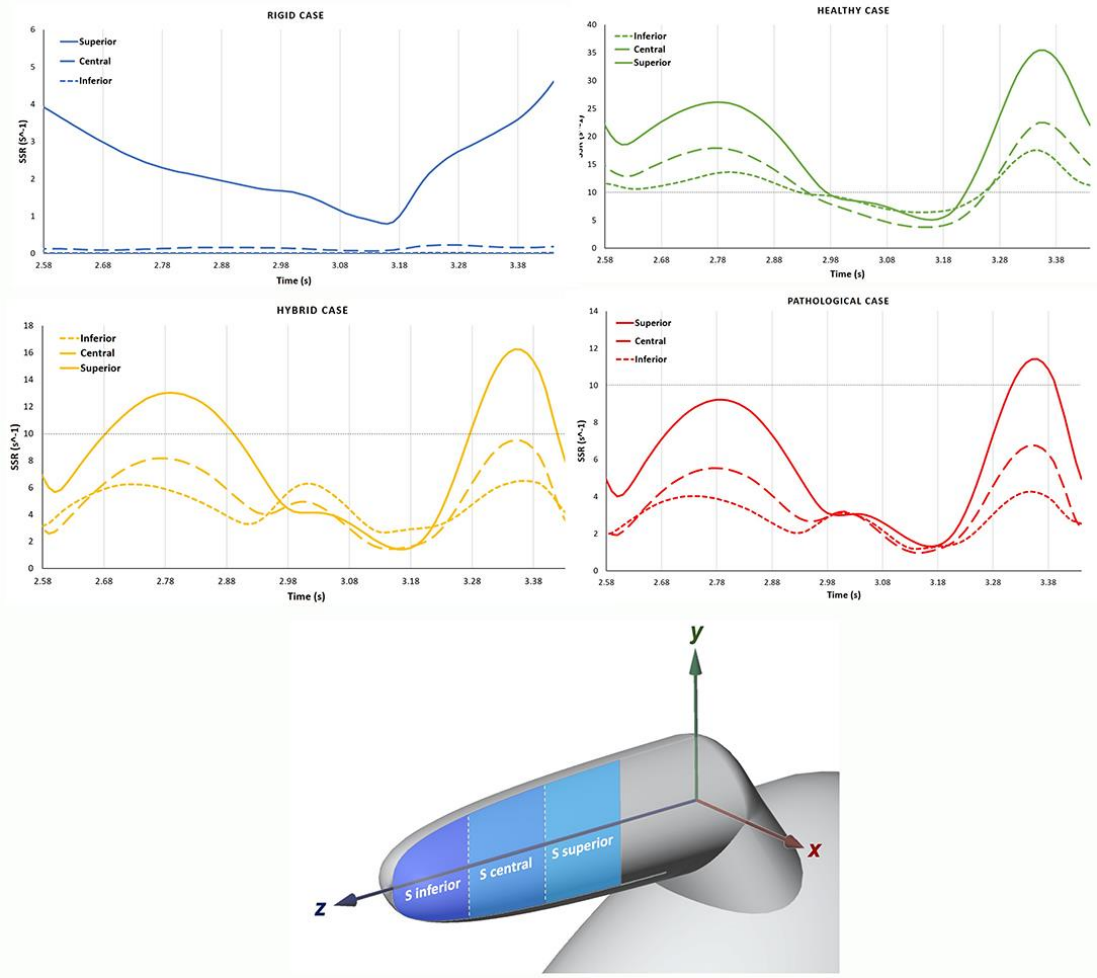

Figure 26 In the top panel, the SSR in the S sections are compared among the different cases, Rigid, Healthy, Pathological and Hybrid. In the bottom panel, the distal part with sagittal (S) sections: Inferior, Central and Superior.

Figure 27 compares the SSR trends for the four scenarios. The difference between the Healthy and Hybrid curves (green and yellow lines) indicates that the alteration in contractility due to atrial fibrillation contributes to a substantial decrease in SSR, which in our simulations is about 50%.

The pathological curve (red line), which also models the volume expansion associated with chronic atrial fibrillation, further exacerbates the reduction in SSR, producing an approximately 30% decrease compared to the hybrid model. In the Rigid model the SSR follows a different trend, maintaining a lower order of magnitude than in other cases. This indicates that the rigid chamber hypothesis, although widely used in the literature, is inadequate for studying the hemodynamic of left atrial appendage.

As previously mentioned, the identification of the central regions of the vortex is a useful indicator of the complex blood flow pattern that occurs in the appendage. Figure 28 represents, for each model, the instantaneous vortex structures within the left atrial appendage at the early ventricular diastolic peak E (corresponding to time t_1 = 0.47 s in Figure 24, left panel) and at peak A of atrial systole (corresponding to the time t_2 = 0.77 s in Figure 24, left panel) of the fourth cardiac cycle. The vortex structures are displayed as iso-boundaries of Q, selecting a suitable positive value. The colour of the outlines indicates the SSR calculated on the surface. For the Rigid model (first row in Figure 27), the vortices are confined to the proximal region of the left atrial appendage and do not expand along the distal direction of the appendage. At time t_2, eddies with higher SSR values are observed. When the left atrial appendage contraction is included for the healthy case (second row in Figure 27), the central regions of the vortex expand in the appendage, reaching its tip with an SSR value greater than 10 s^{-1}.

This indicates better blood washout. In particular, at instant t_1, left atrial appendage reaches its maximum volume (see dark green and light green curves in Figure 24, right panel) and a well-structured vortex is clearly visible.

At this time the SSR varies from 25 to 35 s^{-1} in the first distal region and shows a value of about 20 s^{-1} in the region of the tip of the appendage. At instant t_2 (left atrial contraction phase) blood flows from the appendage to the main atrial chamber; destroy the eddies observed previously and maintain high SSR values at the walls. These events indicate reduced blood stagnation and consequently a lower risk of clot formation. When atrial fibrillation contraction is imposed (in Hybrid and Pathological cases), the left atrial appendage volume change between t_1 and t_2 is reduced compared to the SR contraction (Healthy) model and the wall movement is reversed, with the medial (lower) left atrial appendage displacement of the greater wall than the lateral (upper) one (see light red and dark red lines in Figure 22, right panel). Furthermore, the A wave associated with atrial systole is not present (Bosi et al., 2018). For the Hybrid model (third row in the figure), although the vortex structures are similar to those obtained for the Healthy case, the SSR values are lower. In the Pathological model, at time t_1 (fourth row in Figure 27), the vortices in the appendage appear less pronounced (some structures with very low SSR values can be observed). At time t_2, the vortices still have SSR values of less than 10 s^{-1} in almost the entire volume of the appendage, implying a worse blood washout than in the healthy case. Of course, the results presented are based on atrial fibrillation clinical data on patients with more severe symptoms and idealized anatomies. A great deal of variability is expected, depending on the specific morphologies of the patient and the severity and degree of persistence of the condition.

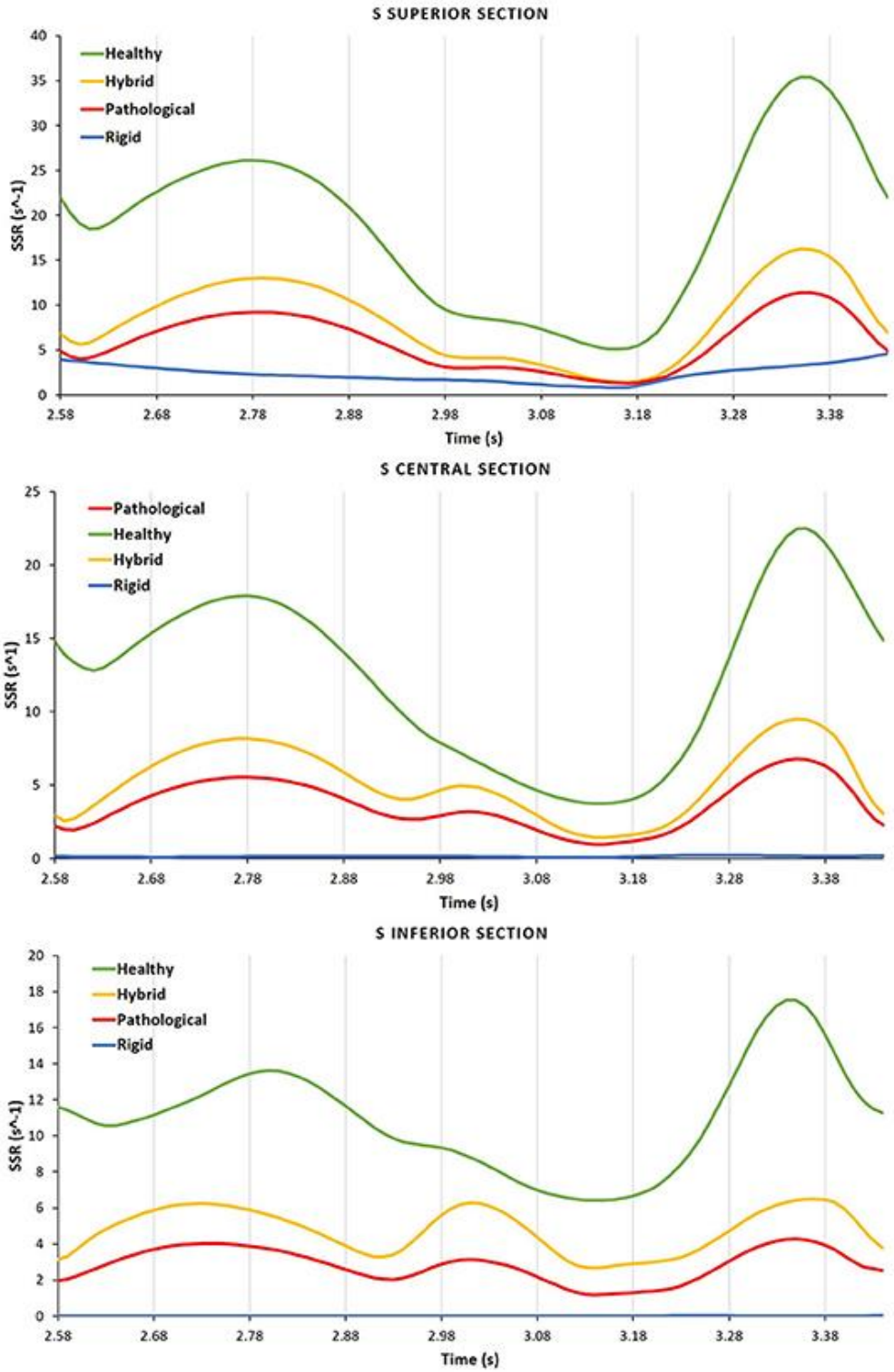

Figure 27 For each case the SSR is analysed in the different S sections, Inferior, Central, and Superior.

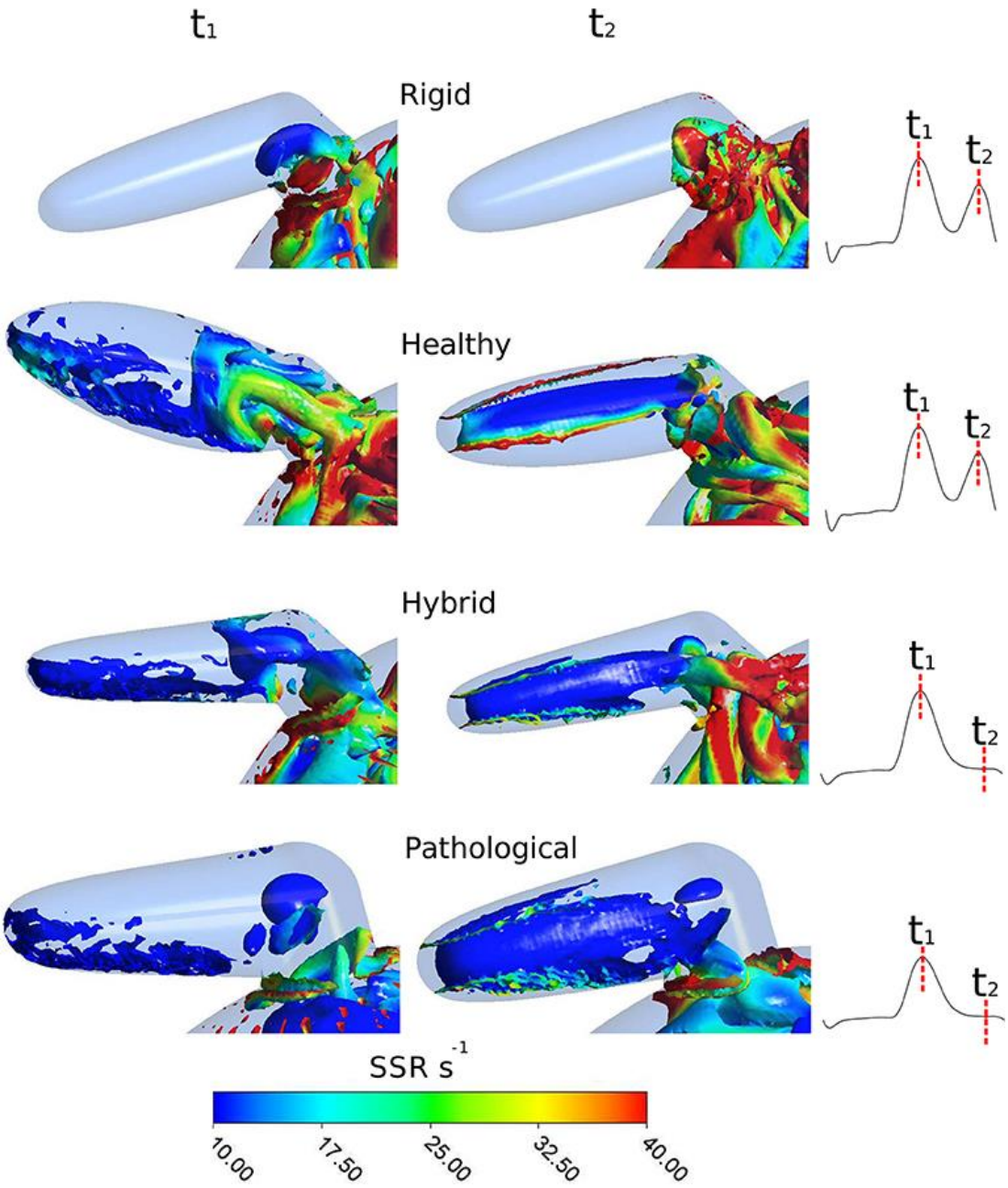

Figure 28 Instantaneous vortex structures within LAA coloured according to the SSR parameter, at E wave peak (corresponding to t_1) and at A wave peak (corresponding to t_2) of the fourth cardiac cycle. To visually appreciate the extent of the regions prone to thrombus formation, the SSR scale starts from 10 s^{-1}. First row: Rigid; second row: Healthy; third row: Hybrid; fourth row: Pathological.

These results further confirm the key role of appendage wall movement in producing safe or potentially thrombogenic hemodynamic conditions.

This suggests that characteristics that influence fluid dynamics in the left atrial appendage, such as contractility and shape, can improve the prediction of ischemic events. In fact, the most used criteria currently adopted for the stratification of patients with atrial fibrillation, such as $ChadS_2$ and CHA_2DS_2-VASc (Kimura et al., 2013; Lip et al., 2010), assign points based on existing diseases (e.g., diabetes and hypertension), age and sex, without considering any direct effects of haemodynamic. In this context, models such as the one presented in this work, based on the analysis of SSR and vorticity in different situations, could find relevant applications in clinical practice, providing more accurate predictions of the risk of ischemic events, especially for low CHA_2DS_2-VASc scores (for example, <2). This will offer a more effective tool to support the most adequate therapeutic selection. Currently, available therapies to minimize ischemic risk in patients with atrial fibrillation include oral anticoagulation, surgical exclusion of the left atrial appendage, and percutaneous occlusion devices of the left atrial appendage (Gan et al., 2014). However, none of the current solutions are free from potentially major complications; oral anticoagulation is associated with bleeding risk (Manzano-Fernández et al., 2008; Onalan et al., 2005), surgical exclusion of left atrial appendage exposes patients to invasive surgery (Ailawadi et al., 2011) and percutaneous devices can be associated with vascular complications, embolic events in the air and peri-device leaks (Lam et al., 2013).

Therefore, a more informed selection of the most suitable therapy for a specific patient with atrial fibrillation, supported by a better understanding of the phenomena responsible for ischemic complications, can play a key role in next generation clinical strategies.

New models need to be implemented to overcome these approximations. Despite these limitations, the study indicates that the modelling of morphological and contractile alterations typically caused by atrial fibrillation pathologies allows to replicate flow conditions that justify the high incidence of observed ischemic events. The altered contraction of the left atrial appendage was found to be the main cause of the worsening of the flow dynamics.

However, the enlargement of the heart chambers associated with chronic atrial fibrillation also appeared to have a relevant effect. This confirms that the left atrial appendage morphological class may play a role in determining thrombogenic haemodynamic conditions in pathological patients. However, the investigation of morphological effects cannot neglect the modelling of left atrial appendage contractility to provide an acceptable analysis of the flow establishing itself in the region. The proposed model lays the foundation for the development of new computational studies to better understand the pathology of atrial fibrillation and the factors that contribute to major complications.

Furthermore, the availability in the literature of clinical data from Tissue Doppler echocardiography, describing left atrial appendage movement associated with other pathologies, leads to new potential applications of the model.

In fact, thanks to its simplified geometry, the model presented is suitable for reproducing other conditions associated with reduced atrial contractility and increased risk of thromboembolic events, such as paroxysmal supraventricular tachycardia and atrial fibrosis (Kamel et al., 2013; Sohns & Marrouche, 2020).

4.2.9 Discussions of the first results

This work allowed to investigate the effect of changes in contractility and shape that occur in patients with atrial fibrillation on local hemodynamic that establishes in the left atrial appendage.

The analysis reveals the essential role of the contractility of the appendage wall on the factors that can favour the formation of thrombus and the consequent ischemic complications.

The model described is based on simplifying hypotheses, such as the laminar Newtonian description of blood and simplified anatomical geometry.

Although these limitations are present, this study indicates that the modelling of the morphological and contractile alterations typically caused by atrial fibrillation pathologies allow to replicate flow conditions that justify the high incidence of observed ischemic events.

This work highlights how the altered contraction of the left atrial appendage was found to be the main cause of the worsening of the flow dynamics.

Volume remodelling of the heart chambers associated with chronic atrial fibrillation appears to have an equally relevant effect.

This confirms that the morphological class of the left atrial appendage may play a role in determining the haemodynamic conditions that favour thrombus formation.

However, investigation of morphological effects cannot neglect modelling of left atrial appendage contractility to provide an acceptable flow analysis.

The proposed model lays the foundations for the development of new computational studies, for example on patient specific models that consider the effects that the structure has on the fluid. Such a model could help to better understand the pathology of atrial fibrillation and the factors that contribute to major complications.

4.3 Patient specific contractile FSI model

The second part of the research work consists in the development of a numerical model capable of implementing patient-specific geometries to be used in FSI simulations. The work is therefore carried out through computational tools such as the principles of segmentation of medical images and with structural, fluidic and fluid-structural interaction numerical approaches.

4.3.1 Model design

The first part of the development of the numerical model involved the anatomical and functional evaluations of the heart chambers under study. Although in the literature there are numerical studies conducted on the left atrial appendage involving patient-specific models and which focus the study on hemodynamic, one of the most significant aspects is the fact that the contractility of the appendage itself is often neglected (Masci et al., 2019; Vella et al., 2021a).

The preliminary study presented ion the previous section has instead considered the alterations of physiological properties and remodelling, through the introduction of geometries of idealised models capable of modulating parameters such as remodelling and contractility (Vella et al., 2021a).

The work described in this section introduces the numerical simulations of fluid structure interactions on patient-specific models, considering geometries representative of the morphological classification identified by the anatomists such as:

chicken wing, windsock, cactus, and cauliflower. The geometrical model considers the entire portion of the left atrial appendage and a part of the left atrium. This geometric development affects both the structural part and the part relating to the fluid.

First step is to introduce the concept of contractility and remodelling in numerical models and to evaluate the combined effect of stresses affecting the left atrial appendage (Benra et al., 2011; Hirschhorn et al., 2020b).

Second step is to perform a stratification of the thromboembolic risk in relation to the different morphologies and based on the evaluation of the volumetric Shear Strain Rate (SSR), both in conditions of sinus rhythm and in conditions of atrial fibrillation. The models were built starting from the scans used in the work of (Bosi et al., 2018)(see Figure 29), and divided into two geometric environments: structural part and fluid part (see Figure 30).

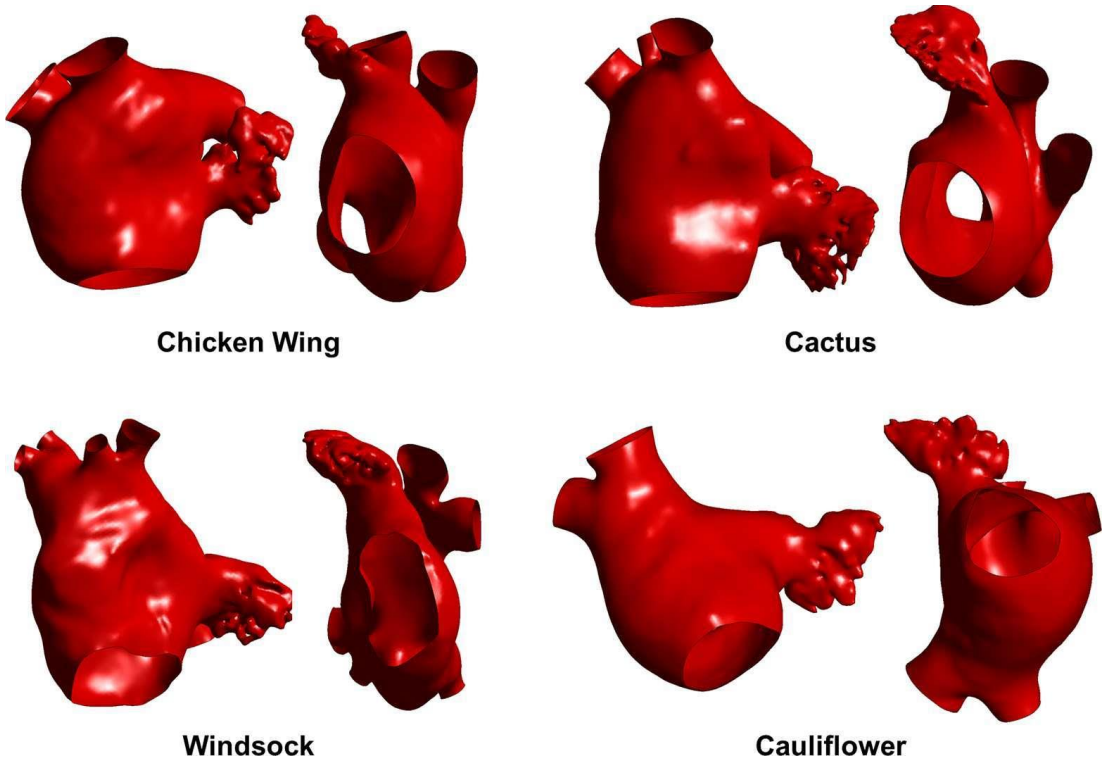

Figure 29 3D reconstruction of the four selected subjects represented in frontal and lateral view (from Bosi et al., 2018)

The structural part was reconstructed starting from the fluid scans for each morphology while the average thickness was chosen according to geometric indications based on a study of mechanical tests of ovine heart(Javani et al., 2016).

In the fluid part, on the other hand, the atrial pressure curve was set in conditions of sinus rhythm and with the necessary corrections in the case of atrial fibrillation.

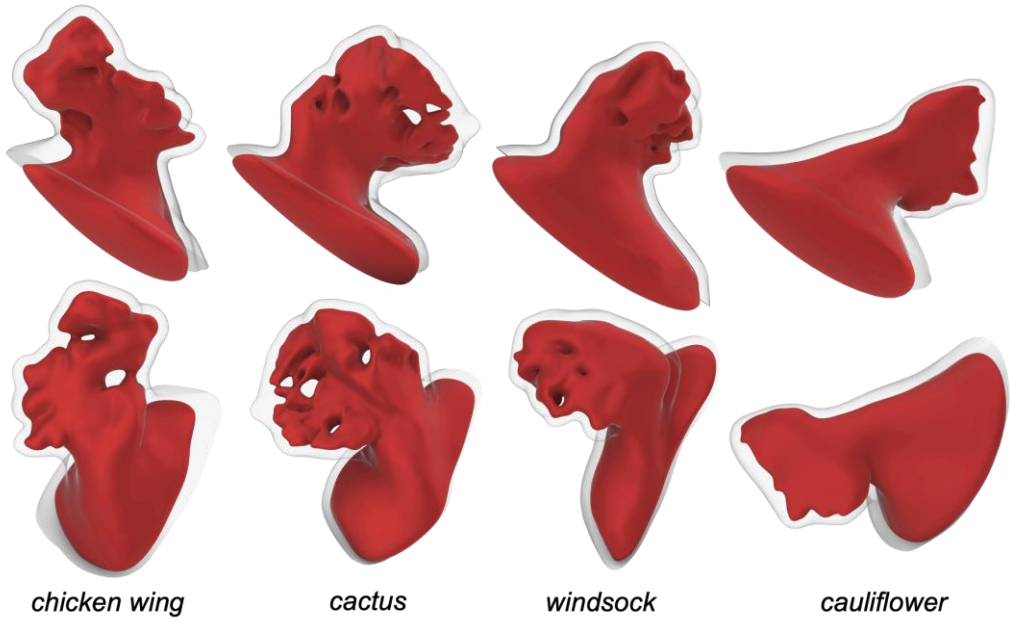

Figure 30 Left atrial appendage CAD models obtained for the four different patient specific shapes, seen from two views.

4.3.2 Anatomical Analysis and Morphologies

The left atrium is characterised by very complex flow patterns, which depend on the number, shape and position of the pulmonary veins, the position and shape of the mitral valve and the orifice of the left atrial appendage, and the conditions of pressure and flow that they act on veins and valves (Otani et al., 2016; Vedula et al., 2015). Therefore, in order to isolate the role of the atrial appendage and avoid introducing the effect of patient-specific characteristics that characterize the surrounding anatomy, it was decided to model and analyse only the appendage.

As clarified in the discussion, this hypothesis does not produce substantial approximations in the determined flow, especially in regions where clot formation is expected.

The commercial software ANSYS 19.2 has been adopted for the fluid-structural interaction simulations (FSI), using the Transient Structural module for the structural part, the ANSYS CFX module for the fluid dynamics part and the System Coupling module for the FSI calculation.

FSI approaches require the definition of a fluid domain and a solid domain. The left atrial appendage geometries analysed were defined starting from the specific patient morphologies used in the work of (Bosi et al., 2018) Figure 29. These are based on radiological scans that return the blood content within the left atrial appendage, and represent the four typical morphologies of the adult population not affected by atrial fibrillation.

The portion considered of the left atrial appendage therefore includes the neck and a portion of the atrium between the proximal part of the left appendage itself and the pulmonary veins.

This removes the boundary conditions from the orifice of the appendage, allowing the contraction of the entire appendage, including its neck region, and the establishment of greater freedom to the parameters of the fluid at the entrance to the left atrial appendage. The morphologies obtained were processed on the Autodesk Meshmixer open-source program, where they have been re-meshed and their imperfections have been corrected (see Figure 31-Figure 34).

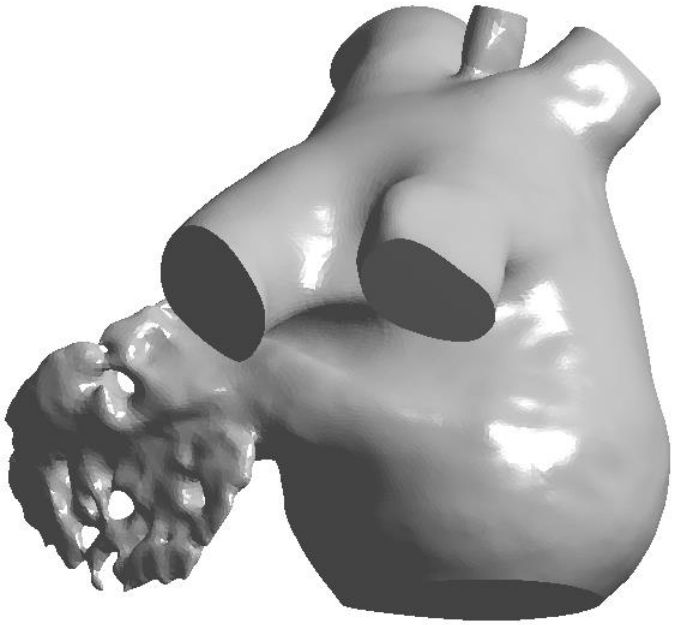

Figure 31 This figure shows the result related to the processing of the atrial model in STL format after post processing in Meshmixer.

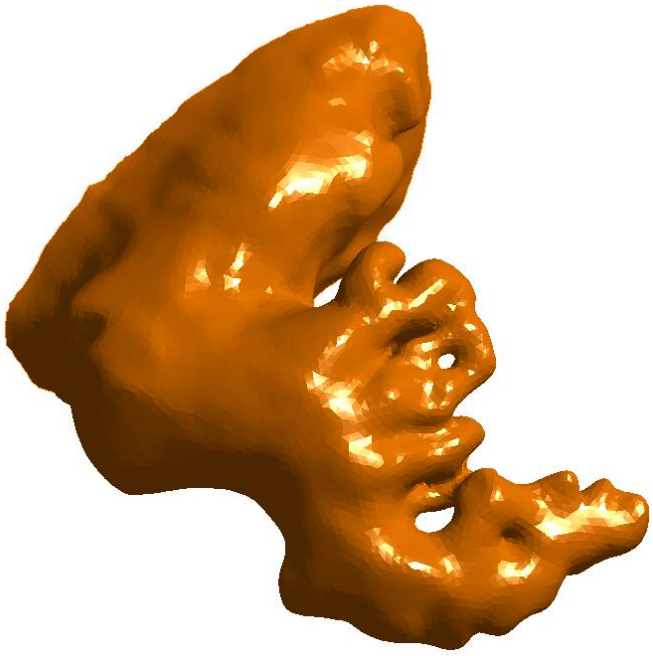

Figure 32 This figure shows the result relating to the processing of the model relating to the left atrial appendix in STL format after post -processing in Meshmixer.

The models obtained were closed with a bulge at the open inlet, obtained from a non-uniform rational base spline (NURBS) tangent to the surface of the wall at the orifice. This acted as an open surface for the application of the fluid boundary conditions.

To create the external surface of the solid left atrial appendage structure, the external blood walls were smoothed, removing all volume discontinuities due to the presence of the trabeculae. The resulting surface was offset outwards by 2.1 mm, chosen on the basis of the average wall thickness measured in the sheep models (Javani et al., 2016), and used as an external mesh in the construction of the solid part.

Specifically, the internal and external meshes were transformed into poly-surfaces and integrated into a solid volume through commercial computer-aided design (CAD) software Rhinoceros 7.0. In order to verify the effect of volume increase associated with persistent atrial fibrillation conditions, a 150% enlarged version of the model was also made (Lacomis et al., 2007).

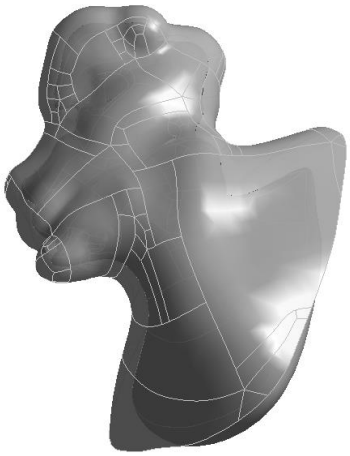

Figure 33 This figure shows the STEP model of the left atrial appendage in the internal and external part after post processing in Rhinoceros.

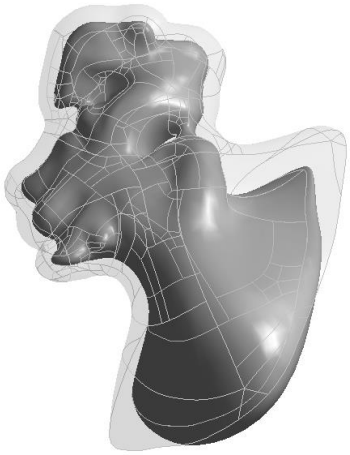

Figure 34 This figure shows the STEP model of the left atrial appendage in the internal part after post processing in Rhinoceros.

4.3.3 CAD Workflow

The settings obtained for the ideal left atrial appendage model were then applied to patient-specific models, classified in the four reference morphologies (Bosi et al., 2018).

Models were processed on various CAD modelling software including Rhinoceros 7 and Meshmixer, and suitably transformed into solid format (.step). The initial shell was updated with a thickness of 2.1 mm according to (Javani et al., 2016), while the internal volume was developed to obtain the fluid domain in the various morphologies. In the figures Figure 35-Figure 38 it is possible to see the first cads of the LAA alone both in the structural part and in the fluid part.

Figure 35 This figure shows the structural part and the part used in the fluid domain for the model patient specific models with mesh Chicken Wing

Cactus

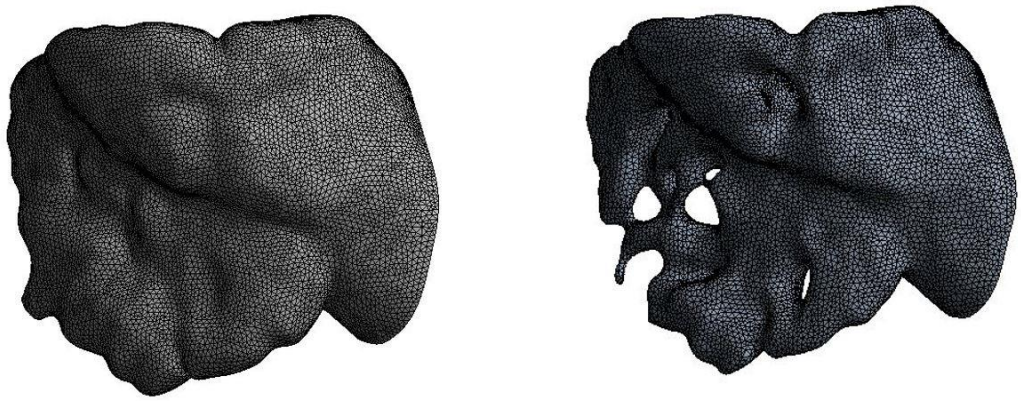

Figure 36 This figure shows the structural part and the part used in the fluid domain for the model patient specific models with mesh Cactus

Cauliflower

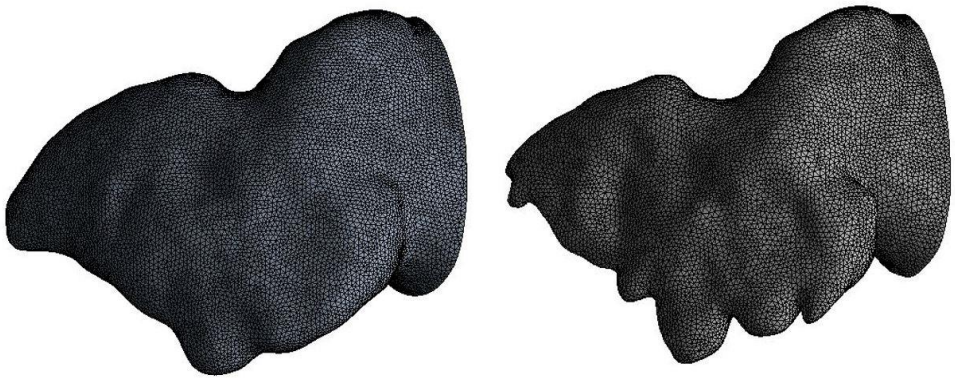

Figure 37 This figure shows the structural part and the part used in the fluid domain for the model patient specific models with mesh Cauliflower

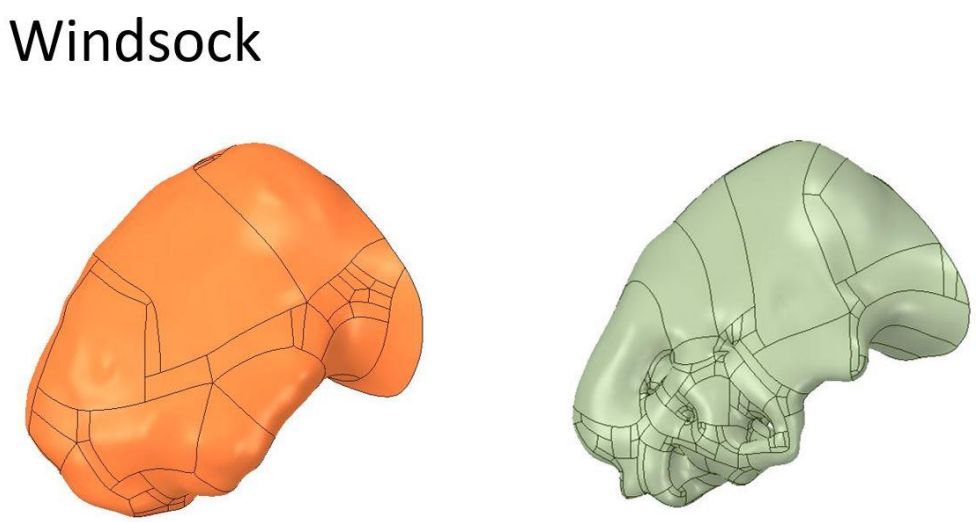

Figure 38 This figure shows the structural part and the part used in the fluid domain for the model patient specific models CAD Windsock model

This process generation of patient-specific models required the setting of leading to editable surfaces in step format for numerical simulations.

This operation used the commands present on Rhinoceros 7. The protocol used to create the models is summarised below:

• Make a discreet cut on the Meshmixer;

• Create the internal structure in STL format eliminating imperfections;

• Import the STL file of the internal structure into Rhinoceros 7 and perform the offset of 2.1 mm;

• Process the offset obtained on the Meshmixer and clean the structural imperfections;

• Import the two STL models on Rhinoceros 7 and create two work levels;

• Perform the Requad Mesh operation on each model;

• Perform the SUB D operation on each model;

• Define a section plan for cutting the left atrium;

• Duplicate the part relating to the internal SUB;

• Use one of the two internal SUB Ds for closing the structural model and one for the fluid model;

• Finally create a PATH at the entrance to the atrium;

• Save the model in STEP format;

4.3.4 Patient Specific Model

The CAD models were imported into ANSYS Workbench and meshed with quadratic tetrahedral elements for the fluid part and with linear tetrahedral elements for the structural part. The mesh density was selected on the basis of a convergence analysis performed on the morphology of the chicken wing, selected for setting all the parameters that were reported as the most common, observed in almost 50% of the population of the patient (di Biase et al., 2012).

In particular, an average mesh density of 70 elements/mm^3 was used for both the structure and the fluid. The four models are represented in Figure 30.

4.3.5 Rheological and mechanical properties

Human blood is a concentrated suspension of cellular elements in plasma. At the scale of the study, it can be considered a homogeneous non-Newtonian fluid with shear thinning, thixotropic and viscoelastic properties (Apostolidis et al., 2015; Chien, 1970; Fedosov et al., 2011). This results in a complex behaviour which changes dynamically as effect of the interplay between different multiscale phenomena occurring at the different flow conditions, and cannot be described by the available phenomenological visco-plastic rheological models (e.g. Casson model (N Casson, 1959)), which are designed to simulate steady-state conditions (Jariwala et al., 2020). Hence, in this work, the fluid was modelled as Newtonian, with a density of 1,062 kg/m³ and a viscosity of 0.0037 Pa·s, replicating the common physical properties of human blood at large shear rates. This is a common assumption, that enables direct comparison of the presented work with similar studies in the literature, whilst providing conservative results. In fact, regions where prolonged stasis is detected are likely to be even more stagnant under *in vivo* conditions, favouring red blood cell aggregation and thrombus formation (Ducci et al., 2016b).

The tissue of the LAA wall exhibits reduced anisotropy, and the typical non-linearly stiffening constitutive behaviour observed in biological soft tissues (Javani et al., 2016), characterised by a low-modulus region, a transient region characterised by a progressive stiffening with strain increases, and a stiff region at larger strains. However, the clinical morphological scans were acquired from pressurised operating hearts, already partially stressed/strained, hence, the wall material was modelled as linear elastic. Anisotropy is reported to be reduced in the wall of the atrium and its appendage (Javani et al., 2016). Hence, for simplicity, the material was modelled as isotropic.

The Young's modulus was set equal to 1.5 MPa, being this intermediate between that reported for the low and high regions in the left atrium of porcine hearts (Momtahan et al., 2015). To account for the material incompressibility, a Poisson's ratio of 0.49 was selected.

During LAA contraction, the volume of the appendage is reported to reduce by approximately 60 % of its maximum value, as a combined effect of the tissue elastic response to the pressure variation and the active contraction of the wall muscle (Li et al., 2015). Therefore, a uniformly distributed pressure was imposed at the open surface of the fluid of the *chicken wing* model, replicating the physiological atrial pressure curve obtained from the Wiggers diagram, and the change of volume due to the muscular contractive action was obtained through the setting of a virtual contraction of the structural part.

4.3.6 Development of FSI numerical model

FSI solutions are a function of how data is exchanged at the boundary or interface between the fluid solver and the structural solver.

The description of displacement in space can be done in two ways:

- Lagrangian description: the observer moves with the body in motion, used in the mechanics of solids;

- Eulerian description: the flow field is described in a fixed volume regardless of the paths of the particles, commonly used in fluid mechanics;

FSI requires a coupling mechanism to provide the information to the respective solver codes in an appropriate manner.

The arbitrary Lagrangian-Eulerian method (ALE method) is a numerical technique that offers the possibility of coupling a Euler and a Lagrange domain to solve fluid-structure coupling problems. The ALE coupling system combines the advantages of the Lagrangian and Eulerian descriptions.

The coupling strategies between the physics of the structural domain and that of fluids are of two types: one-way and fully coupled bidirectional.

In a one-way study, the fluid or structural domain is initially solved independently and the results are used as the model condition when solving the other domain. An example of an appropriate cardiovascular model for a one-way FSI study is the modelling of vessel compliance and distention, whereby the fluid domain is first resolved using CFD to determine the fluid forces on the vessel wall and then the results are used to calculate the deformation of the wall using FEA.

An interpolation phase will couple the two domains with the function of remapping the forces from the nodes of the fluid domain to the nodes of the structural domain. One-way studies have the advantage of the simplicity of the model and require fewer computational resources, but have the limit of not fully capturing the interaction of the fluid and structural domains (Benra et al., 2011). For example, in case of the modelling of the compliance and distension of the vessel, the distensile action will immediately reduce the pressure of the fluid acting on by the vessel, therefore the pressure of the fluid exported in the structural domain is probably higher than in reality with consequent overestimation of distension.

One of the main limitations of one-way studies is that they cannot study transient problems because the state of one domain at a static time is used to determine the state of the other domain at the same time (Hirschhorn et al., 2020b). Another aspect is related to the mesh and the exaggerated deformation of the elements. In the case of a significant deformation of the structural part, they can create conditions of instability with consequent simulation subject to error.

In the bidirectional method the calculation procedure is as follows:

- ✓ An interpolation is performed between the forces of the fluid mesh, in the interface surface, with those of the structure mesh;
- ✓ A convergent solution is thus obtained in the structural domain, in response to the acting forces;
- ✓ At this point the response of the structural part comes into play, which is understood in terms of displacement of the nodes relative to the mesh of the solid domain;
- ✓ The cycle closes when the convergence downstream of the interpolation of the displacements of the interface nodes with the fluid domain mesh is reached;
- ✓ The time steps are repeated iteratively.

The change from one temporal step to another is determined by a limit threshold within which to contain the variations between the forces relative to the fluid domain and the displacements relative to the structural field.

The final choice fell on the bidirectional method. The model was fine-tuned to the ideal geometry, considering only the left atrial appendage. The encouraging results on the ideal model led to the transfer of the same parameterization to patient-specific models.

4.3.7 Two Coupling Methods for Numerical Analysis

The first FSI analysis was performed on a cylindrical model, thus modelling the blood flow in an artery. The model consists in associating a transient structural analysis and a CFD analysis with a coupling system; The computational setup is described in Figure 39:

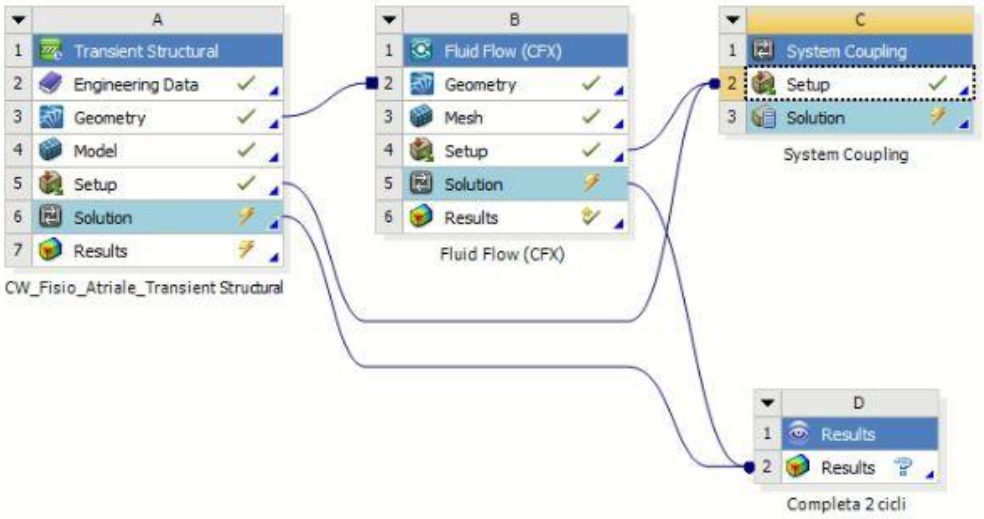

Figure 39 This figure shows the schematic used in FSI simulations using ANSYS Workbench software. In this diagram it is possible to identify the module relating to the structural part, the fluid part and the coupling module.

The characteristics initially set on the cylindrical model are:

- Tube diameter 1.5 cm, tube length 10 cm;
- A constant speed at the Inlet of 0.5 m/s;
- A constant pressure of 13332 Pa in the outlet;
- The structuring model is considered elastic with a density of 1120 kg/m^{-3};
- Young 1.08 MPa;
- Poisson 0.49;

After having carried out some tests on an example of simple geometry such as the cylinder, the FSI computational model was transferred to the geometry of the left atrial appendage of the population specific model (Vella et al., 2021a).

The initial model also included the atrial chamber but, due to the verification of a lack of stabilization of the flows inside the left atrium, it was decided to reduce the analysis to the appendage only. This simplification introduced in the model has allowed the reduction of the computational effort with consequent obtaining of the results in a shorter time.

The CAD model consists of a part used for the Transient structural simulation, with an average thickness of about 2.1 mm, a mesh consisting of about 180000 quadratic elements and 265000 nodes. The interior of the model, on the other hand,

constitutes the fluid domain and is composed of approximately 197,000 elements and 270,000 nodes for a volume equal to 2.80E-06 mm^3 (see Figure 40).

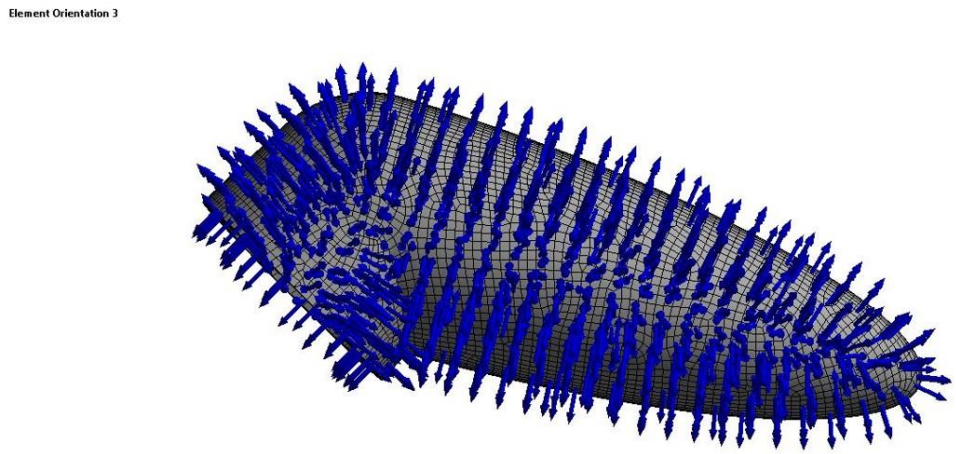

Figure 40 This figure shows the CAD model relating to the idealized geometry of the left atrial appendage only. For each element of the mesh there is also the local reference system relative to the z axis.

4.4 Boundary Condition

The setup of the boundary conditions is done on the left atrial appendage model of the population-specific geometry. It was necessary to carry out a series of tests before obtaining the final conditions implemented on the patient specific models.

4.4.1 Pressure Contribution

The pressure contribution was obtained from the physiological atrial pressure curves, present in the Wiggers diagram (Wiggers & Katz, 1922; Wright et al., 2020).

This curve was also processed on MATLAB, in order to obtain a slightly smoothed trend, and repeated for four cardiac cycles.

The pressure curve acts on the internal walls of the atrial appendage, while a fixed support was applied to the surface of the orifice. The time instant T_0 of the cycle coincides with the pressure value P = 0, at the beginning of filling phase (ventricular diastole) as shown in the thermal curve (see Figure 43)

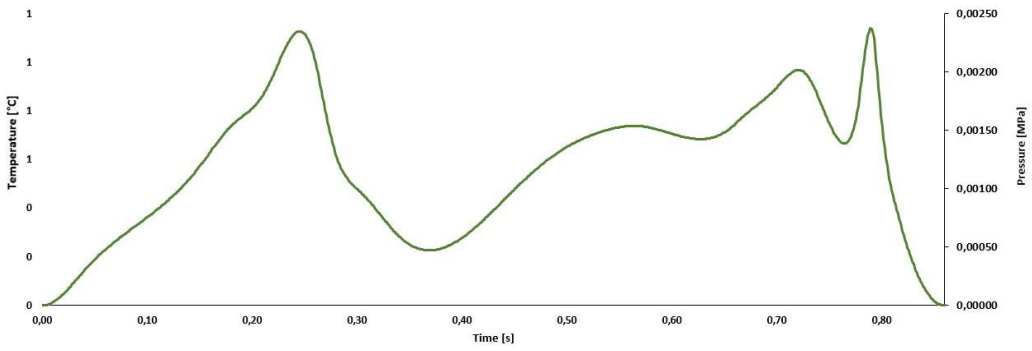

Figure 41 This figure shows the atrial pressure curve used in the numerical model and applied to the fluid directly on the portion called Inlet.

This choice was then replaced by the application of the pressure curve directly on the fluid inlet. The results of the fluid volume change obtained according to the imposition of the pressure curve directly on the walls of the structure were superimposable to the volume changes obtained by the imposition of pressure directly on the fluid.

4.4.2 Thermal Contraction

It was possible to obtain a contraction of the walls of the left atrial appendage that simulates muscle activation by exploiting virtual temperature drops, and specially set coefficients of thermal contraction of the material. The setting of the thermal expansion coefficients considered the conservation of the volume.

This exploited of a local reference system, for each element of the mesh (see Figure 45), which made it possible to simultaneously obtain a contraction in the plane and an expansion along the thickness, in the phase of filling the appendage.

Before finalizing this setup, the invariability of the volume of the contracting solids was verified on a cubic geometric model (Figure 42).

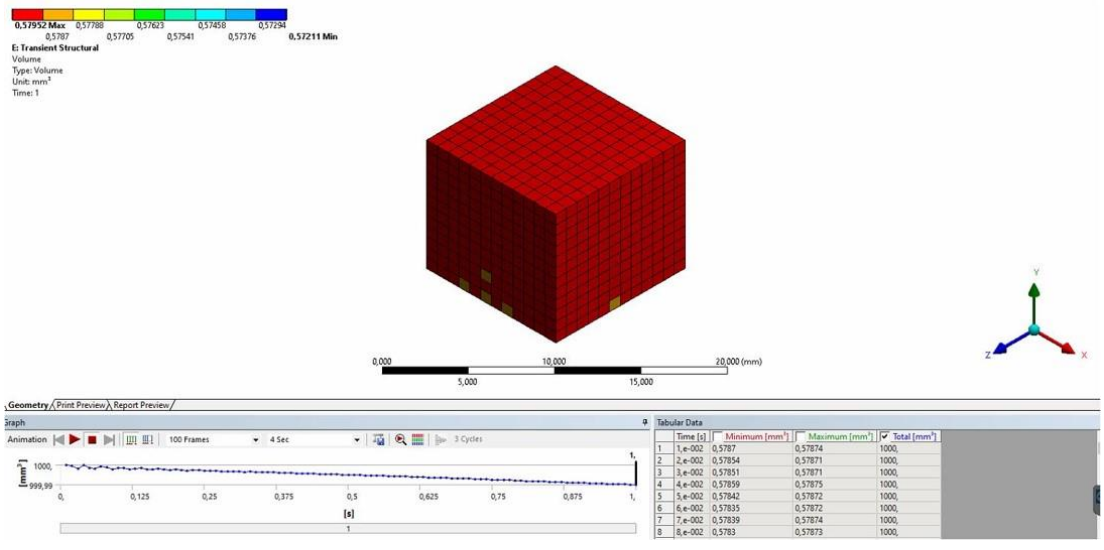

Figure 42 shows the result relating to the simulation tests on a simple geometric model which confirms how the application of a thermal load with the correct setup of the thermal expansion coefficients guarantees the conservation of the volume.

Having ascertained that the volume of the structural part subjected to thermal variation remained unchanged, it was possible to draw a thermal curve like the one in Figure 43 which, after a series of tests and with the correct setup, returned a volume variation adequate to what was indicated in the studies in the literature (Li et al., 2015).

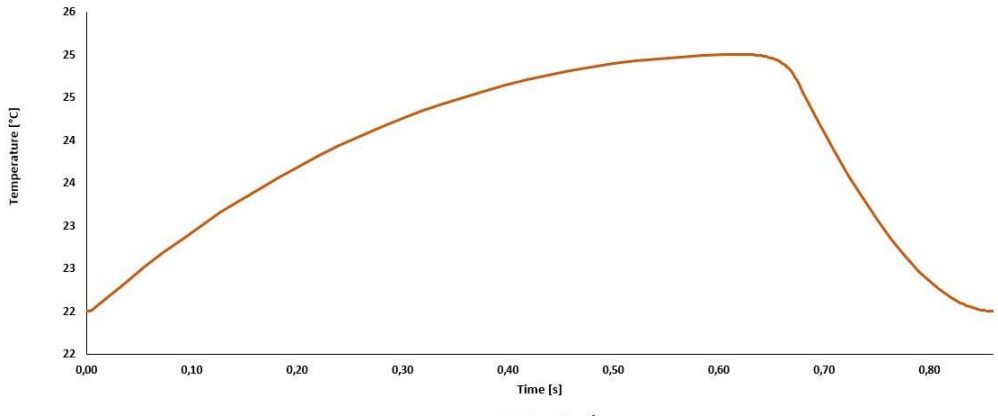

Figure 43 This figure shows the thermal curve used to describe the phases of active contraction of the left atrial appendage starting from its minimum volume configuration.

The final simulation setup that resulted in a volume variation of about 60% consists of a modulus of elasticity equal to 0.5 MPa and thermal expansion coefficients equal to: $C_x = 0.024$; $C_y = 0.024$; $C_z = -0.048$; The superimposition of the effects is shown below.

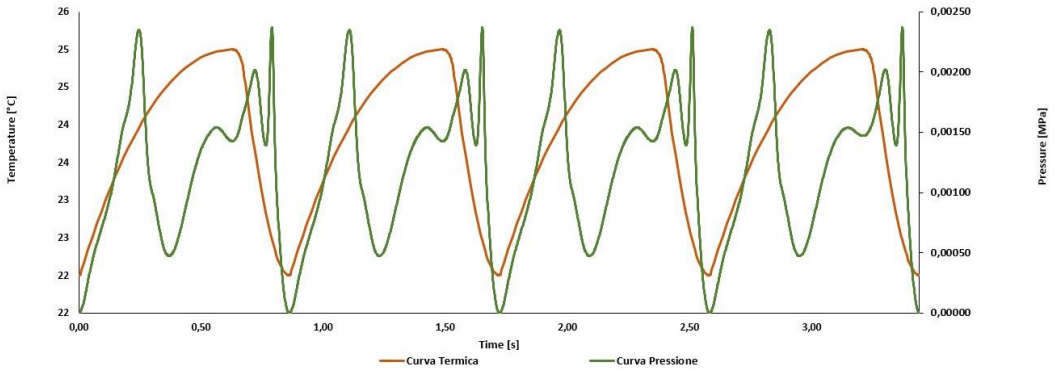

Figure 44 shows the overlap of curves. In green it is possible to identify the pressure curve while the thermal curve in brown.

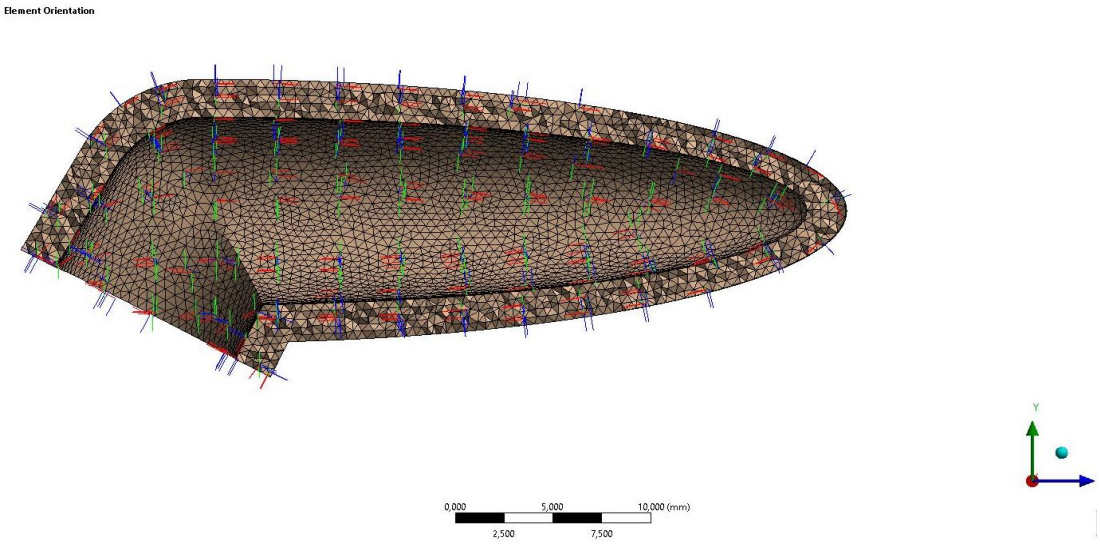

Figure 45 Sectional view of the left atrial appendage with local reference system in the ideal CAD model

4.4.3 Numerical Model Workflow

The numerical model used in the FSI simulations involves the use of three calculation modules: the structural part defined in Transient Structural, the fluid dynamic part defined in Fluid Flow (CFX) and the part of the coupling defined in system coupling (see Figure 39) plus a module additional, denoted Result, read-only of the results.

The geometric model is loaded on the module of the structural part, both the component of the solid domain and that of the fluid domain, the latter is suppressed in the setup. The same geometry is connected to the Fluid Flow module (CFX) where the structural part is suppressed, in the opposite way this time.

The part of the material setup is defined in the Transient Structural module as for example the one shown in Figure 46 . The material is defined linear elastic with the definition of the coefficients of thermal expansion foreseen for each direction.

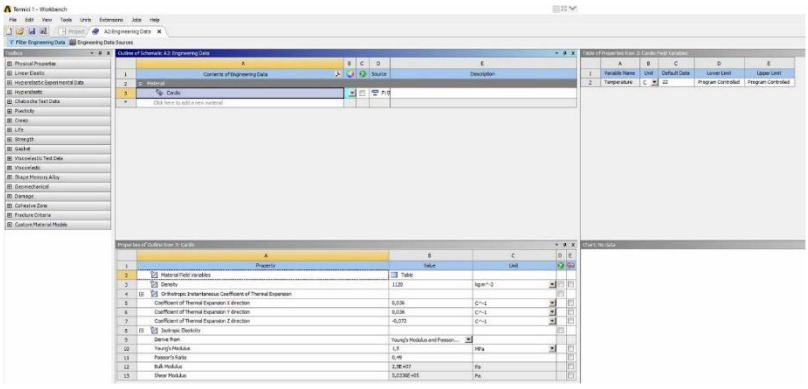

Figure 46 Example of a model setup used to define the material within the Transient Structural module

The setup of the material used in the fluid was developed using a Newtonian fluid model with the introduction of the density value equal to 1060 [kg m^{-3}] like that of blood (see Figure 47).

The setup of the analysis involves the use of the same time step in both modules: Transient Structural and Fluid Flow (CFX).

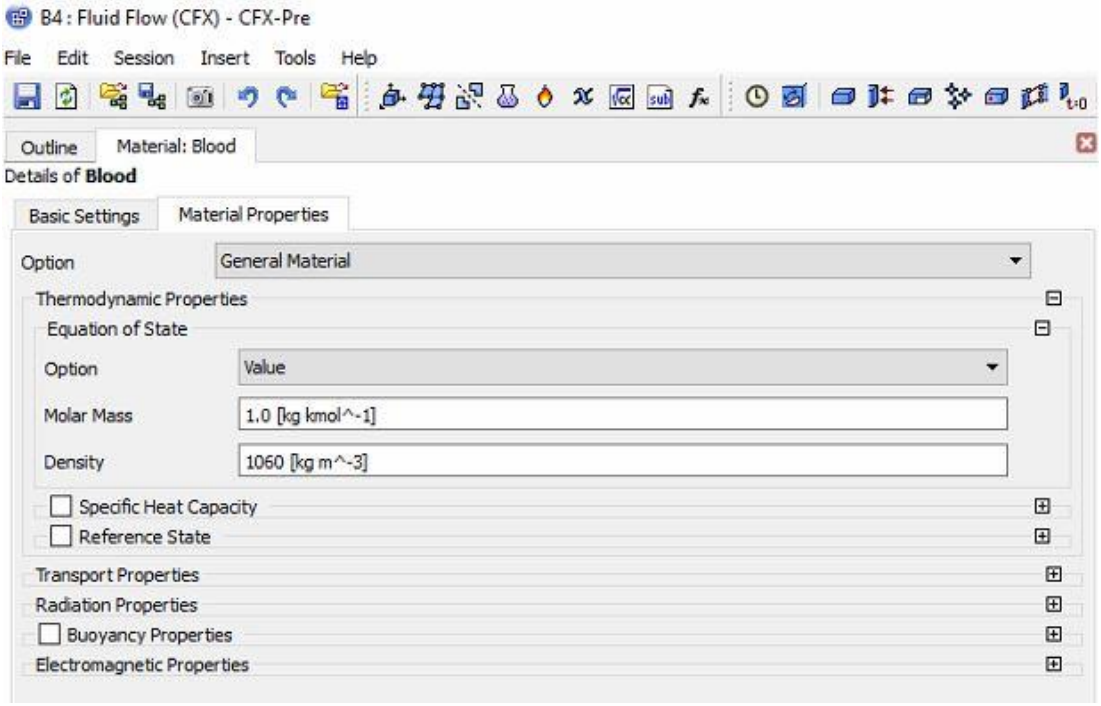

Figure 47 Example of a model setup used to define the fluid domain material within the Fluid Flow (CFX) module.

Finally, in the System Coupling set, it is possible to define the data transfers for each module where the source and target for the structural part and for the fluid part are defined (see Figure 48 and Figure 49).

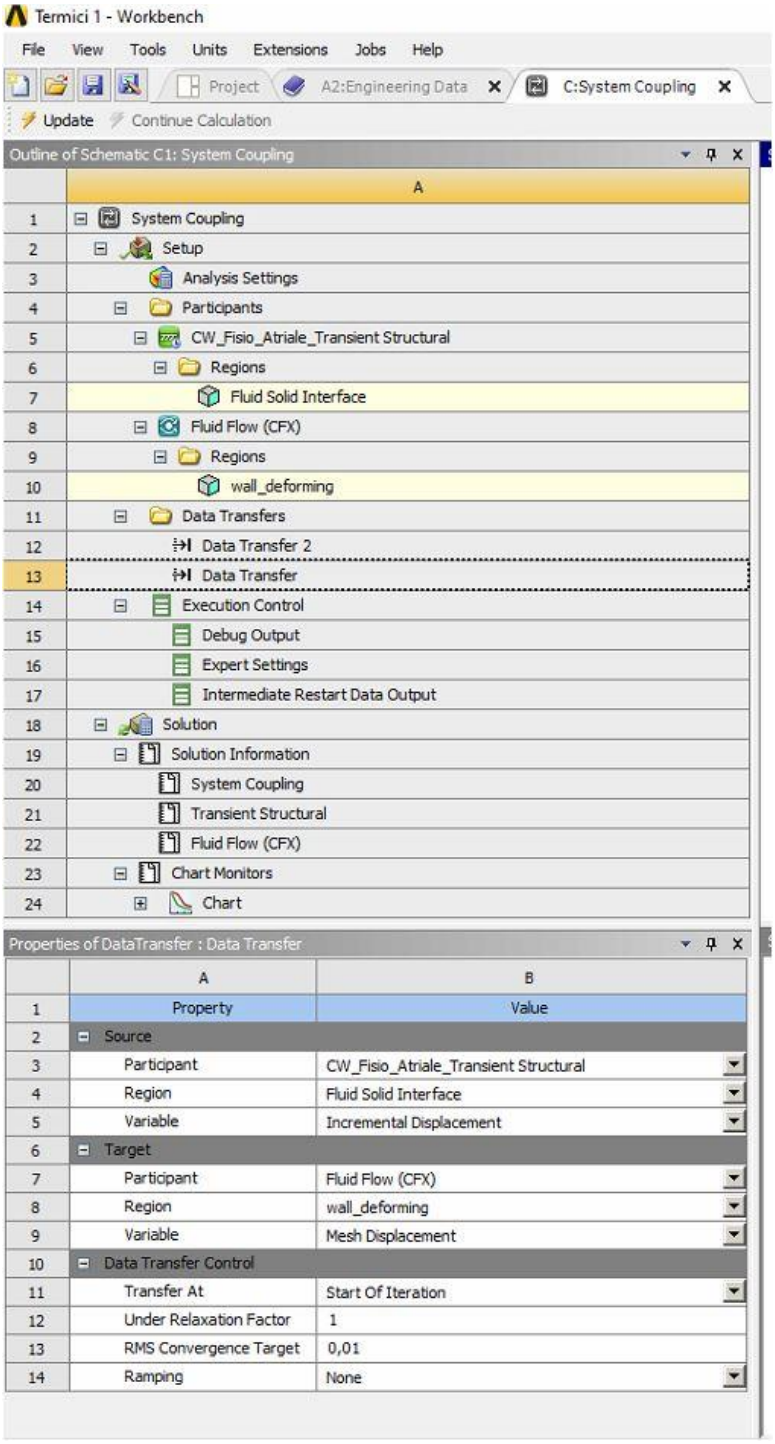

Figure 48 Example of the data transfer setup related to the Transient Structural part within the System Coupling module

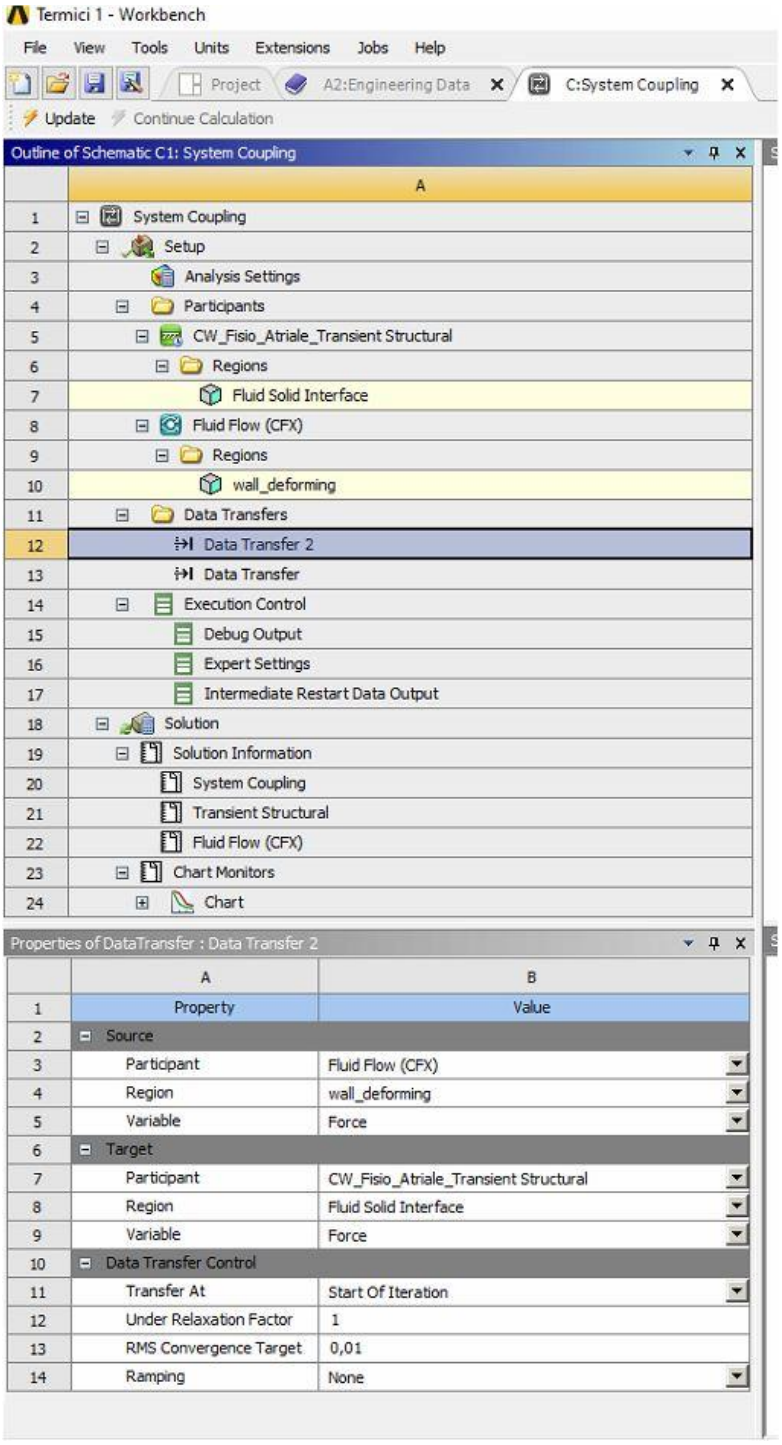

Figure 49 Example of the data transfer setup related to the Fluid Flow (CFX) part inside the System Coupling module

4.4.4 Results FSI population-specific LAA model

The evaluation of the SSR was carried out on a longitudinal section plane of the left atrial appendage. The value was averaged over a surface bounded by the volume of the fluid. The volume variation of about 60%, obtained through the application of a pressure on the internal walls of the left atrial appendage and an artificial thermal contraction produced an average value of SSR on the section plane of the fluid consistent with the physiological conditions of a subject with sinus rhythm.

Figure 50 shows the trend of the volume variation on the fluid of ideal geometry, Figure 51 shows the section where to evaluate the velocity in the plane of the orifice on left atrial appendage, always relative to the ideal geometric model (population specific model).

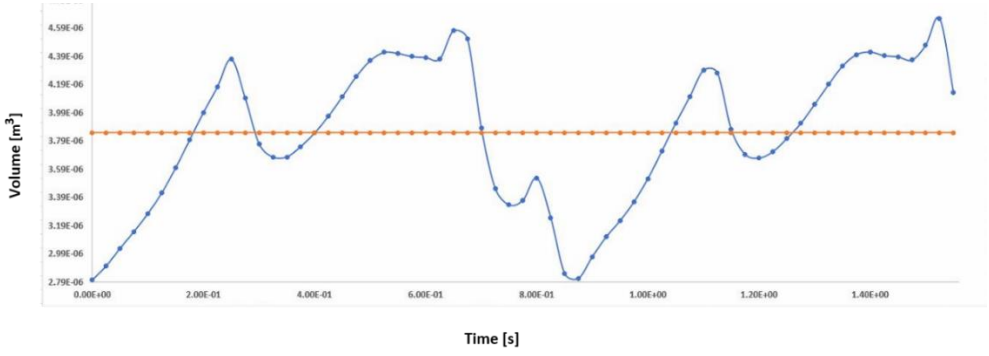

Figure 50 shows the trend relative to the volume variation on the geometry representative of the ideal model.

One of the parameters associated with thromboembolic risk assessments is the velocity measured at the orifice of the left atrial appendage.

Although this parameter is used by clinicians as a reference, the ranges of measured values are lower than those expected for a sinus rhythm condition.

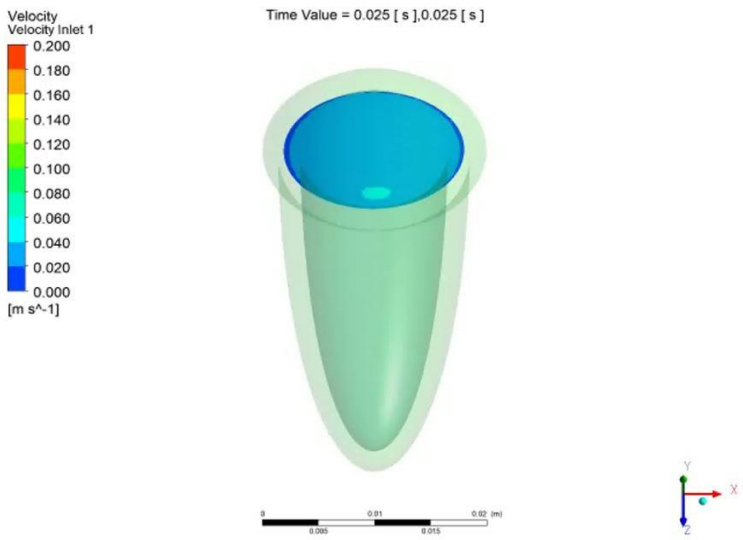

Figure 51 shows the trend relative to average speed rating in the orifice plan of left atrial appendage ideal model.

4.5 Setting of boundary conditions to the final model

During contraction of the left atrial appendage, the volume of the appendage is reduced by approximately 60% of its maximum value, as a combined effect of the elastic response of the tissue to the change in pressure and to the active contraction of the wall muscle (Li et al., 2015). Therefore, the uniformly distributed pressure was imposed on the open fluid surface of the chicken wing model, replicating the physiological atrial pressure curve obtained from the Wiggers diagram (see Figure 52), and the volume change due to muscle contracting action was obtained through the setting up a virtual contraction of the structural part.

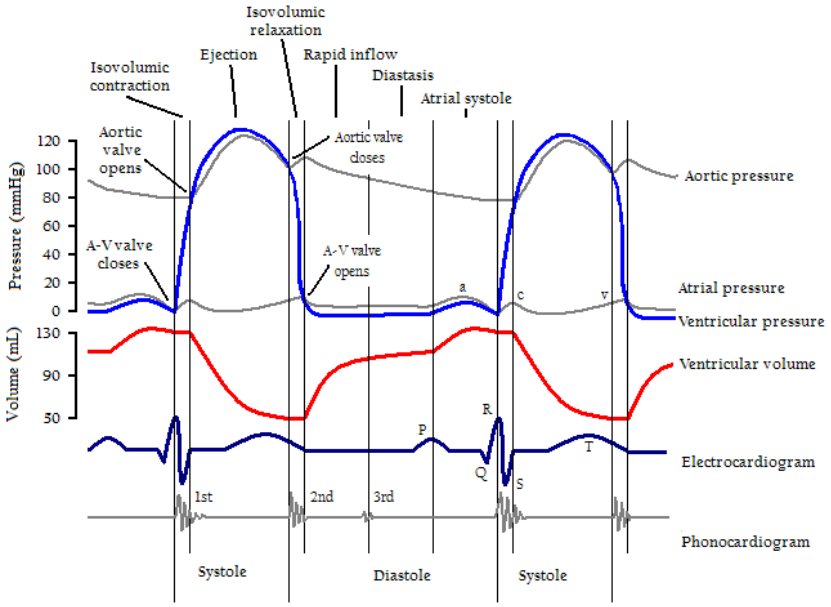

Figure 52 shows the Wiggers diagram. The diagram displaying the time variations in cardiac electrical and mechanical functions as recorded by a polygraph (from https://commons.wikimedia.org/wiki/File: Wiggers_Diagram.png)

The contraction was defined through the orthotropic thermal expansion coefficients of the structural elements. In particular, a local reference system was imposed for each element of the mesh, with the x-y plane parallel to the internal wall.

The coefficient of thermal expansion along the wall thickness (local z direction) was defined to maintain volume conservation (each contraction along the plane corresponds to an expansion along the thickness), thus imitating cardiac muscle behaviour (see Figure 53).

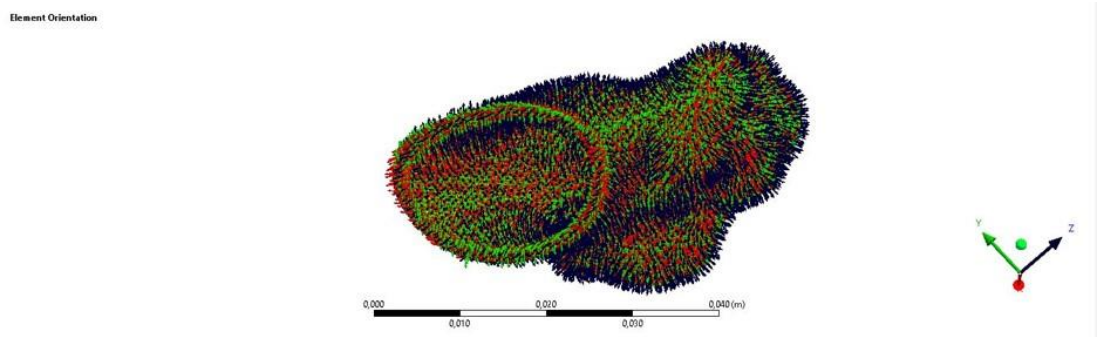

Figure 53 shows the element orientation using in left atrial appendage patient specific model.

Then, the virtual temperature change applied to the structure to simulate active contraction was adapted to replicate clinical assessments of left atrial appendage fill and empty volumes under healthy conditions for chicken wing morphology.

In particular, the thermal expansion coefficients were set equal to 0.05 in the directions in the plane (*x* and *y*), and equal to -0.10 in the out-of-plane direction (z); and the temperature curve was varied between 0 and 5 °C, in order to obtain a relative volume variation during the cycle of about 60%.

For the FSI simulation, the timestep used is 21.5 ms. Figure 54 shows a cross section of the model of the structural domain of the chicken wing at maximum expansion and maximum contraction.

The entire procedure described was first applied to the ideal model, the work of fine-tuning the model was characterized by the parameterisation of the model on the geometry of the only atrial appendage already used in the geometries relating to CFD simulations. Finally, a transposition of the parameters was carried out on the various patient specific models.

The same material parameters were applied to all the geometries represented by the morphological families. Figure 54 shows a representation of the chicken wing morphology in two different phases of the cardiac cycle.

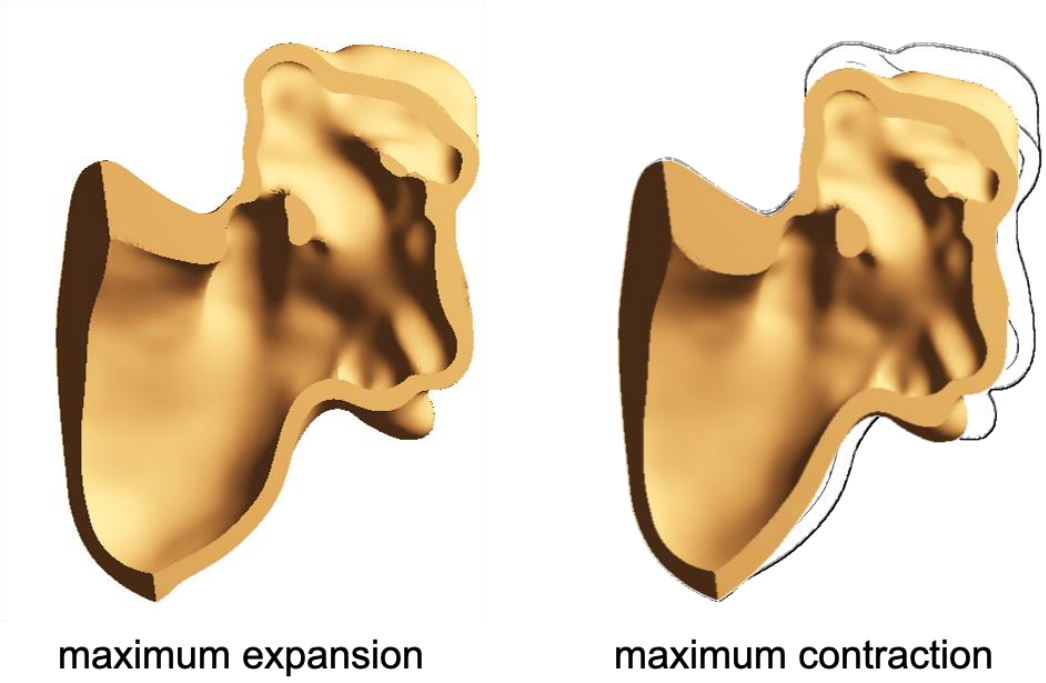

Figure 54 Cross section of the chicken wing model at the maximum expansion (left) and at the maximum con-traction (right).

4.5.1 First Patient Specific Numerical Simulation

The study approach followed in the simulation of the ideal model is repeated in the Patient Specific models (see Figure 55); The setting work to obtain an overall volume variation of 60% was repeated for the most recurrent morphology: chicken wing.

Once the optimal combination of loads and supports on this morphology provided both, same boundary conditions were applied in the remaining three morphologies identified. The SSR and the speed at the orifice become periodic and well stabilised already at the second cycle (see Figure 56-Figure 57).

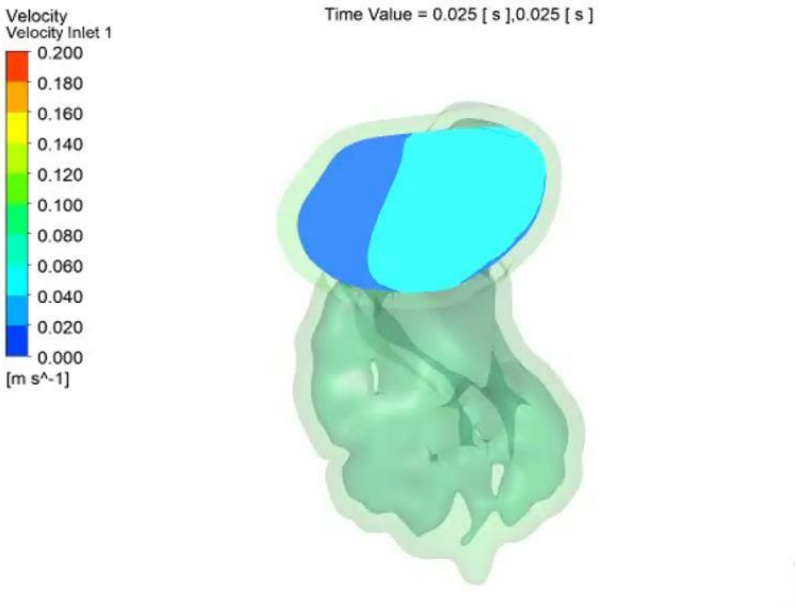

Figure 55 shows the trend for the evaluation of the mean velocity in the plane of the orifice of the left atrial appendage compared to the specific model for the patient.

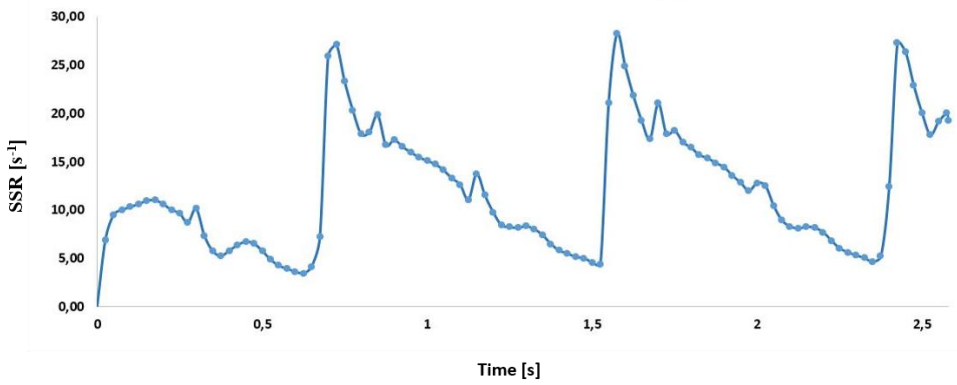

Figure 56 shows three-cycle SSR trend of a Patient Specific model

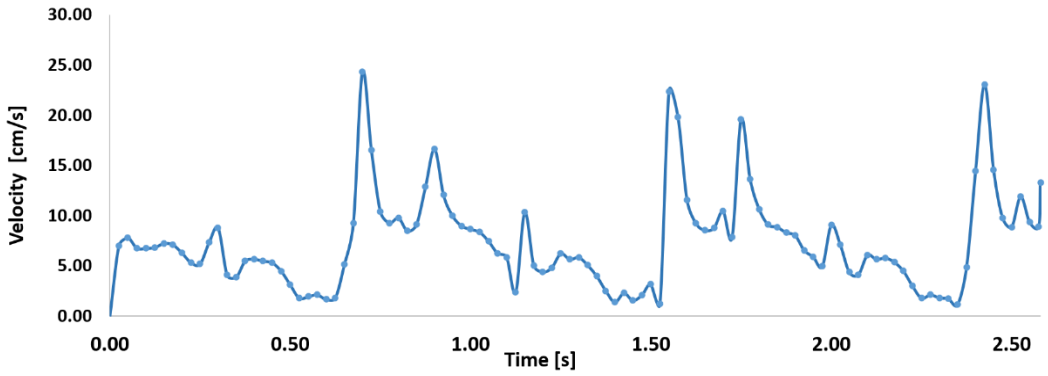

Figure 57 shows three-cycle velocity trend of a Patient Specific model

4.5.2 Complete models setup

The final study analyses three precise and distinct operating conditions:

- **Sinus rhythm**
- **Acute atrial fibrillation**
- **Chronic atrial fibrillation**

To simulate sinus rhythm conditions, uniformly distributed pressure was applied on the open fluid surface, based on the physiological atrial pressure described in the Wiggers diagram (Wiggers & Katz, 1922; Wright et al., 2020).

Then, as described above, a virtual temperature change was applied to the structure to simulate active contraction (see Figure 58)

For the simulation of acute and chronic AF conditions, no active contraction was enforced (by applying a constant virtual temperature equal to 0 °C), and the pressure

curve applied at the fluid free surface was modified to account for the lack of atrial contraction (Fukunami et al., 1991; Steinberg et al., 1993.; Weng et al., 2020; Yagishita et al., 2018).

Hence, the structure only undergoes passive expansion due to the pressure curve imposed at the opening surface of the fluid. In the case of chronic AF, typically associated with remodelling, the enlarged version of the appendage was used.

The simulated heart rate was of 70 beats/min, corresponding to a duration of each cycle equal to 860 ms. This is an idealised condition in the case of AF, which is characterised by irregular rhythm, and was adopted to allow direct comparison of the results, isolating the effect of the loss of contraction and remodelling.

Up to six cardiac cycles were simulated for each morphology and a stabilization of flows was detected for all cases as early as the second cycle.

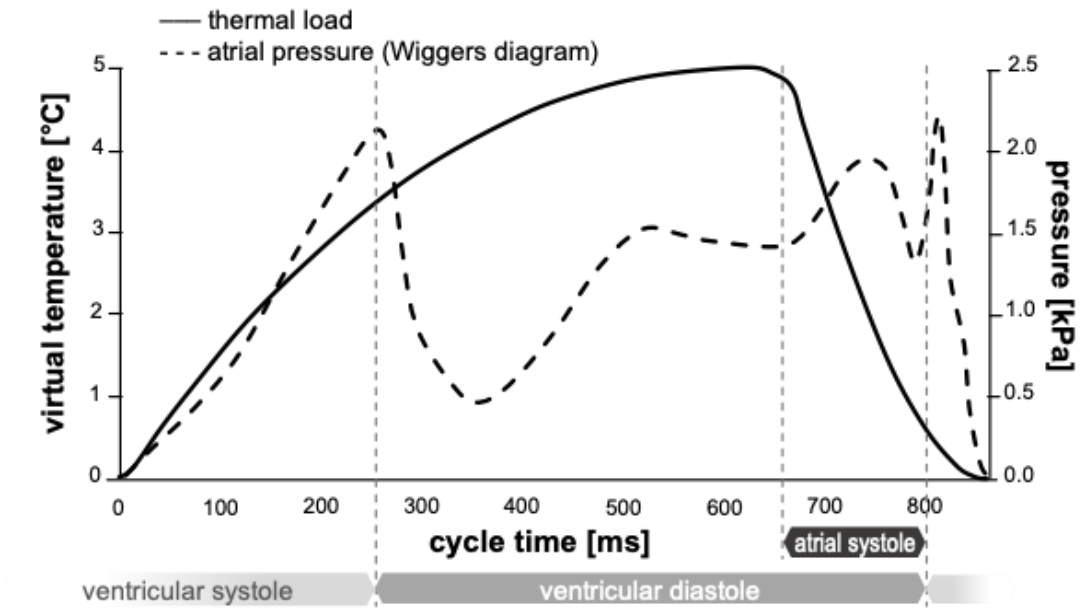

Figure 58 Thermal load (continuous line) and physiological atrial pressure curve (dashed line).

4.6 FSI Patient-Specific Results

In total, four different patient-specific models associated with the different morphological classes of the left atrial appendage (chicken wing, cactus, windsock and cauliflower) were analysed. Three conditions were analysed for each patient specific morphology: sinus rhythm, acute atrial fibrillation and chronic atrial fibrillation, for a total of 12 different numerical simulations.

The volume changes obtained for the different cases are summarized in Table 5

Table 5 Percental volume change simulated for all models and all operating conditions.

	Sinus Rhythm	*AF Acute*	*AF Chronic*
Chicken Wing	56.15 %	3.24 %	3.30 %
Cactus	57.86 %	4.10 %	4.46 %
Windsock	57.43 %	2.50 %	2.77 %
Cauliflower	74.12 %	3.84 %	3.85 %

The physical quantities analysed in the models are the Shear Strain Rain (SSR) and the peak velocity at the orifice of the left atrial appendage. Since all analyses become periodic after the second cycle; outcomes were evaluated during the third cardiac cycle.

The diagrams of Figure 59 represent the mean wall SSR calculated in the region from the neck of the left atrial appendage (cross section of the smallest orifice) to its distal end, during the cardiac cycle, for the four appendages in the three different conditions. For clarity, the time in the diagrams is relative to the cycle represented (ranges from 0 to 860 ms) rather than the analysis time (from 1,720 to 2,580 ms).

The colour maps in Figure 60 represent the distribution of the wall SSR at the respective peak of the mean wall SSR identified by the diagrams of Figure 59.

To support a more effective visualization of the wall SSR range, a logarithmic rainbow scale is used in the images, with the red colour indicating the regions of lower shear rate, where blood clotting is promoted.

In order to identify regions of potential thrombosis risk, the fluid wall that remains exposed throughout the cycle to SSR values below 10 and 5 s^{-1} is represented in Figure 61. These thresholds have been selected to better identify the regions with low and very low persistent shear rate, where the aggregation of red blood cells is expected to be more pronounced, with a consequent increase in viscosity (in the real case) and in coagulation (Ranucci et al., 2014).

The percentage of the left atrial appendage area exposed to SSR values below 10 and 5 s^{-1} for the entire cycle is summarised in Table 6.

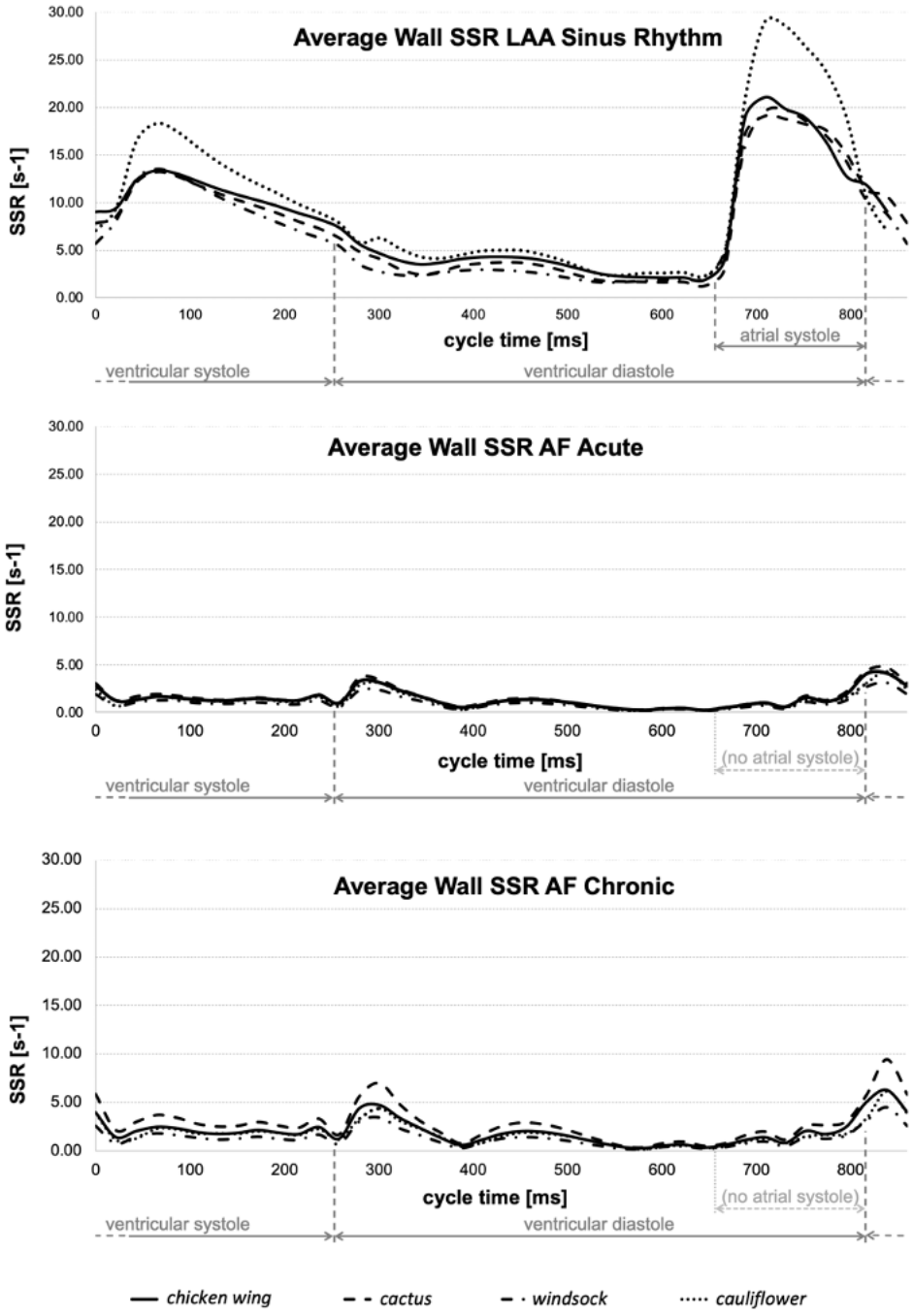

Figure 59 Average wall SSR estimated for all models in sinus rhythm (top), acute AF (middle) and chronic AF (bottom) conditions.

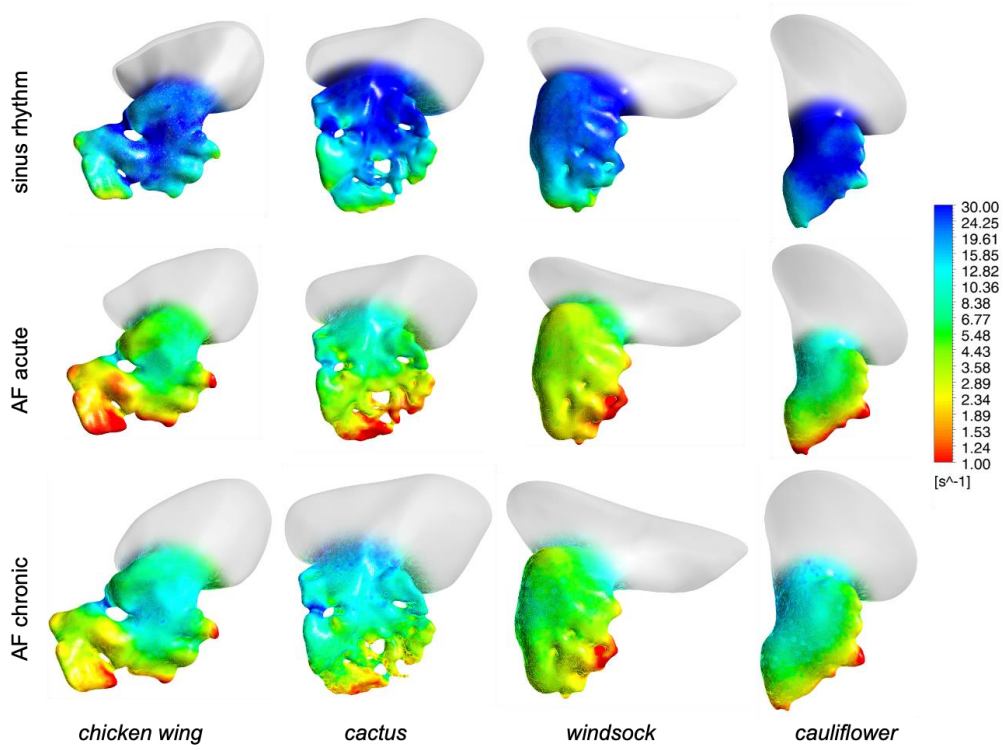

Figure 60 Colour maps of the maximum wall SSR at the instant of the cycle when they reach the maximum value, estimated for all models and all operating conditions.

Table 6 Percentage of left atrial appendage area exposed to SSR values below 10 and 5 s^{-1} for cycle

	Sinus Rhythm		*AF Acute*		*AF Chronic*	
	$< 5\ s^{-1}$	$< 10\ s^{-1}$	$< 5\ s^{-1}$	$< 10\ s^{-1}$	$< 5\ s^{-1}$	$< 10\ s^{-1}$
Chicken Wing	3 %	17 %	64 %	93 %	52 %	76 %
Cactus	3 %	11 %	55 %	93 %	33 %	63 %
Windsock	4 %	17 %	86 %	100 %	60 %	96 %
Cauliflower	0	3 %	64 %	95 %	46 %	79 %

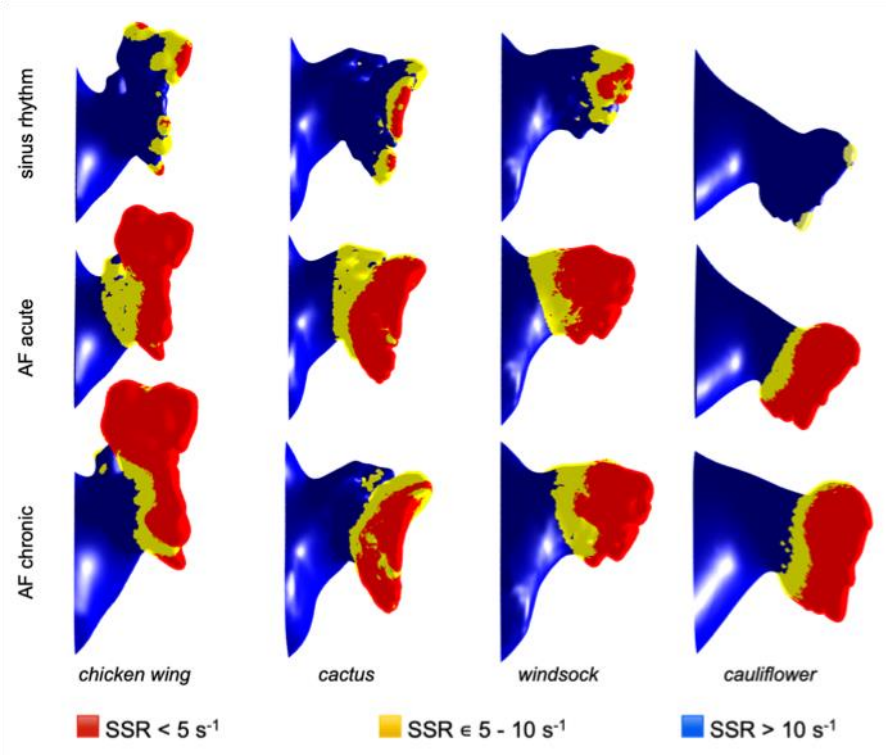

Figure 61 Risk area maps in: a) Sinus Rhythm, b) AF Acute and c) AF Chronic

To obtain the risk maps, a reading protocol in the .csv format returned by ANSYS Workbench was developed through the MatLab calculation code.

Within the cardiac cycle examined, the SSR values relating to each trn printed in the numerical simulation were extracted.

The output files were acquired from the code together with the coordinates of the nodes and the geometry of the model.

The aim was to design a tool capable of developing a colour map where to identify SSR values below a certain threshold for the entire duration of the cycle.

This tool, if appropriately implemented, can return information useful for a customizable evaluation of the parameters related to the evaluation of the thrombo-embolic risk.

The same tool allows to obtain the curves of the SSR values as a function of the percentage of associated risk area (see Figure 62).

The script is reported in full in the appendage in the example relating to the chicken wing model in sinus rhythm.

In the clinical setting, velocity remains the most commonly used parameter for hemodynamic evaluation (Fukuda, 2003). Therefore, the maximum predicted velocity during the cycle at the cross-section of the left atrial appendage orifice for the different simulations was determined and reported in the Table 7.

Table 7 Maximum velocity in: Sinus Rhythm, AF Acute and AF Chronic [cm/s]

	Sinus Rhythm	*AF Acute*	*AF Chronic*
Chicken Wing	15	2.5	4.6
Cactus	10	2.8	4.4
Windsock	15	2.2	3.5
Cauliflower	20	1.9	4.7

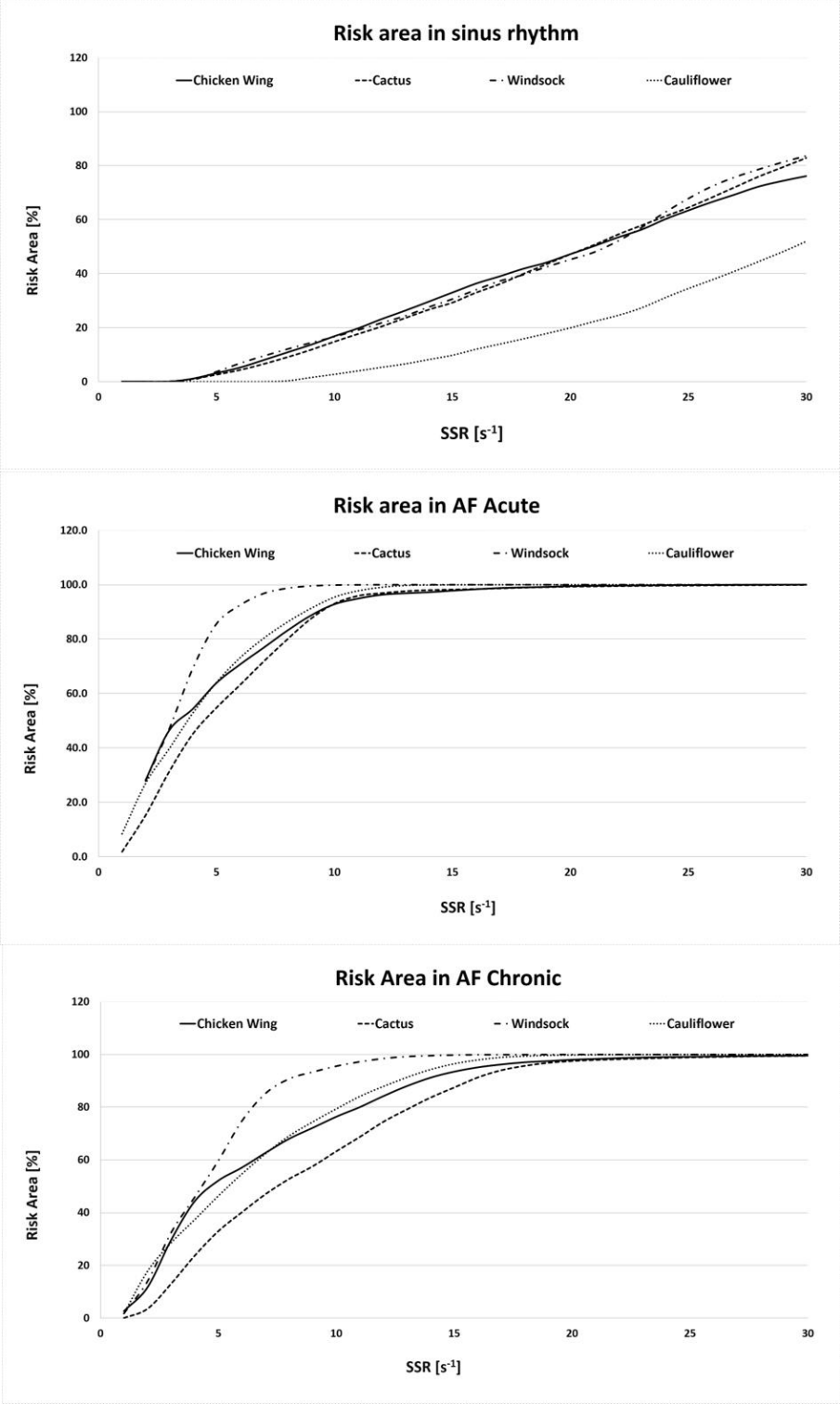

Figure 62 Risk Area curve for each model for all operating conditions

4.7 Comparison of Patient Specific Models Belonging to the Same Morphological Class

To deepen the morphological analysis, a comparison was made with two other models belonging to the same morphological family.

The morphology used as a reference is the Chicken Wing, as the most common in the population. A comparison was made between three models classified within this morphological group.

The geometric models representative of the compared chicken wing morphologies are represented in Figure 63. The ‘chicken wing’ model is the same one used in previous simulations; the ‘chicken wing 1’ and ‘chicken wing 2’ models both belong to other patients without cardiovascular disease.

The acquisition and development processes of each of them are the same used in the four previous simulations and illustrated in the materials and methods chapter.

The boundary conditions are also the same, so as to make a measurement comparable with the previous ones. However, the operating conditions analysed are two: sinus rhythm and acute atrial fibrillation. The condition of chronic atrial fibrillation is not taken into consideration.

This first comparison allows to carry out an evaluation between models belonging to the same morphology and models belonging to the four different families previously illustrated.

The volume changes obtained for the different cases are summarized in Table *8*.

While in the comparison made between the different morphologies in Figure 59 there was an evident difference only in the model without trabecular (the Cauliflower), Figure 59 indicates how in sinus rhythm conditions there are no significant differences between the three geometries belonging to the same family.

Table 8 Percental volume change simulated for tree chicken wing models and two operating conditions.

	Sinus Rhythm	*AF Acute*
Chicken Wing	56.15 %	3.24 %
Chicken Wing 2	47.01 %	2.10 %
Chicken Wing 3	41.18 %	3.82 %

Figure 63 Left atrial appendage CAD models obtained for the tree different patient specific chicken wing shapes.

The significantly more evident result is appreciable in the comparative analysis carried out in AF Acute conditions (see Figure 64).

Within the same morphological family, we find evident differences and compared to the four different morphologies they seem to be more marked.

The colour maps in Figure 65 represent the wall SSR distribution at the respective peak of the average wall SSR identified by the diagrams in Figure 64.

Consistently with previous representations, in order to obtain more effective visualisation of the wall SSR interval, a logarithmic rainbow scale is used in the images, with the red colour indicating the regions of lower shear rate, where blood clotting is promoted.

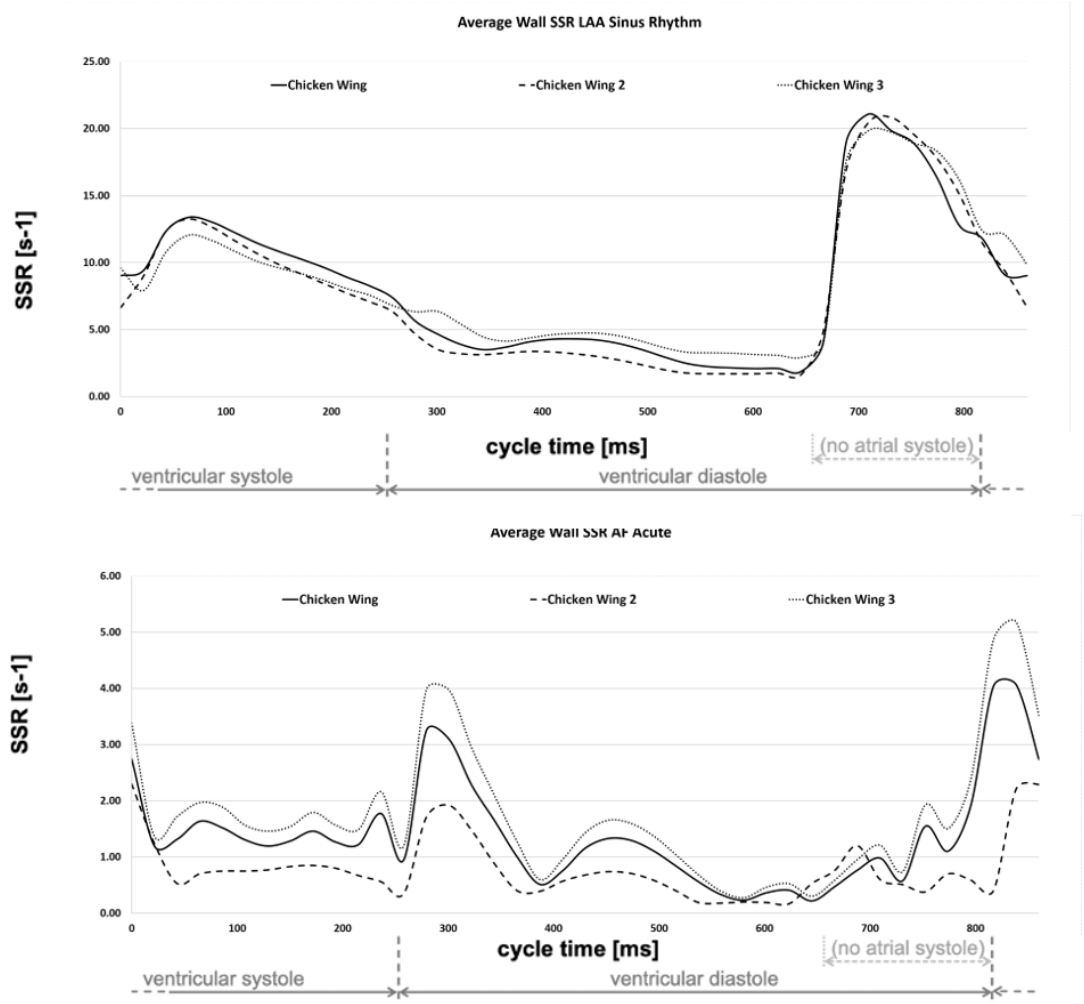

Figure 64 Average wall SSR estimated for tree chicken wing models in sinus rhythm (top) and, acute AF chronic AF (bottom) conditions.

To identify the regions of potential risk of thrombosis, Figure 66 shows the fluid wall that remains exposed throughout the cycle to SSR values below 10 and 5 $s^{-1.}$ The percentage of the left atrial appendage area exposed to SSR values below 10 and 5 s^{-1} for the entire cycle is summarized in Table 9.

The morphologies analysed, belonging to the same family, in the case in question Chicken Wing describe SSR curves that record values that differ significantly from each other. This evidence is especially marked in the AF Acute regimen. For these reasons, these early results suggest that the current morphological classification is inadequate in terms of evaluating thromboembolic risk.

Starting from the assumption that a specific left atrial appendage is identified in a specific family, it is not excluded that this registers an exposure to thromboembolic risk other than that which is expected.

Although there is a grouping based on morphological assessments, this same classification does not have a direct correlation with the probability of clot formation under conditions of atrial fibrillation.

Therefore, it is possible to hypothesize that the introduction of other parameters influences the exposure to thromboembolic risk more than the exposure to a specific morphological family.

In fact, the first results suggest that it is possible to identify other anatomical parameters that directly influence the probability of formation of a clot such as the number of folds, trabeculae rather than the presence of more or less pronounced lobes.

It remains correct to note that the sample of cases to be evaluated should be expanded to confirm this first indication, however

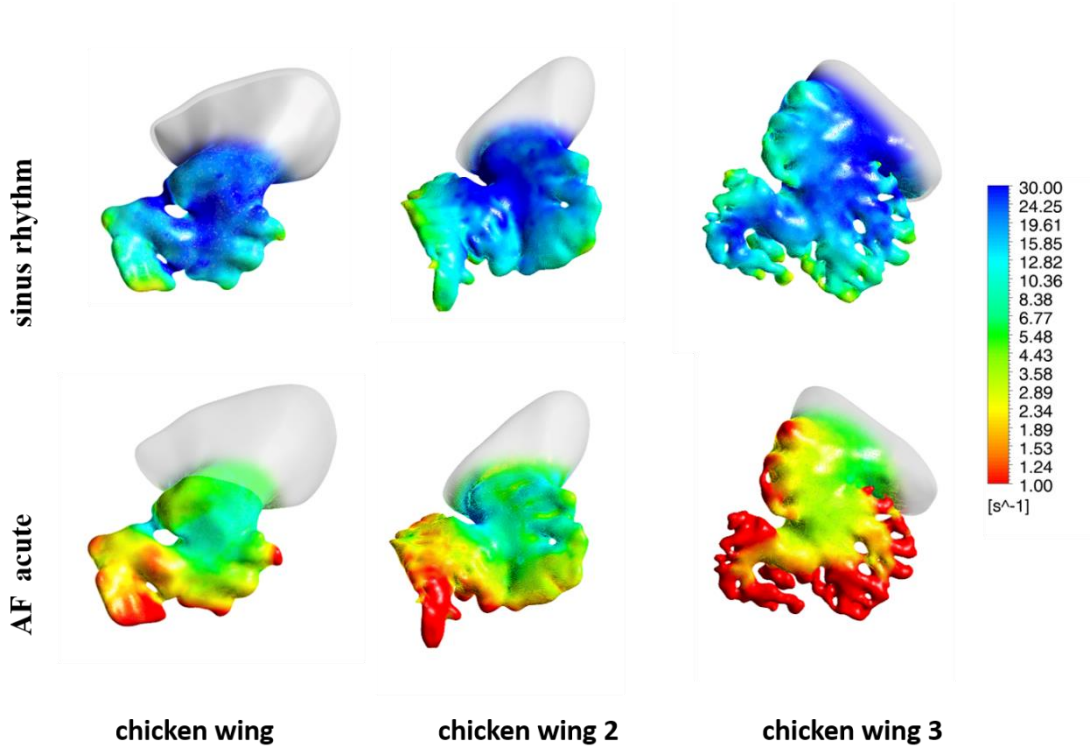

Figure 65 Colour maps of the maximum wall SSR at the instant of the cycle when they reach the maximum value, estimated for tree models and two operating conditions for Chicken Wing morphology

Table 9 Percentage of left atrial appendage area exposed to SSR values below 10 and 5 s-1 for cycle for tree chicken wing models

	Sinus Rhythm		*AF Acute*	
	$< 5\ s^{-1}$	$< 10\ s^{-1}$	$< 5\ s^{-1}$	$< 10\ s^{-1}$
Chicken Wing	3 %	17 %	64 %	93 %
Chicken Wing 2	3 %	22 %	94 %	99 %
Chicken Wing 3	3 %	21 %	61 %	83 %

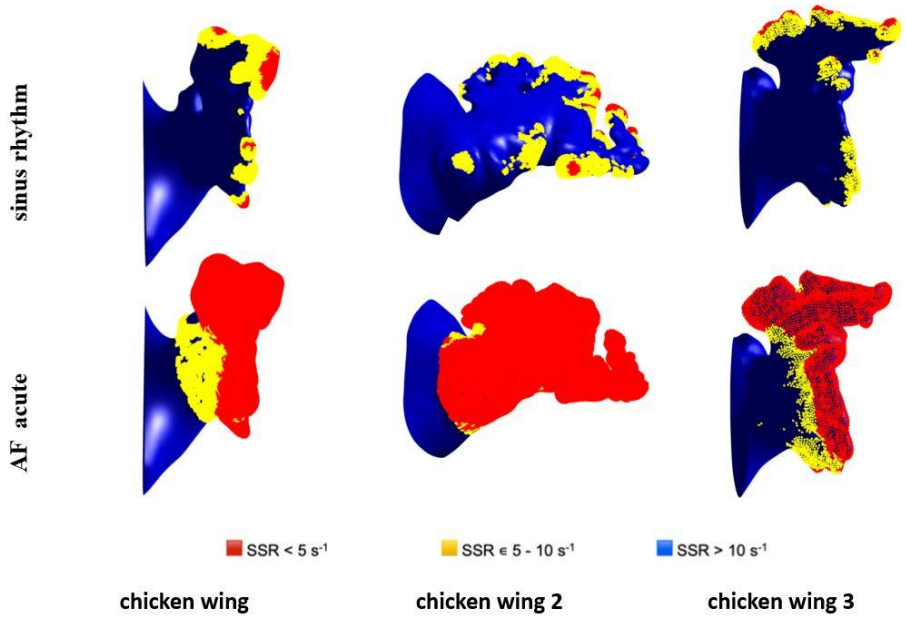

Figure 66 Risk area maps in: Sinus Rhythm and AF Acute for each chicken wing model

Also, in this case an evaluation is made of the maximum speed expected during the cycle at the cross section of the orifice of the left atrial appendage for the three different simulations of the chicken wing models and reported in Table 10.

The curves of the SSR values as a function of the percentage of associated risk area are finally represented in Figure 67

Table 10 Maximum velocity in: Sinus Rhythm and AF Acute [cm/s] for each chicken wing model

	Sinus Rhythm	*AF Acute*
Chicken Wing	15	2.5
Chicken Wing 2	12	2.4

Chicken Wing 3	13	4.1

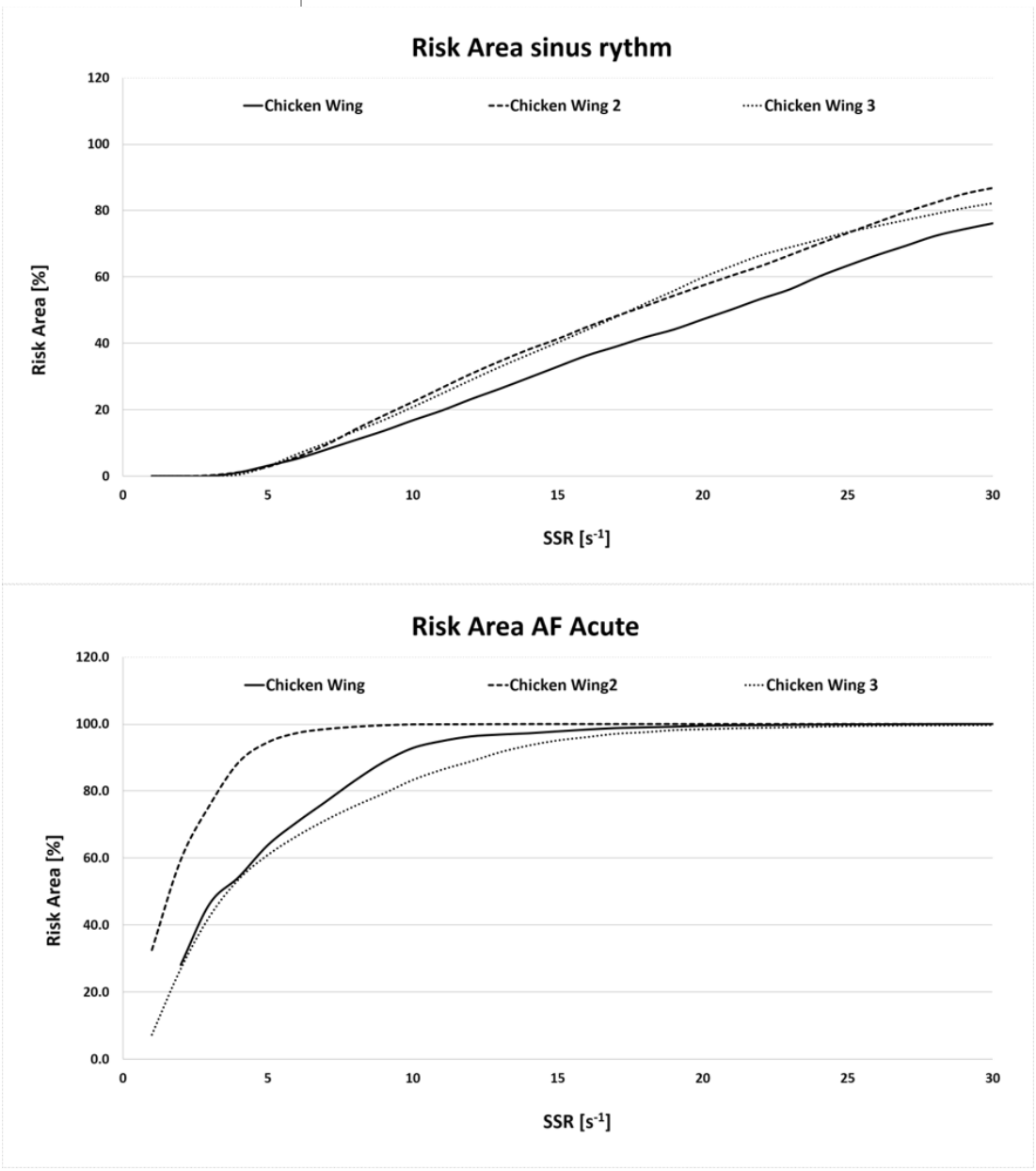

Figure 67 Risk Area curve for each chicken wing model

5. Discussion

Although the material properties and contraction parameters were set for the chicken wing model, under sinus rhythm conditions they produce very similar percentage volume changes in all models (approximately 57%), with the exception of cauliflower, which experiences volume variations around 30% largest (Table 5). The different behaviour of this model could be associated with the fact that it was the only one in which the trabecular structures were absent. These can act as connecting rods between the two main walls defining the appendage chamber, thus reducing the ability of the left atrial appendage to substantially change its shape under the effect of internal and external loads.

These differences are well reflected in the mean wall SSR in the left atrial appendage region, which is very similar for chicken wing, cactus, and windsock patterns throughout the cardiac cycle, peaking during active contraction. at values around 20 s^{-1} and seems to be amplified by about 30% for cauliflower (Figure 59 above).

In conditions of acute and chronic atrial fibrillation, the volume changes are drastically reduced for all cases by more than an order of magnitude, with the cactus model showing the greatest volume change and the windsock the lowest, both for acute and chronic conditions (Table 5).

Volume variations for chronic models were expected to be slightly greater, due to the stronger displacements produced by the same pressure acting on larger sections.

Interestingly, although the mean wall SSR in the left atrial appendage region still appears to relate well to the change in volume for each condition, it only decreases to about one-fifth of that expected in acute sinus rhythm and to a third in the case of the chronic case. Globally, the SSR levels predicted by the models compare well with those indicated in Vella (2021a), although that study identified higher values observed in acute conditions than in extended chronic conditions. This discrepancy may be due to the fact that in Vella (2021a) displacements of the walls of the left atrial appendage were imposed, limiting the interaction between the different extension of the wall and the elastic expansion and recoil of the structure. This suggests that FSI approaches are better suited to capture the different factors that control the phenomenon.

Comparison of the diagrams in Figure 59 for sinus rhythm and atrial fibrillation conditions indicates that the increase in wall SSR is not only associated with the active contraction that produces atrial systole, but the consequent relaxation phase is equally important. This produces a sustained increase in SSR for ventricular systole. During this phase, when there is no flow exiting the atrial chamber through the mitral valve, relaxation of the left atrial appendage produces a movement of flow that prevents blood stasis and all the potential associated risks (a similar effect is to be expected for the atrium).

The colour maps of the wall SSR distribution (Figure 60) indicate that, under normal conditions, the shear rate decreases at the distal edges and, in particular, after the trabeculae and at the lobes.

Knees, like those that characterise the main body of the chicken wing and the windsock, are also associated with some reduction in cutting speed.

These effects become more pronounced and extensive in conditions of left atrial fibrillation, especially in acute configurations, maintaining the same spatial distribution.

The risk maps in Figure 61 offer a clearer view of the regions where flow conditions that promote thickening and clotting of the blood are most likely to occur. These at-risk regions are extremely small (less than 5% of the left atrial appendage surface is constantly below 5 s^{-1}) and confined to the distal portion of the lobes for the healthy case, but occupy over 55% under conditions of acute atrial fibrillation.

This confirms that the active contraction of the left atrial appendage plays a clear and marked role on the correct hemodynamic of the region, allowing adequate washing and reducing the risk of clot formation.

The risk maps also show very clearly the crucial role of the lobes (Figure 61a) and knees (see yellow regions in Figure 61b) in establishing low shear regions.

The general behaviour appears to be very homogeneous for all models, with the exception of the major changes in volume during the cycle and the wall SSR predicted for cauliflower under sinus rhythm conditions (this morphology is rare and reported in only about 3% of patients, according to Di Biase (2012).

In conditions of atrial fibrillation, despite the significant morphological differences, all models are well aligned in terms of shear rate and predicted risk level.

The predicted orifice velocities were lower than those clinically detected by clinical studies (Fukuda, 2003).

As regards the comparative analysis between morphologies belonging to the same class, the relevant aspect is mainly recorded in conditions of atrial fibrillation. The same models identified as belonging to the chicken wing class present a markedly different exposure to thromboembolic risk.

In particular, the chicken wing 2 morphology presents a percentage of the most exposed risk area of all. This evidence is maintained in the curves present in the diagram of Figure 64, in addition to presenting the peak of maximum velocity at the lowest orifice among the three.

Consistent with the hypothesis that the current morphological classification has some limitations, relative to the associated thromboembolic risk, and that other parameter that could be defined morpho-structural such as folds and trabeculae can be associated with the evaluation of thromboembolic risk.

A direct comparison is not possible, since the velocity measured in patients by echocardiography also includes orifice movement as an effect of atrial movement, which not is considered in the model presented. Interestingly, although velocities decrease substantially as a result of atrial fibrillation (Table 3), no direct relationship can be found between the magnitude of the velocity at the orifice and the risk estimate. In fact, the velocity at the orifice depends on the rate of variation of the volume and on the cross section of the orifice, so it is not directly related to the hemodynamic that is established in the distal portion of the appendage.

5.1 Limitations

The study is based on a series of hypotheses and simplifications about the modelled region, the boundary conditions, the material properties and the rheological characteristics of the blood. Although analysis of the atrial appendage alone may overlook the effect of complex fluid dynamics established in the left atrium, the magnitude of this contribution on the estimated velocities and shear rates on the left atrial appendage from previous studies typically dissipates in the first third of appendage.

Furthermore, flow patterns in the atrium are highly dependent on a number of boundary conditions, such as pressure in each pulmonary vein or flow through the mitral valve, modelling of which requires additional assumptions and uncertainties.

The wall tissue was modelled as linear elastic, with an intermediate Young's modulus between that in the regions of low and high stiffness in animal tests. Although this choice simplifies the study and avoids substantial alterations in patient-specific morphologies, the compliance of the atrial wall contributes directly to the component of volume change associated with the passive response to pressure. Hence, its role on the AF behaviour may be relevant. Furthermore, it is not known whether and how this parameter changes during remodelling.

This also applies to the wall thickness, which was selected on the basis of animal data and maintained for all models.

The boundary conditions, in terms of inlet pressure and contraction, were designed on the basis of the scarce information available found on volume changes and applied identically to all models.

The availability of tests from healthy and post-mortem human specimens with atrial fibrillation would be essential to increase the reliability of the model. Finally, the blood was assumed to be Newtonian, thus underestimating the increase in viscosity in regions of prolonged low shear rate. This is a conservative assumption, which underestimates the expected stagnation and clotting potential.

5.2 Presentation of the results

Memories presented at national conferences and seminars:

- Vella, D., **Musotto, G.**, Bosi, G. M., B. Zuccarello & Burriesci, G. "Influence of Cardiac Chambers Contractility on Embolic Thrombus Risk", presented al 48° Convegno Nazionale AIAS, Assisi, 4-7 September 2019.

- Vella, D., **Musotto, G.**, Bosi, G. M., B. Zuccarello & Burriesci, G; "Prediction of thromboembolic events in Atrial Fibrillation" presented al Ri.MED Research Retreat, Palermo, 23 October 2019.

- **Musotto G**., Monteleone A., Vella D., Zuccarello B., Bosi G. M., & Burriesci, G; "A thrombotic risk numerical study based on the left atrial appendage morphology" presented al Ri.MED Research Retreat, Palermo, 17 December 2021.

Memories presented at international conferences (accepted):

- **Musotto G**, Monteleone A., Vella D., Bosi G. M., Zuccarello B., Pantano A, Pitarresi G. Burriesci, G; "A Patient Specific numerical study of Fluid Structure Interaction (FSI) to evaluate a thromboembolic risk map on the Left Atrial Appendage. *9th World Congress of Biomechanics* – 10-14th July 2022.

Scientific article in international journals.

- Vella, D., Monteleone, A., **Musotto, G.**, Bosi, G. M., & Burriesci, G. (2021). Effect of the Alterations in Contractility and Morphology Produced by Atrial Fibrillation on the Thrombosis Potential of the Left Atrial Appendage. *Frontiers in Bioengineering and Biotechnology*, vol. 9, pp.147-160.

Submitted and being evaluated:

- **Musotto G**, Monteleone A, Vella D., Di Leonardo S., Viola A., Pitarresi G., Zuccarello B., Pantano A., Cook A., Bosi, G. M., & Burriesci, G., "The role of patient specific morphological features of the left atrial appendage on the thromboembolic risk under atrial fibrillation"; *Frontiers in Cardiovascular Medicine;*

6. Conclusion

This work begins with an in-depth study of the problem of atrial fibrillation and explores the numerical methods currently used to study the problem from a computational point of view.

A study work related to population specific geometric models is presented, using CFD simulations, that underline the importance of the contractile effect of the left atrial appendage and of volumetric remodulations due to the pathological condition.

Then, four different patient-specific geometric models of the left atrial appendage are analysed and a comparative study between three models belonging to the same morphological family (chicken wing) is performed. This is necessary to study the mechanisms that promote clot formation under conditions of atrial fibrillation.

The analysis performed through computational fluid-structure interaction simulations (FSI), modelling the active and passive contractility of the left atrial appendage walls in sinus rhythm and atrial fibrillation condition, also simulating left atrial appendage remodelling typically caused by persistent atrial fibrillation.

The study confirms that the active contractility of the left atrial appendage muscle wall is essential to ensure physiologically healthy flow and its impairment caused by AF conditions is the main factor promoting hemodynamic conditions related to thromboembolic risk.

Left atrial appendage remodelling typically produced by persistent atrial fibrillation may result in improved flow conditions, due to increased passive motility of the appendage walls.

There appeared to be some correlation between the change in volume experienced by the left atrial appendage during the cardiac cycle and the SSR. The greatest changes in volume are recorded in sinus rhythm regime and are similar for all analysed models, with the exception of Cauliflower. Of all morphologies, the latter is devoid of trabeculae connecting the two main walls of the left atrial appendage, thus increasing the ability of the left atrial appendage to substantially change its shape with respect to the contractile surface.

No substantial differences were observed between models in terms of critical flow parameters, indicating that morphological class may not be directly associated with thromboembolic risk. However, regions with very low SSR appeared to be concentrated in specific anatomical areas among the various models studied, particularly in the lobes, after highly trabeculated regions and in areas characterized by sudden bends. These can act as nucleation sites for clot formation. The presence of trabeculae also appeared to play a role in limiting the percentage change in volume under healthy conditions, which was similar for all models except the one without trabeculations, which showed substantially greater volume changes. Although the blood velocity at the left atrial appendage orifice can obviously distinguish between healthy cases and those with atrial fibrillation, in diseased conditions this does not appear to be directly related to the risk of clotting.

The observations summarised above suggest that a different classification, based on local characteristics rather than the global macroscopic form of left atrial appendage, may serve as the best descriptor of thromboembolic risks and FSI models that allow simulation of active contraction and interaction between tissues and blood are fundamental to provide a better understanding of the phenomenon.

7. Appendix

7.1.1 MATLAB script for the evaluation of results maps

```
clear all;close all;clc

importstl=stlread('CW.stl');
files = dir('*.csv');
num_files = length(files);
results = cell(length(files), 1);

% Coordinates of the Chicken Wing Sinus Rhythm plane

p0=[0.133794  0.14817  -0.19746];

p1=[0.145571  0.158883 -0.199698];

p2=[0.150725  0.153238 -0.205536];

% Equation of the plane ax+by+cz+d=0

a=det([p1(2)-p0(2) p1(3)-p0(3)
    p2(2)-p0(2) p2(3)-p0(3)]);

b=-det([p1(1)-p0(1) p1(3)-p0(3)
    p2(1)-p0(1) p2(3)-p0(3)]);

c=det([p1(1)-p0(1) p1(2)-p0(2)
    p2(1)-p0(1) p2(2)-p0(2)]);

d=-a*p0(1)-b*p0(2)-c*p0(3);

% Distance from the floor

 p=rand(1,3);
dist=((a*p(1)+b*p(2)+c*p(3)+d))/sqrt(a^2+b^2+c^2);



for i = 1:num_files
  results{i} = csvread(files(i).name,6,0);
  node_list(i,:) = results{i}(1:end,1);
  x(i,:) = results{i}(1:end,2);
  y(i,:) = results{i}(1:end,3);
  z(i,:) = results{i}(1:end,4);
  SSR(i,:) = results{i}(1:end,5);
End
```

```
% node is contained in results{i}(1:end,1)
% x is contained in results{i}(1:end,2)
% x is contained in results{i}(1:end,3)
% x is contained in results{i}(1:end,4)
% SSR is contained in results{i}(1:end,5)

nl = size(node_list,2);

% Calculation of the number of nodes of the LAA

nodi_LAA = 0;
fuori = zeros(nl);
for i = 1:1
       for n = 1:nl
           p=[x(i,n) y(i,n) z(i,n)];
           dist=((a*p(1)+b*p(2)+c*p(3)+d))/sqrt(a^2+b^2+c^2);

            if dist > 0
                fuori(n) = 1;
            else
                nodi_LAA = nodi_LAA+1;
             end
       end
end

% Calculation of the average temporal SSR

mean_SSR = zeros(length(num_files),num_files);


time = [0:0.0215:0.86-0.0215];



for i = 1:num_files
    for n = 1:nl
         if fuori(n) == 0
             val = SSR(i,n);
             mean_SSR(i) = mean_SSR(i)+val;
         end
    end
end
mean_SSR = mean_SSR/nodi_LAA;

figure
plot(time,mean_SSR)

mean_SSR = mean_SSR';
time = time';
```

```
% ------------------------------------------------------------------------
-
% Threshold value of SSR: variable

for rt = 1:1:100

    SSR_t(rt) = rt;
    check = zeros(nl);
    for i = 1:num_files
        for n = 1:nl
            if fuori(n) == 0
                if (SSR(i,n) > SSR_t(rt))
                    check(n) = 1;
                end
            end
        end
    end

    count = 0;
    for n = 1:nl
        if fuori(n) == 0
            if ( check(n) == 0)
                count = count+1;
            end
        end
    end

    % Percent of contour nodes which have a SSR value under the defined
    % Threshold value (SSR_t) for the whole period of the cardiac cycle

    percent(rt) = count/nodi_LAA*100;
end
figure
plot(SSR_t,percent,'-r','LineWidth',2)
ylabel('Risk Area %')
xlabel('SSR Threshold Value [1/s]')

excel (:,1) = SSR_t (:);
excel (:,2) = percent (:);
```

```
% ------------------------------------------------------------------------
-

% Threshold value of SSR

SSR_t = 5;
%%%%%%%%%%%%%%
SSR_t2 = 10;
%%%%%%%%%%%%%%

check = zeros(nl);
for i = 1:num_files
    for n = 1:nl
        if fuori(n) == 0
            if (SSR(i,n) > SSR_t)
                check(n) = 1;
            end
        end
    end
end

count = 0;

for n = 1:nl
    if fuori(n) == 0
        if ( check(n) == 0)
            count = count+1;
            x_t(count) = x(1,n);
            y_t(count) = y(1,n);
            z_t(count) = z(1,n);
        end
    end
end

% Percent of contour nodes which have a SSR value under the defined
% Threshold value (SSR_t) for the whole period of the cardiac cycle

percent = count/nodi_LAA*100 % with SSR_t = 5


check = zeros(nl);
for i = 1:num_files
    for n = 1:nl
        if fuori(n) == 0
            if SSR(i,n) > SSR_t2
                check(n) = 1;
            end
        end
    end
end

count = 0;
for n = 1:nl
    if fuori(n) == 0
```

```
        if ( check(n) == 0)
            count = count+1;
            x_t2(count) = x(1,n);
            y_t2(count) = y(1,n);
            z_t2(count) = z(1,n);
        end
    end
end

% Percent of contour nodes which have a SSR value under the defined
% Threshold value (SSR_t) for the whole period of the cardiac cycle


figure
%plot3(x(1,:),y(1,:),z(1,:),'.b')
%hold on
plot3(x_t2,y_t2,z_t2,'.y','MarkerSize',20)
hold on
plot3(x_t,y_t,z_t,'.r','MarkerSize',20)
hold on
trimesh(importstl,'Edgecolor','none','Facecolor','b')

% trimesh(importstl,'Edgecolor','none','Facecolor',[0.99 0.99 0.99])
light
lighting phong

axis image
title('SSR Chicken Wing Sinus Rhythm')
legend ('Over 10', 'Between 5 and 10','Less than 5')

% hold on
% plot3(p0(1),p0(2),p0(3),'*b','MarkerSize',50)
% hold on
% plot3(p1(1),p1(2),p1(3),'*b','MarkerSize',50)
% hold on
% plot3(p2(1),p2(2),p2(3),'*b','MarkerSize',50)

%
% [xp,yp] = meshgrid(0.1:0.01:0.2,0.1:0.01:0.2);
% xp=0:0.01:0.1;
% yp=0:0.01:0.1;
% zp=(-a*xp-b*yp-d)/c;
% p=[0.132893905000000    0.144480765000000   -0.179775879000000]
% dist=((a*p(1)+b*p(2)+c*p(3)+d))/sqrt(a^2+b^2+c^2);
%
% figure
% plot3(x(1,:),y(1,:),z(1,:),'.b',p(1),p(2),p(3),'.r',xp,yp,zp,'k')
% axis image
```

7.1.2 Presentation of the first results

The results briefly described above were presented at the 48th AIAS National Conference, held in Assisi between 4 and 7 September 2019. The results of the comparison of models in sinus rhythm conditions and in pathological conditions of atrial fibrillation, confirmed the importance of introducing deformability, with lower SSR values in atrial fibrillation conditions than those recorded in sinus rhythm. These latest results were presented in poster format at the Ri.MED Foundation Retreat 2019 held in Palermo on 23 October 2019. (See Figure 68).

The work was further investigated and elaborated through the comparison carried out between four numerical models.

This study made it possible to obtain a broader evaluation of the problem that led to the publication of the document by (Vella et al., 2021a).

The presentation of this preliminary study was fundamental to investigate the problem of hemodynamic of the left atrial appendage with the numerical approach of FSI simulations.

This last model, although it had a greater computational effort required, allowed to achieve results that considered the complexity of the phenomenon and thus have a more precise response in terms of precision.

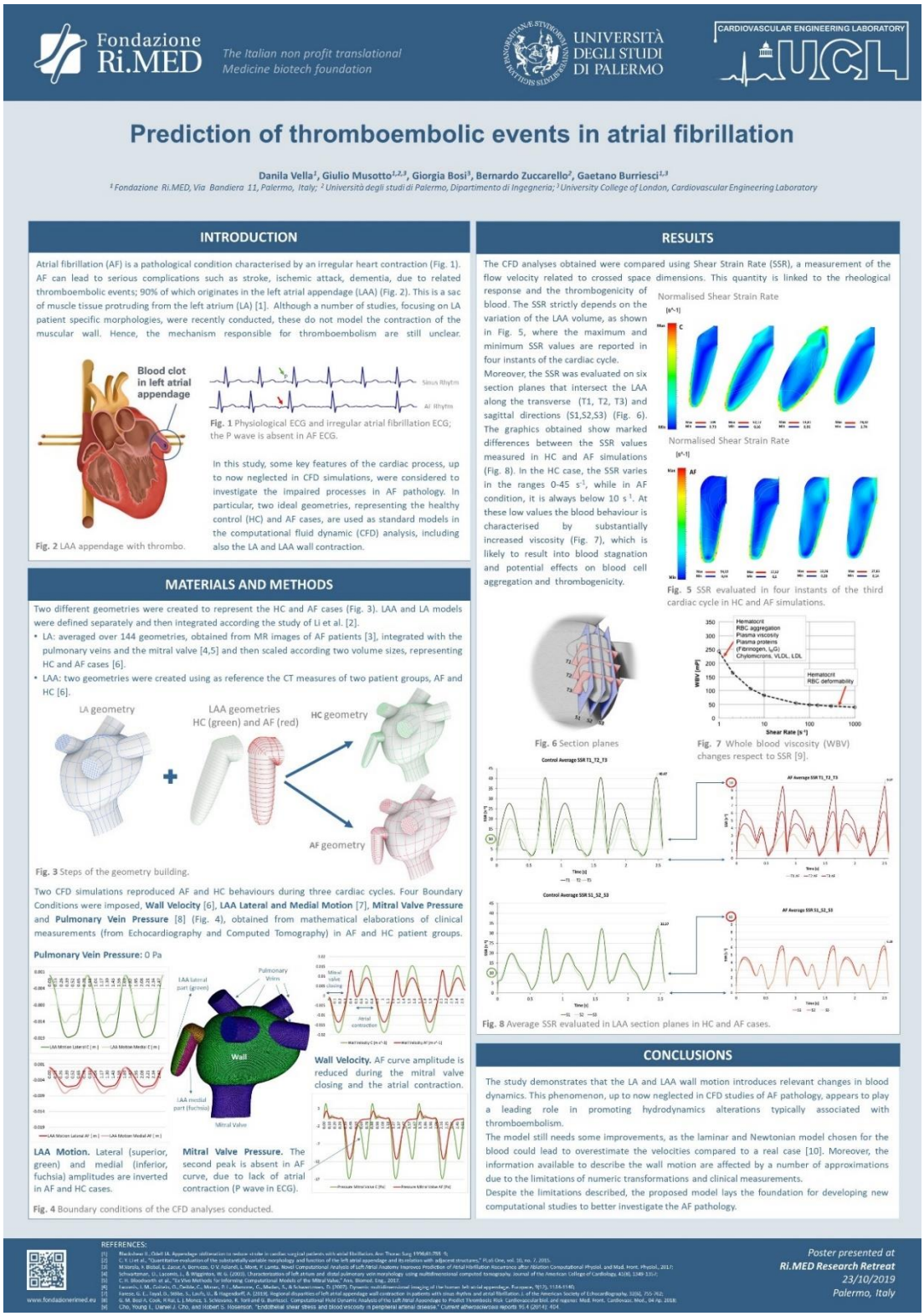

Figure 68 Poster Retreat of the Ri.MED Foundation held in Palermo on 23 October 2019.

8. Bibliography

Abrignani, M. G., & Colivicchi, F. (2015). Thromboembolic and hemorrhagic risk stratification in patients with atrial fibrillation. Part I: the thromboembolic risk. *Monaldi Archives for Chest Disease*, *80*(2). https://doi.org/10.4081/monaldi.2013.80

Ailawadi, G., Gerdisch, M. W., Harvey, R. L., Hooker, R. L., Damiano, R. J., Salamon, T., & Mack, M. J. (2011). Exclusion of the left atrial appendage with a novel device: Early results of a multicenter trial. *The Journal of Thoracic and Cardiovascular Surgery*, *142*(5), 1002-1009.e1. https://doi.org/10.1016/j.jtcvs.2011.07.052

Al-Saady, N. M., Obel, O. A., & Camm, A. J. (1999a). Left atrial appendage: structure, function, and role in thromboembolism. *Heart*, *82*(5), 547–554. https://doi.org/10.1136/hrt.82.5.547

Al-Saady, N. M., Obel, O. A., & Camm, A. J. (1999b). Left atrial appendage: structure, function, and role in thromboembolism. *Heart*, *82*(5), 547–554. https://doi.org/10.1136/hrt.82.5.547

Anand, M., Rajagopal, K., & Rajagopal, K. R. (2005). A Model for the Formation and Lysis of Blood Clots. *Pathophysiology of Haemostasis and Thrombosis*, *34*(2–3), 109–120. https://doi.org/10.1159/000089931

Apostolidis, A. J., Armstrong, M. J., & Beris, A. N. (2015). Modeling of human blood rheology in transient shear flows. *Journal of Rheology*, *59*(1), 275–298. https://doi.org/10.1122/1.4904423

Badimon, L., Badimon, J. J., Galvez, A., Chesebro, J. H., & Fuster, V. (1986). Influence of arterial damage and wall shear rate on platelet deposition. Ex vivo study in a swine model. *Arteriosclerosis: An Official Journal of the American Heart Association, Inc.*, *6*(3), 312–320. https://doi.org/10.1161/01.ATV.6.3.312

Benra, F.-K., Dohmen, H. J., Pei, J., Schuster, S., & Wan, B. (2011). A Comparison of One-Way and Two-Way Coupling Methods for Numerical Analysis of Fluid-Structure Interactions. *Journal of Applied Mathematics*, *2011*, 1–16. https://doi.org/10.1155/2011/853560

Björck, S., Palaszewski, B., Friberg, L., & Bergfeldt, L. (2013). Atrial Fibrillation, Stroke Risk, and Warfarin Therapy Revisited. *Stroke*, *44*(11), 3103–3108. https://doi.org/10.1161/STROKEAHA.113.002329

Bloodworth, C. H., Pierce, E. L., Easley, T. F., Drach, A., Khalighi, A. H., Toma, M., Jensen, M. O., Sacks, M. S., & Yoganathan, A. P. (2017). Ex Vivo Methods for Informing Computational Models of the Mitral Valve. *Annals of Biomedical Engineering*, *45*(2), 496–507. https://doi.org/10.1007/s10439-016-1734-z

Bosi, G. M., Cook, A., Rai, R., Menezes, L. J., Schievano, S., Torii, R., & Burriesci, G. (2018). Computational Fluid Dynamic Analysis of the Left Atrial Appendage to Predict Thrombosis Risk. *Frontiers in Cardiovascular Medicine*, *5*. https://doi.org/10.3389/fcvm.2018.00034

Budge, L. P., Shaffer, K. M., Moorman, J. R., Lake, D. E., Ferguson, J. D., & Mangrum, J. M. (2008). Analysis of in vivo left atrial appendage morphology in patients with atrial fibrillation: a direct comparison of transesophageal echocardiography, planar cardiac CT, and segmented three-dimensional cardiac CT. *Journal of Interventional Cardiac Electrophysiology*, *23*(2), 87–93. https://doi.org/10.1007/s10840-008-9281-7

Cabral, K. P. (2013). Pharmacology of the new target-specific oral anticoagulants. *Journal of Thrombosis and Thrombolysis*, *36*(2), 133–140. https://doi.org/10.1007/s11239-013-0929-5

Cadroy, Y., Horbett, T. A., & Hanson, S. R. (1989). Discrimination between platelet-mediated and coagulation-mediated mechanisms in a model of complex thrombus formation in vivo. *The Journal of Laboratory and Clinical Medicine*, *113*(4), 436—448. http://europepmc.org/abstract/MED/2522978

Casa, L. D. C., & Ku, D. N. (2017). Thrombus Formation at High Shear Rates. *Annual Review of Biomedical Engineering*, *19*(1), 415–433. https://doi.org/10.1146/annurev-bioeng-071516-044539

Chien, S. (1970). Shear Dependence of Effective Cell Volume as a Determinant of Blood Viscosity. *Science*, *168*(3934), 977–979. https://doi.org/10.1126/science.168.3934.977

Chnafa, C., Mendez, S., & Nicoud, F. (2014). Image-based large-eddy simulation in a realistic left heart. *Computers & Fluids*, *94*, 173–187. https://doi.org/10.1016/j.compfluid.2014.01.030

Colilla, S., Crow, A., Petkun, W., Singer, D. E., Simon, T., & Liu, X. (2013). Estimates of Current and Future Incidence and Prevalence of Atrial Fibrillation in the U.S. Adult Population. *The American Journal of Cardiology*, *112*(8), 1142–1147. https://doi.org/10.1016/j.amjcard.2013.05.063

Dawson, A. G., Asopa, S., & Dunning, J. (2010). Should patients undergoing cardiac surgery with atrial fibrillation have left atrial appendage exclusion? *Interactive CardioVascular and Thoracic Surgery*, *10*(2), 306–311. https://doi.org/10.1510/icvts.2009.227991

Dedè, L., Menghini, F., & Quarteroni, A. (2021). Computational fluid dynamics of blood flow in an idealized left human heart. *International Journal for Numerical Methods in Biomedical Engineering*, *37*(11). https://doi.org/10.1002/cnm.3287

di Biase, L., Santangeli, P., Anselmino, M., Mohanty, P., Salvetti, I., Gili, S., Horton, R., Sanchez, J. E., Bai, R., Mohanty, S., Pump, A., Cereceda Brantes, M., Gallinghouse, G. J., Burkhardt, J. D., Cesarani, F., Scaglione, M., Natale, A., & Gaita, F. (2012). Does the Left Atrial Appendage Morphology Correlate With the Risk of Stroke in Patients With Atrial Fibrillation? *Journal of the American College of Cardiology*, *60*(6), 531–538. https://doi.org/10.1016/j.jacc.2012.04.032

di Fusco, S. A., Colivicchi, F., Aspromonte, N., Tubaro, M., Aiello, A., & Santini, M. (2017). Direct oral anticoagulants in patients undergoing cardioversion: insight from randomized clinical trials. *Monaldi Archives for Chest Disease*, *87*(1). https://doi.org/10.4081/monaldi.2017.805

Ducci, A., Pirisi, F., Tzamtzis, S., & Burriesci, G. (2016a). Transcatheter aortic valves produce unphysiological flows which may contribute to thromboembolic events: An in-vitro study. *Journal of Biomechanics*, *49*(16), 4080–4089. https://doi.org/10.1016/j.jbiomech.2016.10.050

Ducci, A., Pirisi, F., Tzamtzis, S., & Burriesci, G. (2016b). Transcatheter aortic valves produce unphysiological flows which may contribute to thromboembolic events: An in-vitro study. *Journal of Biomechanics*, *49*(16), 4080–4089. https://doi.org/10.1016/j.jbiomech.2016.10.050

European Heart Association. (n.d.). *CHA2DS2-VASc*. Retrieved May 3, 2022, from https://www.heartassociation.eu/e-se-il-mio-score-cha2ds2-vasc-fosse-uguale-uno/?lang=it

Farese, G. E., Tayal, B., Stöbe, S., Laufs, U., & Hagendorff, A. (2019). Regional Disparities of Left Atrial Appendage Wall Contraction in Patients With Sinus Rhythm and Atrial Fibrillation. *Journal of the American Society of Echocardiography*, *32*(6), 755–762. https://doi.org/10.1016/j.echo.2019.01.016

Fedorov, A., Beichel, R., Kalpathy-Cramer, J., Finet, J., Fillion-Robin, J.-C., Pujol, S., Bauer, C., Jennings, D., Fennessy, F., Sonka, M., Buatti, J., Aylward, S., Miller, J. v., Pieper, S., & Kikinis, R. (2012). 3D Slicer as an image computing platform for the Quantitative Imaging Network. *Magnetic Resonance Imaging*, *30*(9), 1323–1341. https://doi.org/10.1016/j.mri.2012.05.001

Fedosov, D. A., Pan, W., Caswell, B., Gompper, G., & Karniadakis, G. E. (2011). Predicting human blood viscosity in silico. *Proceedings of the National Academy of Sciences*, *108*(29), 11772–11777. https://doi.org/10.1073/pnas.1101210108

Fukuda, N. (2003). Transthoracic Doppler echocardiographic measurement of left atrial appendage blood flow velocity: comparison with transoesophageal measurement. *European Journal of Echocardiography*, *4*(3), 191–195. https://doi.org/10.1016/S1525-2167(02)00166-X

Fukunami, M., Yamada, T., Ohmori, M., Kumagai, K., Umemoto, K., Sakai, A., Kondoh, N., Minamino, T., & Hoki, N. (n.d.). *Detection of Patients at Risk for Paroxysmal Atrial Fibrillation During Sinus Rhythm by P Wave-Triggered Signal-Averaged Electrocardiogram*. http://ahajournals.org

Furie, B., & Furie, B. C. (2008). Mechanisms of Thrombus Formation. *New England Journal of Medicine*, *359*(9), 938–949. https://doi.org/10.1056/NEJMra0801082

Gorelick, P. B. (2004). TIA incidence and prevalence: The Stroke Belt perspective. *Neurology*, *62*(Issue 8, Supplement 6), S12–S14. https://doi.org/10.1212/WNL.62.8_suppl_6.S12

Hagiwara, Y., Fujita, H., Oh, S. L., Tan, J. H., Tan, R. S., Ciaccio, E. J., & Acharya, U. R. (2018). Computer-aided diagnosis of atrial fibrillation based on ECG Signals: A review. *Information Sciences*, *467*, 99–114. https://doi.org/10.1016/j.ins.2018.07.063

Hindricks, G., Potpara, T., Dagres, N., Arbelo, E., Bax, J. J., Blomström-Lundqvist, C., Boriani, G., Castella, M., Dan, G.-A., Dilaveris, P. E., Fauchier, L., Filippatos,

G., Kalman, J. M., la Meir, M., Lane, D. A., Lebeau, J.-P., Lettino, M., Lip, G. Y. H., Pinto, F. J., … Zakirov, N. U. (2021). 2020 ESC Guidelines for the diagnosis and management of atrial fibrillation developed in collaboration with the European Association for Cardio-Thoracic Surgery (EACTS). *European Heart Journal*, *42*(5), 373–498. https://doi.org/10.1093/eurheartj/ehaa612

Hirschhorn, M., Tchantchaleishvili, V., Stevens, R., Rossano, J., & Throckmorton, A. (2020a). Fluid–structure interaction modeling in cardiovascular medicine – A systematic review 2017–2019. *Medical Engineering & Physics*, *78*, 1–13. https://doi.org/10.1016/j.medengphy.2020.01.008

Hirschhorn, M., Tchantchaleishvili, V., Stevens, R., Rossano, J., & Throckmorton, A. (2020b). Fluid–structure interaction modeling in cardiovascular medicine – A systematic review 2017–2019. *Medical Engineering & Physics*, *78*, 1–13. https://doi.org/10.1016/j.medengphy.2020.01.008

Holmes, D. R., Reddy, V. Y., Turi, Z. G., Doshi, S. K., Sievert, H., Buchbinder, M., Mullin, C. M., & Sick, P. (2009). Percutaneous closure of the left atrial appendage versus warfarin therapy for prevention of stroke in patients with atrial fibrillation: a randomised non-inferiority trial. *The Lancet*, *374*(9689), 534–542. https://doi.org/10.1016/S0140-6736(09)61343-X

Jariwala, S., Horner, J. S., Wagner, N. J., & Beris, A. N. (2020). Application of population balance-based thixotropic model to human blood. *Journal of Non-Newtonian Fluid Mechanics*, *281*, 104294. https://doi.org/10.1016/j.jnnfm.2020.104294

Javani, S., Gordon, M., & Azadani, A. N. (2016). Biomechanical Properties and Microstructure of Heart Chambers: A Paired Comparison Study in an Ovine Model. *Annals of Biomedical Engineering*, *44*(11), 3266–3283. https://doi.org/10.1007/s10439-016-1658-7

Jia, D., Jeon, B., Park, H.-B., Chang, H.-J., & Zhang, L. T. (2019). Image-Based Flow Simulations of Pre- and Post-left Atrial Appendage Closure in the Left Atrium. *Cardiovascular Engineering and Technology*, *10*(2), 225–241. https://doi.org/10.1007/s13239-019-00412-7

Kalaria, R. N., Maestre, G. E., Arizaga, R., Friedland, R. P., Galasko, D., Hall, K., Luchsinger, J. A., Ogunniyi, A., Perry, E. K., Potocnik, F., Prince, M., Stewart, R., Wimo, A., Zhang, Z.-X., & Antuono, P. (2008). Alzheimer's disease and vascular dementia in developing countries: prevalence, management, and risk factors. *The Lancet Neurology*, *7*(9), 812–826. https://doi.org/10.1016/S1474-4422(08)70169-8

Kamel, H., Elkind, M. S. V., Bhave, P. D., Navi, B. B., Okin, P. M., Iadecola, C., Devereux, R. B., & Fink, M. E. (2013). Paroxysmal Supraventricular Tachycardia and the Risk of Ischemic Stroke. *Stroke*, *44*(6), 1550–1554. https://doi.org/10.1161/STROKEAHA.113.001118

Khan, A. A., & Lip, G. Y. H. (2019). The prothrombotic state in atrial fibrillation: pathophysiological and management implications. *Cardiovascular Research*, *115*(1), 31–45. https://doi.org/10.1093/cvr/cvy272

Kimura, T., Takatsuki, S., Inagawa, K., Katsumata, Y., Nishiyama, T., Nishiyama, N., Fukumoto, K., Aizawa, Y., Tanimoto, Y., Tanimoto, K., Jinzaki, M., & Fukuda, K. (2013). Anatomical characteristics of the left atrial appendage in cardiogenic stroke with low CHADS2 scores. *Heart Rhythm*, *10*(6), 921–925. https://doi.org/10.1016/j.hrthm.2013.01.036

Kim, Y., Kim, K., & Park, Y. (2012). Measurement Techniques for Red Blood Cell Deformability: Recent Advances. In *Blood Cell - An Overview of Studies in Hematology*. InTech. https://doi.org/10.5772/50698

Korhonen, M., Muuronen, A., Arponen, O., Mustonen, P., Hedman, M., Jäkälä, P., Vanninen, R., & Taina, M. (2015). Left Atrial Appendage Morphology in Patients with Suspected Cardiogenic Stroke without Known Atrial Fibrillation. *PLOS ONE*, *10*(3), e0118822. https://doi.org/10.1371/journal.pone.0118822

Krahn, A. D., Manfreda, J., Tate, R. B., Mathewson, F. A. L., & Cuddy, T. E. (1995). The natural history of atrial fibrillation: Incidence, risk factors, and prognosis in the manitoba follow-up study. *The American Journal of Medicine*, *98*(5), 476–484. https://doi.org/10.1016/S0002-9343(99)80348-9

Lacomis, J. M., Goitein, O., Deible, C., Moran, P. L., Mamone, G., Madan, S., & Schwartzman, D. (2007a). Dynamic multidimensional imaging of the human left atrial appendage. *EP Europace*, *9*(12), 1134–1140. https://doi.org/10.1093/europace/eum227

Lacomis, J. M., Goitein, O., Deible, C., Moran, P. L., Mamone, G., Madan, S., & Schwartzman, D. (2007b). Dynamic multidimensional imaging of the human left

atrial appendage. *EP Europace*, *9*(12), 1134–1140. https://doi.org/10.1093/europace/eum227

Lansberg, M. G., Albers, G. W., Beaulieu, C., & Marks, M. P. (2000). Comparison of diffusion-weighted MRI and CT in acute stroke. *Neurology*, *54*(8), 1557–1561. https://doi.org/10.1212/WNL.54.8.1557

Leiderman, K., & Fogelson, A. L. (2011). Grow with the flow: a spatial-temporal model of platelet deposition and blood coagulation under flow. *Mathematical Medicine and Biology*, *28*(1), 47–84. https://doi.org/10.1093/imammb/dqq005

Li, C.-Y., Gao, B.-L., Liu, X.-W., Fan, Q.-Y., Zhang, X.-J., Liu, G.-C., Yang, H.-Q., Feng, P.-Y., Wang, Y., & Song, P. (2015). Quantitative Evaluation of the Substantially Variable Morphology and Function of the Left Atrial Appendage and Its Relation with Adjacent Structures. *PLOS ONE*, *10*(7), e0126818. https://doi.org/10.1371/journal.pone.0126818

Lim, K. H., Yeo, J. H., & Duran, C. M. (2005). Three-dimensional asymmetrical modeling of the mitral valve: a finite element study with dynamic boundaries. *J Heart Valve Dis*, *14*(3), 386–392.

Lip, G. Y. H., Nieuwlaat, R., Pisters, R., Lane, D. A., & Crijns, H. J. G. M. (2010). Refining Clinical Risk Stratification for Predicting Stroke and Thromboembolism in Atrial Fibrillation Using a Novel Risk Factor-Based Approach. *Chest*, *137*(2), 263–272. https://doi.org/10.1378/chest.09-1584

Manzano-Fernández, S., Pastor, F. J., Marín, F., Cambronero, F., Caro, C., Pascual-Figal, D. A., Garrido, I. P., Pinar, E., Valdés, M., & Lip, G. Y. H. (2008).

Increased Major Bleeding Complications Related to Triple Antithrombotic Therapy Usage in Patients With Atrial Fibrillation Undergoing Percutaneous Coronary Artery Stenting. *Chest*, *134*(3), 559–567. https://doi.org/10.1378/chest.08-0350

Masci, A., Barone, L., Dedè, L., Fedele, M., Tomasi, C., Quarteroni, A., & Corsi, C. (2019). The Impact of Left Atrium Appendage Morphology on Stroke Risk Assessment in Atrial Fibrillation: A Computational Fluid Dynamics Study. *Frontiers in Physiology*, *9*. https://doi.org/10.3389/fphys.2018.01938

Mason, P. K., Lake, D. E., DiMarco, J. P., Ferguson, J. D., Mangrum, J. M., Bilchick, K., Moorman, L. P., & Moorman, J. R. (2012). Impact of the CHA2DS2-VASc Score on Anticoagulation Recommendations for Atrial Fibrillation. *The American Journal of Medicine*, *125*(6), 603.e1-603.e6. https://doi.org/10.1016/j.amjmed.2011.09.030

Mega, J. L., & Simon, T. (2015). Pharmacology of antithrombotic drugs: an assessment of oral antiplatelet and anticoagulant treatments. *The Lancet*, *386*(9990), 281–291. https://doi.org/10.1016/S0140-6736(15)60243-4

Momtahan, N., Poornejad, N., Struk, J. A., Castleton, A. A., Herrod, B. J., Vance, B. R., Eatough, J. P., Roeder, B. L., Reynolds, P. R., & Cook, A. D. (2015). Automation of Pressure Control Improves Whole Porcine Heart Decellularization. *Tissue Engineering Part C: Methods*, *21*(11), 1148–1161. https://doi.org/10.1089/ten.tec.2014.0709

Mori, M., Kanzaki, H., Amaki, M., Ohara, T., Hasegawa, T., Takahama, H., Hashimura, K., Konno, T., Hayashi, K., Yamagishi, M., & Kitakaze, M. (2011). Impact of reduced left atrial functions on diagnosis of paroxysmal atrial fibrillation: Results from analysis of time-left atrial volume curve determined by two-dimensional speckle tracking. *Journal of Cardiology*, *57*(1), 89–94. https://doi.org/10.1016/j.jjcc.2010.08.006

Nattel, S. (2002). New ideas about atrial fibrillation 50 years on. *Nature*, *415*(6868), 219–226. https://doi.org/10.1038/415219a

Nattel, S., & Harada, M. (2014). Atrial Remodeling and Atrial Fibrillation. *Journal of the American College of Cardiology*, *63*(22), 2335–2345. https://doi.org/10.1016/j.jacc.2014.02.555

N Casson. (1959). A flow equation for pigment-oil suspensions of the printing ink type. *Rheology of Disperse Systems Rheology of Disperse Systems*, *Pergamon Press* , 84–104.

Nedios, S., Kornej, J., Koutalas, E., Bertagnolli, L., Kosiuk, J., Rolf, S., Arya, A., Sommer, P., Husser, D., Hindricks, G., & Bollmann, A. (2014). Left atrial appendage morphology and thromboembolic risk after catheter ablation for atrial fibrillation. *Heart Rhythm*, *11*(12), 2239–2246. https://doi.org/10.1016/j.hrthm.2014.08.016

Olesen, J., Torp-Pedersen, C., Hansen, M., & Lip, G. (2012). The value of the CHA2DS2-VASc score for refining stroke risk stratification in patients with atrial

fibrillation with a CHADS2 score 0–1: A nationwide cohort study. *Thrombosis and Haemostasis*, *107*(06), 1172–1179. https://doi.org/10.1160/TH12-03-0175

Onalan, O., Lashevsky, I., Hamad, A., & Crystal, E. (2005). Nonpharmacologic stroke prevention in atrial fibrillation. *Expert Review of Cardiovascular Therapy*, *3*(4), 619–633. https://doi.org/10.1586/14779072.3.4.619

OSTERMAYER, S., RESCHKE, M., BILLINGER, K., TREPELS, T., BUSCHEK, F., BAYARD, Y., & SIEVERT, H. (2003). Percutaneous Closure of the Left Atrial Appendage. *Journal of Interventional Cardiology*, *16*(6), 553–556. https://doi.org/10.1046/j.1540-8183.2003.01055.x

Otani, T., Al-Issa, A., Pourmorteza, A., McVeigh, E. R., Wada, S., & Ashikaga, H. (2016). A Computational Framework for Personalized Blood Flow Analysis in the Human Left Atrium. *Annals of Biomedical Engineering*, *44*(11), 3284–3294. https://doi.org/10.1007/s10439-016-1590-x

Petty, G. W., Brown, R. D., Whisnant, J. P., Sicks, J. D., O'Fallon, W. M., & Wiebers, D. O. (1999). Ischemic Stroke Subtypes. *Stroke*, *30*(12), 2513–2516. https://doi.org/10.1161/01.STR.30.12.2513

Ranucci, M., Laddomada, T., Ranucci, M., & Baryshnikova, E. (2014). Blood viscosity during coagulation at different shear rates. *Physiological Reports*, *2*(7), e12065. https://doi.org/10.14814/phy2.12065

Sanfilippo, A. J., Abascal, V. M., Sheehan, M., Oertel, L. B., Harrigan, P., Hughes, R. A., & Weyman, A. E. (1990). Atrial enlargement as a consequence of atrial

fibrillation. A prospective echocardiographic study. *Circulation*, *82*(3), 792–797. https://doi.org/10.1161/01.CIR.82.3.792

Schwartzman, D., Lacomis, J., & Wigginton, W. G. (2003). Characterization of left atrium and distal pulmonary vein morphology using multidimensional computed tomography. *Journal of the American College of Cardiology*, *41*(8), 1349–1357. https://doi.org/10.1016/S0735-1097(03)00124-4

Seo, J. H., Vedula, V., Abraham, T., Lardo, A. C., Dawoud, F., Luo, H., & Mittal, R. (2014). Effect of the mitral valve on diastolic flow patterns. *Physics of Fluids*, *26*(12), 121901. https://doi.org/10.1063/1.4904094

Sohns, C., & Marrouche, N. F. (2020). Atrial fibrillation and cardiac fibrosis. *European Heart Journal*, *41*(10), 1123–1131. https://doi.org/10.1093/eurheartj/ehz786

Steinberg, J. S., Zelenkofske, S., Wong, S.-C., Gelernt, M., Sciacca, R., Scd, E., & Menchavez, E. (n.d.). *Value of the P-Wave Signal-Averaged ECG for Predicting Atrial Fibrillation After Cardiac Surgery*. http://ahajournals.org

Stoddard, M. F., Dawkins, P. R., Prince, C. R., & Ammash, N. M. (1995). Left atrial appendage thrombus is not uncommon in patients with acute atrial fibrillation and a recent embolic event: A transesophageal echocardiographics tudy. *Journal of the American College of Cardiology*, *25*(2), 452–459. https://doi.org/10.1016/0735-1097(94)00396-8

Varela, M., Bisbal, F., Zacur, E., Berruezo, A., Aslanidi, O. v., Mont, L., & Lamata, P. (2017a). Novel Computational Analysis of Left Atrial Anatomy Improves

Prediction of Atrial Fibrillation Recurrence after Ablation. *Frontiers in Physiology*, *8*. https://doi.org/10.3389/fphys.2017.00068

Varela, M., Bisbal, F., Zacur, E., Berruezo, A., Aslanidi, O. v., Mont, L., & Lamata, P. (2017b). Novel Computational Analysis of Left Atrial Anatomy Improves Prediction of Atrial Fibrillation Recurrence after Ablation. *Frontiers in Physiology*, *8*. https://doi.org/10.3389/fphys.2017.00068

Vedula, V., George, R., Younes, L., & Mittal, R. (2015). Hemodynamics in the Left Atrium and Its Effect on Ventricular Flow Patterns. *Journal of Biomechanical Engineering*, *137*(11). https://doi.org/10.1115/1.4031487

Vella, D., Monteleone, A., Musotto, G., Bosi, G. M., & Burriesci, G. (2021a). Effect of the Alterations in Contractility and Morphology Produced by Atrial Fibrillation on the Thrombosis Potential of the Left Atrial Appendage. *Frontiers in Bioengineering and Biotechnology*, *9*. https://doi.org/10.3389/fbioe.2021.586041

Vella, D., Monteleone, A., Musotto, G., Bosi, G. M., & Burriesci, G. (2021b). Effect of the Alterations in Contractility and Morphology Produced by Atrial Fibrillation on the Thrombosis Potential of the Left Atrial Appendage. *Frontiers in Bioengineering and Biotechnology*, *9*. https://doi.org/10.3389/fbioe.2021.586041

Weng, L. C., Hall, A. W., Choi, S. H., Jurgens, S. J., Haessler, J., Bihlmeyer, N. A., Grarup, N., Lin, H., Teumer, A., Li-Gao, R., Yao, J., Guo, X., Brody, J. A., Müller-Nurasyid, M., Schramm, K., Verweij, N., van den Berg, M. E., van Setten,

J., Isaacs, A., … Lubitz, S. A. (2020). Genetic determinants of electrocardiographic P-wave duration and relation to atrial fibrillation. *Circulation: Genomic and Precision Medicine*, 389–395. https://doi.org/10.1161/CIRCGEN.119.002874

Whitlock, R. P., Belley-Cote, E. P., Paparella, D., Healey, J. S., Brady, K., Sharma, M., Reents, W., Budera, P., Baddour, A. J., Fila, P., Devereaux, P. J., Bogachev-Prokophiev, A., Boening, A., Teoh, K. H. T., Tagarakis, G. I., Slaughter, M. S., Royse, A. G., McGuinness, S., Alings, M., … Connolly, S. J. (2021). Left Atrial Appendage Occlusion during Cardiac Surgery to Prevent Stroke. *New England Journal of Medicine*, *384*(22), 2081–2091. https://doi.org/10.1056/NEJMoa2101897

Wiggers, C. J., & Katz, L. N. (1922). The contour of the ventricular volume curves under different conditions. *American Journal of Physiology-Legacy Content*, *58*(3), 439–475.

Wright, B. E., Watson, G. L., & Selfridge, N. J. (2020). The Wright table of the cardiac cycle: a stand-alone supplement to the Wiggers diagram. *Advances in Physiology Education*, *44*(4), 554–563. https://doi.org/10.1152/advan.00141.2019

Yaghi, S., Song, C., Gray, W. A., Furie, K. L., Elkind, M. S. V., & Kamel, H. (2015). Left Atrial Appendage Function and Stroke Risk. *Stroke*, *46*(12), 3554–3559. https://doi.org/10.1161/STROKEAHA.115.011273

Yagishita, A., Goya, M., & Hirao, K. (2018). Simultaneous recording of the P wave during atrial fibrillation. In *Circulation* (Vol. 138, Issue 18, pp. 2057–2060).

Lippincott Williams and Wilkins. https://doi.org/10.1161/CIRCULATIONAHA.118.037198